Spring 2011

Computational Investigation of the Bioactive Selenium Compounds Ebselen and Selenious Acid

Sonia Antony
Old Dominion University

COMPUTATIONAL INVESTIGATION OF THE BIOACTIVE SELENIUM COMPOUNDS EBSELEN AND SELENIOUS ACID

by

Sonia Antony
M.Sc. May 2001, University of Kerala, India
M.S. May 2006, Old Dominion University

A Dissertation Submitted to the Faculty of
Old Dominion University in Partial Fulfillment of the
Requirements for the Degree of

DOCTOR OF PHILOSOPHY

CHEMISTRY

OLD DOMINION UNIVERSITY
May 2011

Approved by:

Craig A. Bayse (Director)

Patricia Pleban (Member)

Paula Mazzer (Member)

Christopher Osgood (Member)

ABSTRACT

COMPUTATIONAL INVESTIGATION OF THE BIOACTIVE SELENIUM COMPOUNDS EBSELEN AND SELENIOUS ACID

Sonia Antony
Old Dominion University, 2011
Director: Dr. Craig A. Bayse

Selenium, a toxic element, is required in trace quantities for the proper functioning of biological systems. The experimental mechanistic study of the reactions of ebselen and selenious acid is difficult due to complexity of the reaction mixtures and the presence of short-lived intermediates. Computational modeling of the reactivity of these species can give us an insight into their mechanisms, but the process is complicated by proton exchanges associated with the mechanistic steps. In gas phase modeling, this may be corrected to a certain level using the solvent assisted proton exchange (SAPE) method. SAPE is a modeling technique that mimics solvent participation in proton transfer associated with chemical reactions. Within this microsolvation method, explicit water molecules allow relay of a proton between the protonation and deprotonation sites of the reactants and the products. In this dissertation, density functional theory (DFT) and solvent assisted proton exchange (SAPE) are used to explore proposed mechanisms for (a) the reactions of ebselen under normal cellular conditions and under oxidative stress, (b) the reactions of selenite with thiols, and (c) the reduction of a zinc finger model compound by ebselen. The activation barriers obtained by SAPE for the these mechanisms fall within the limits expected for a catalytic system at physiological temperatures, and are significantly lower than studies which force direct proton transfer.

The results suggest that under normal cellular conditions, ebselen reacts with thiol to form the corresponding selenenyl sulfide, a terminal pathway in the antioxidant activity of the compound. Under oxidative stress, ebselen catalyzes the reduction of oxidants through a thioselenurane intermediate. In the thiol reduction of selenite to the selenotrisulfide, formation of a selenurane intermediate is predicted to be the rate determining step. The initial reduction of a zinc finger model complex with ebselen is shown to be a low-barrier reaction consistent with experimental rate constants.

This dissertation is dedicated to my parents, Celine and Antony.

ACKNOWLEDGMENTS

I would like to thank my parents for providing me a convent school education. My teachers were my inspiration, and I am grateful for their dedication and hard work. Thanks to my alma maters: St. Joseph's Convent Girls High school, Fatima Mata National College, and Mar Ivanios College. I thank Uncle Sach, and Aunt Jessy, for encouraging and helping me to pursue higher studies in the United States. Thank you for providing for me and allowing me to be a part of your family for the past three years.

As an international student, I felt a very warm atmosphere at the campus of Old Dominion University. The office of the international student and scholar services has been very helpful since my arrival in the United States. The Department of Chemistry and Biochemistry provided me funding and a friendly environment. I am grateful to Dr. Kenneth Brown and Dr. Richard Gregory for providing me teaching assistantship. I would like to express my gratitude to Dr. Williams, Alicia, Janice, Valerie, Tammy, Lennis, Dr. Dobrydneva, and John Hill for their friendship and help. I would also like to thank Dr. John Cooper, my Master's advisor, for funding and advice. My sincere appreciation to the OCCS and its staff members for all their help, especially: Charlotte, Allen and Ruben. I enjoyed the company of the students in the Chemistry Department including, Erin, Sean, Mindy, Josh, Jeff, Jasprina, Trebbeca, Anna, and Rajaa. I thank my lab mates Patricia and Lenora for their encouragement and moral support. It was a pleasure working with you and I enjoyed your company very much. I will miss our daily chat at lunch time.

My eternal gratitude to the army of people who supported me through prayers, including Fr. Tim, Fr. Joy, Deacon Bob, Sr. Elena Mary, Sr. Agatha, my parents, Aunt

Jessy, Aunt Leela, Aunt Barbara, Aunt Cicily, Uncle John, my brother Sojan, Shiny, Patricia Lutz, Janice, Tamrae Harper, and many more. I thank you all for enriching my faith in Christ, and I thank God almighty for all the blessings.

I am very grateful to my committee members Dr. Patricia Pleban, Dr. Paula Mazzer, and Dr. Christopher Osgood for all their help, valuable time and advice. I appreciate the research funding through the NSF grant. A very special thanks to my advisor, Dr. Craig Bayse, for the constant help with my projects, writing papers, and support in getting my degree. I would not have been able to complete this work if it was not for your support and encouragement.

TABLE OF CONTENTS

LIST OF TABLES

LIST OF FIGURES

Figure Page

LIST OF SCHEMES

CHAPTER 1

INTRODUCTION

Selenium Chemistry

The element selenium was discovered in 1817 by a Swedish scientist Jons Jacob Berzelius while investigating the cause of illness among the workers in a sulfuric acid manufacturing plant.[1] Initially, Se was believed to be toxic because it caused "alkali disease" in cattle that grazed on selenium-accumulating plants.[2] The potential beneficial nature of selenium was established when Swartz and Foltz proved that Se could alleviate liver necrosis in rats.[3] A selenium-deficient diet has shown to cause "White muscle disease" in cattle and "Keshan" disease among humans, and both have similar symptoms.[4] Se-deficient individuals are susceptible to the disease causing virus strain of Keshan disease.[5] Kashin Beck disease is caused by the deficiency of Se, and is found in preadolescents and adolescents, affecting the limb joints and hence affecting growth.[6] Selenium and iodine deficiency can result in impaired thyroid metabolism.[7,8,9] The supplementation of selenium is believed to reduce the risk of arthritis, cardiovascular disease, and cancer.[10] Thus, selenium, once thought to be toxic, was found to be an essential trace element, and its deficiency or supplementation is associated with a number of diseases.

This dissertation follows the format of *Journal of Physical Chemistry A*.

Rotruck et al. confirmed the presence of Se in the antioxidant enzyme glutathione peroxidase (GPx), [11] a tetrameric protein with one selenium atom per subunit.[12] Further experiments by Epp et al. proved that Se was incorporated through a selenocysteine (SeCys) residue, which is necessary for the activity.[13] SeCys is also found in the active site of thioredoxin reductase (TRxR), selenoprotein P, and other redox-related selenoenzymes.[7] Thus, the major biological role of selenium is to prevent oxidative damage to lipids, DNA, and other cellular components by removing reactive oxygen species (ROS).[14] Specifically, GPx converts hydrogen peroxide, a reactive oxygen species (ROS), into water.[14]

Scheme 1. Catalytic cycle of GPx.

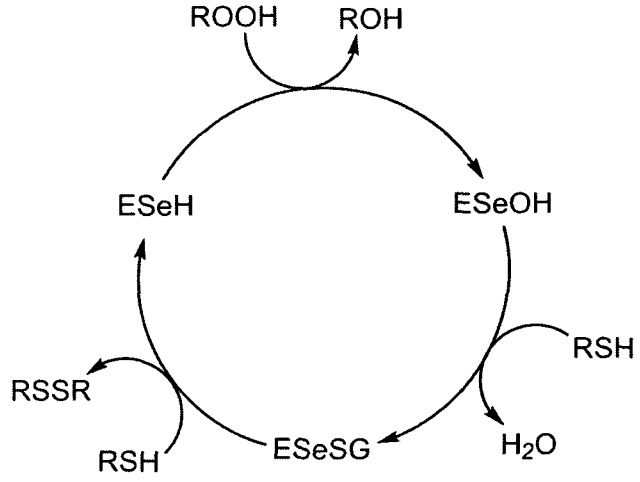

The importance of Se lies in the fact that it can shuttle between different oxidation states due to its low redox potential, which makes it suitable for catalytic activity.[15] GPx undergoes a simple catalytic cycle (Scheme 1) with the selenol form of the enzyme as the active form which reacts with peroxide to form the corresponding selenenic acid.[13] Reduction of the acid with an equivalent of thiol gives the selenenyl sulfide intermediate, with subsequent reaction producing a disulfide and regenerating the selenol to complete the catalytic cycle.[13,16] Among these three steps, the formation of disulfide has been shown to be the rate-determining step.

Many organo-selenium compounds of pharmacological importance were synthesized after recognizing selenium as a micronutrient.[14] One compound, ebselen, a cyclic selenenamide, was found to be a non-toxic GPx mimic with anti-inflammatory and anti-artherosclerotic properties.[17] Ebselen has been widely studied for its various physiological activities and undergoes more complex reaction pathways than GPx due to the Se-N covalent bond.[17] Ebselen reacts with ROS and thiols forming various metabolites and some metabolites reduce the peroxides in the membranes and lipoproteins.[17] Ebselen inhibits apoptosis and studies have shown that it considerably reduces the oxidative damage dealt by the large concentrations of ROS produced by stroke.[18-21] Studies have shown that the compound's activity varies depending on the reaction conditions.[14] Additionally, Daiber et al.'s study of the reaction of ebselen and peroxynitrite showed that the reaction is difficult to monitor under physiological conditions, because there are too many reactions and multi-equilibria systems to follow experimentally.[22]

Scheme 2. Metabolic pathways of selenium compounds from food source.[23]

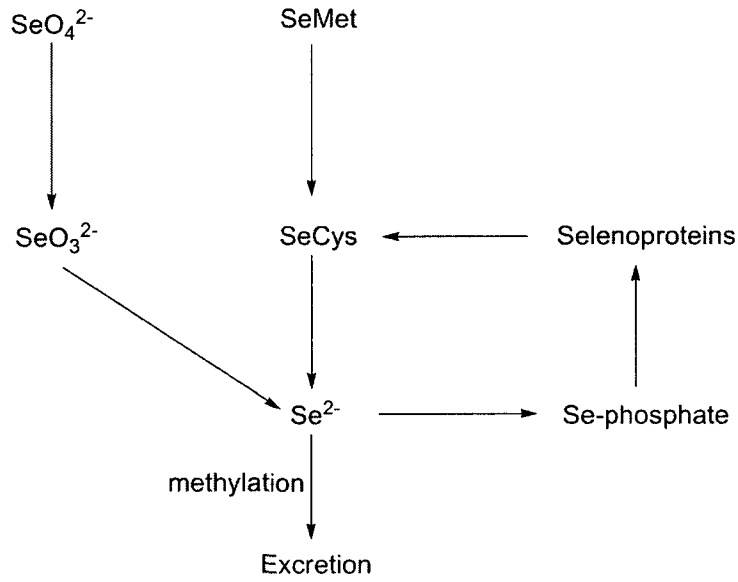

Ebselen cannot be used as a supplement for Se deficiency because its selenium is not bioavailable.[24] Instead, adding Se to the soil where crops were grown reduced selenium deficiency and improved the health of the population. Plants take up inorganic forms of Se (SeO_3^{2-} and SeO_4^{2-})[25] and convert them to selenoamino acids such as selenomethione and methylselenocysteine (Scheme 2).[23] Selenious acid and its salts are known to be toxic[26], but limited consumption has potent anti-inflammatory properties by inhibiting the RNS-producing enzymes.[27] Thiols, such as GSH and thioredoxin, can convert selenite into a selenotrisulfide by a non-enzymatic reaction.[28] GSSeSG is an efficient substrate for the mammalian thioredoxin reductase and oxidizes reduced thioredoxin.[29,30] These selenotrisulides are a source of Se atoms for selenophosphate and selenocysteine synthesis. For example, 3-mercaptopyruvate sulfur transferase (MST) and

glyceraldehyde-3-phosphate dehydrogenase (GAPDH) are SSeS binding proteins which release the substrate form of Se for bacterial selenophosphate synthase (SPS),[31] an important enzyme that is involved in the synthesis of selenocysteine and 2-selenouridine.[32,33]

In addition to the beneficial effect described so far, ebselen and selenite inhibit DNA binding by zinc finger transcription factors (TFs) such as API, TFIIIA and SP1.[34-37] The proposed mechanism is through the reaction with the cysteine thiol groups of the TFs resulting in the ejection of Zn and the unfolding of the functional protein.[38] Labaree et al. confirmed the presence of RSSeSR when a reaction was conducted between sodium selenite and a zinc finger model compound, but a dithiol and selenol were present in the reaction of ebselen; in both cases zinc was released from the coordination site.[38] The reaction with the zinc-binding thiolates and hence the inhibition of TF may be responsible for the anti-inflammatory and anti-cancer effects of selenium compounds.[38]

The mechanistic pathways of biological reactions involving selenium compounds have been experimentally investigated by several researchers under various conditions.[22,39-44] Sometimes, it is difficult to obtain a clear idea of the reaction mechanism due to the complex reaction mixtures and multi-equilibria involved in the reaction. Density-functional theory (DFT) has emerged as a valuable tool in predicting the geometry and energies of reactions, but these typically gas-phase calculations do not include the role of solvent. The proton transfer reactions that we are modeling occur in biological systems, where the presence of water cannot be neglected. Purely gas-phase calculations give a very high barrier due to a strained transition state for a direct proton transfer reaction. Implicit bulk solvation correction does not account for any hydrogen

bonding, and hence does not improve the activation barriers, and molecular dynamics simulations using explicit bulk solvation are generally computationally expensive. The inclusion of a solvent network of a minimum number of water molecules in a gas-phase DFT calculation has been shown predict activation barriers with a reasonable level of accuracy.[45] This microsolvation technique is called solvent-assisted proton exchange (SAPE) and simulates mild acid/base catalysis by the bulk water. SAPE models use a hydrogen-bonded network of solvent to connect the heavy atom proton donor and acceptor to relay the protons through the solvent network and give lower, more realistic activation barriers.

In this dissertation, we use DFT and these explicit solvation methods to predict the pathways of ebselen under normal cellular conditions and oxidative stress, the mechanistic steps involved in the conversion of selenious acid to selenotrisulfide, and the reactions of ebselen with zinc finger proteins. The theoretical basis for my study is included in the following part of this Chapter.

Theoretical basis for my computational study[46-48]

The failure of classical dynamics to explain the wave-like nature of microscopic particles led in part to the development of quantum mechanics (QM). In QM, the physical properties of a microscopic system can be described by a wave function Ψ. Physical observables can be obtained by applying the appropriate operators on this wave function. For example, from the time-independent Schrödinger equation (eq 1), the energy, E, (the observable) can be obtained by using the Hamiltonian operator $\hat{H}$ on the wave function Ψ.

$$\hat{H}\Psi = E\Psi \quad (1)$$

The Schrodinger equation falls into the category of equations known as the partial differential eigenvalue equations in which an operator acts on a function and returns the function multiplied by a scalar (the eigenvalue). Using QM, the energetics of a reacting system at the molecular level (microscopic level) can be determined from the structure of the reactants, transition states and products. In this dissertation, the mechanistic pathways involved in the reaction of ebselen and selenious acid is predicted based on the activation energy barriers obtained from QM calculations; thus complementing the experimental research.

Expressing the time independent Schrodinger's equation for a hydrogen atom gives eq 2:

$$\left\{-\frac{\hbar^2}{2m}\nabla^2 + \hat{V}\right\}\Psi(r) = E\Psi(r) \quad (2)$$

The Hamiltonian operator is composed of two parts – kinetic energy and potential energy.

$$\hat{H} = -\frac{\hbar^2}{2m}\nabla^2 + \hat{V} \quad (3)$$

Equation 3 represents the Hamiltonian for a hydrogen atom and the kinetic energy operator is

$$\hat{K} = -\frac{\hbar^2}{2m}\nabla^2 \quad (4)$$

where m is the mass of the electron, $\hbar$ is Planck's constant divided by 2π, and $\nabla^2 = \left(\frac{\partial^2}{\partial x^2} + \frac{\partial^2}{\partial y^2} + \frac{\partial^2}{\partial z^2}\right)$

Potential energy operator for the interaction between a single electron and nucleus is

$$\hat{V} = -\frac{Ze^2}{4\pi\varepsilon_o r} \qquad 5$$

Based on the model for hydrogen atom, the total energy of a system of N electrons and M nuclei is obtained by using the Hamiltionian,

$$\hat{H} = -\sum_{i=1}^{N}\frac{1}{2}\nabla_i^2 - \sum_{A=1}^{M}\frac{1}{2M_A}\nabla_A^2 - \sum_{i=1}^{N}\sum_{A=1}^{M}\frac{Z_A}{r_{iA}} + \sum_{i=1}^{N}\sum_{j>i}^{N}\frac{1}{r_{ij}} + \sum_{A=1}^{M}\sum_{B>A}^{M}\frac{Z_A Z_B}{R_{AB}} \qquad 6$$

where $\hat{H}$ is expressed in atomic units and each term on the right hand side represents the kinetic energy of the electrons, the kinetic energy of the nuclei, coulomb attraction between the electrons and nuclei, repulsion between the electrons, and the repulsion between the nuclei respectively. M_A is the ratio of the mass of nucleus A to the mass of an electron; Z_A is the atomic number of nucleus A and ∇_i^2 involves differentiation with respect to the coordinates of the i^{th} electron and the A^{th} nucleus.

Using the appropriate operators, the expectation value of any quantity such as the energy can be obtained as shown below.

$$\int \Psi^* \hat{H} \Psi d\tau = \int \Psi^* E \Psi d\tau \qquad 7$$

where Ψ^* is the complex conjugate of Ψ. Rearranging eq 7 gives the expectation value, E.

$$E = \frac{\int \Psi^* H \Psi d\tau}{\int \Psi^* \Psi d\tau} \qquad 8$$

a. The Born-Oppenheimer Approximation[47]

The real representation of a wave function for a many particle molecular system is difficult to express, since the motion of each particle is correlated with that of other particles. In order to reduce the complications, an approximate wave function may be obtained by assuming the velocity of the nuclei to be negligible, since nuclei are much heavier than electrons. Under this approach, known as the Born-Oppenheimer approximation, the kinetic energy of the nuclei (second term in eq 8) is zero and the potential energy due to the nuclear-nuclear repulsion (last term in eq 8) is a constant which is be added to the electronic energy. The terms involving the electrons are called the electronic Hamiltonian describing the motion of N electrons in the field of M point charges.

$$\hat{H}_{elec} = -\sum_{i=1}^{N}\frac{1}{2}\nabla_i^2 - \sum_{i=1}^{N}\sum_{A=1}^{M}\frac{Z_A}{r_{iA}} + \sum_{i=1}^{N}\sum_{j>i}^{N}\frac{1}{r_{ij}} \qquad 9$$

The sum of the first two terms is called the one electron Hamiltonian.

The solution to a Schrodinger equation involving the electronic Hamiltonian,

$$\hat{H}_{elec}\varphi_{elec} = \varepsilon_{elec}\varphi_{elec} \qquad 10$$

where φ is the electronic wave function describing the motion of the electrons which is explicitly dependent on the electronic coordinates but parametrically dependent on the nuclear coordinates and so does the eigenvalue, the electronic energy. The total energy for the system under the Born-Oppenheimer approximation is given by eq 11.

$$\varepsilon_{tot} = \varepsilon_{elec} + \sum_{A=1}^{M}\sum_{B>A}^{M}\frac{Z_A Z_B}{R_{AB}} \qquad 11$$

The wavefunction as described above does not include the spin of the electrons. The antisymmetry (Pauli's exclusion) principle states that "A many-electron wave function must be antisymmetric with respect to the interchange of the coordinate x of any two electrons"

$$\varphi(x_1, \cdots x_i, \cdots x_j, \cdots x_N) = -\varphi(x_1, \cdots x_j, \cdots x_i, \cdots x_N) \quad 12$$

Applying the antisymmetric wave function to multi-electron Hamiltonian (eq 11) with the inclusion of spin leads to the Hartree-Fock equations (eq 13 and 14)

$$\hat{F}(i)\varphi_i = \varepsilon_i \varphi_i \quad 13$$

$$\hat{F}(i) = -\frac{1}{2}\nabla_i^2 - \sum_{A=1}^{M} \frac{Z_A}{r_{iA}} + V^{HF}(i) \quad 14$$

where $\hat{F}(i)$ is the one-electron Fock operator for each electron "i", φ_i is the ith spin orbital and ε_i is the eigenvalue of the ith spin orbital. Solution to the HF equation provides both the wavefunction and the energy of the system.

b. Electron correlation and exchange[47]

As a result of Pauli's exclusion principle, a small amount of electron correlation is included in the HF method. The pure HF wave function does not include the dependence on the distance between electrons of opposite spin, whereas the exact wave function does. The energy associated with the exchange of spatial coordinates of electrons is termed the "exchange energy" which is a special case of electron interaction. The rest of the interactions between electrons that are not included in the exchange part and the classical coulombic interaction are termed the "electron correlation".

$$E_{corr} \equiv E_{exact} - E_{HF} \quad 15$$

The correlation energy is defined as the difference between the exact energy and the Hartree-Fock energy. In the HF method, the electron correlation is treated in an average way, which means each electron is considered to moving in the average potential field of the rest of the electrons. The electrons may get closer and the resulting HF energy is above the true energy. This treatment results in poor prediction of bond distances and bond dissociation energies. In order to overcome this drawback of HF theory, expensive post Hartree Fock ab initio methods or density functional theory (DFT) may be used.

c. Density Functional theory

The density of electrons depends only on the number of electrons, position of the nuclei, and the charges of the nuclei.

$$N = \int \rho(r) dr \quad 16$$

According to the early approximations in the Hohenberg theorem, energy is a functional of density.[49]

$$E = E[\rho] \quad 17$$

Later, the Kohn-Sham (KS) theorem was developed to include the exchange and correlation effects in an approximate way.[50] The kinetic energy of the interacting systems and the non-interacting systems are different, even though the electron density is the same. In order to solve this problem, the kinetic energy term that is not included in the original Hamiltonian is built into the exchange-correlation functional, which was originally intended for the non-classical potential energy, as in the HF equation. Hence,

$$E(\rho) = T_s[\rho] + V_{re}[\rho] + J[\rho] + T_C[\rho] + E_{ncl}[\rho] \quad 18$$

The terms on the right-hand side are the kinetic energy of the non-interacting electrons, the nuclear-electron interaction, the classical electron-electron interactions, the corrections to the kinetic energy, and the corrections to the non-classical electron-electron interactions, respectively. The last two terms arise due to the interacting nature of the electrons, and those are collectively called the exchange correlation energy E_{xc}.

$$E_{xc} = (T[\rho] - T_S[\rho]) + (E_{ee}[\rho] - J[\rho]) = T_C[\rho] + E_{ncl}[\rho] \quad 19$$

where $T[\rho]$ is the true kinetic energy and $E_{ee}[\rho]$ is the true electron-electron interaction energy.

KS molecular orbitals are constructed from non-interacting systems with the assumption that for an interacting system with the same density, an external potential can be determined, which in turn determines the Hamiltonian and the wave function. The one-electron KS operator (h_i^{KS}) operates on the molecular orbital, χ_i, to give the energy (eq 20):

$$h_i^{KS}\chi_i = \varepsilon_i\chi_i \quad 20$$

This equation is similar to the Fock equation for a one electron system (eq 13).

Local density approximation:[46,51] The concept of local density approximation (LDA) is based on the idea of a uniform electron gas, where the electron density, ρ, is a constant value throughout the system. If N is the number of electrons and V is the volume of electron gas, then the density can be written by eq 21:

$$\frac{N}{V} = \rho \qquad 21$$

The concept of a homogeneous electron gas is unrealistic, because the electron density varies rapidly in most atoms and molecules, but LDA still has a prominent place in DFT, because its exchange and correlation energy functional have been shown to predict better results than the HF method.[46,48]

$$\varepsilon_{xc} = \int \rho(r)\varepsilon_{xc}[(\rho)]\, dr \qquad 22$$

$$\varepsilon_{xc} = \varepsilon_x + \varepsilon_c \qquad 23$$

$$\varepsilon_x = \frac{-9\alpha}{8}\left(\frac{3}{\pi}\right)^{1/3} \rho^{1/3}(r) \qquad 24$$

The exchange functional is frequently called the Slater exchange, and is abbreviated by S. From the results of the highly accurate Monte-Carlo simulations by Ceperly and Alder,[52] different expressions of ε_c were developed by various authors.[53] Vosko, Wilk, and Nusair[53] derived an expression for ε_c (VWN5) based on Ceperly and Alder's work and also by random phase approximation (VWN)[53] from the following equation.

$$\varepsilon_c^i =$$

$$\frac{A}{2}\left\{ln\frac{r_s}{r_s+b\sqrt{r_s}+c} + \right.$$

$$\left.\frac{2b}{\sqrt{4c-b^2}}tan^{-1}\left(\frac{\sqrt{4c-b^2}}{2\sqrt{r_s}+b}\right) - \frac{bx_0}{x_0^2+bx_0+c}\left\{ln\frac{(\sqrt{r_s}-x_0)^2}{r_s+b\sqrt{r_s}+c} + \frac{2(b+2x_0)}{\sqrt{4c-b^2}}tan^{-1}\left(\frac{\sqrt{4c-b^2}}{2\sqrt{r_s}+b}\right)\right\}\right\} \qquad 25$$

where r_s is the density parameter, and the empirical constants A, x_0, b, and c have a different set of values for i=0 and i=1. Since DFT uses combinations of separate

functional designed to handle exchange and correlation, VWN, in combination with Slater's exchange, is called the SVWN method.

If the LDA is extended to the unrestricted spin case, then it is called the local spin density approximation (LSDA). Even though the electron density is not uniform for real systems, the results obtained by LSDA are comparable to, or better than, those obtained from the Hartree-Fock approximation. LSDA gives good results for equilibrium geometries, dipole moments, and vibrational frequencies, even though it gives inaccurate molecular atomization energies.[48]

Generalized gradient approximation method:[46] One drawback of LSDA theory is that in reality, the electron density is not spatially uniform. The generalized gradient approximation (GGA) is obtained when LSDA is corrected for the variation of electron densities, ρ^{α} and ρ^{β}. This approach was initially referred to as non-local DFT, and later referred to as the generalized gradient approximation (GGA). Most gradient-corrected functionals are expressed as an enhancement factor added to the LDA functional. The exchange correlation functional can be divided into two parts:

$$E_{xc}^{GGA} = E_{x}^{GGA} + E_{c}^{GGA} \qquad 26$$

$$E_{x}^{GGA} = E_{X}^{LSD} - \sum_{\sigma} F[x_{\sigma}]\, \rho_{\sigma}(r)^{4/3} dr \qquad 27$$

$$x = \frac{|\nabla \rho_{\sigma}|}{(\rho_{\sigma})^{4/3}} \qquad 28$$

The enhancement factor put forward by different people led to the development of various GGA exchange functionals. [54-58] Becke[54] developed a widely popular GGA exchange functional (B or B88) by introducing an empirical parameter based on the

exchange energies of the noble gas elements.[55] Using the enhancement factor as a function of the reduced density gradient, prominent functionals such as B86 by Becke[59], P by Perdew[56], and PBE[57,58] by Perdew, Burke and Ernzerhof were developed. Similarly, GGA correlation functionals such as B88[54], P86[56], PW91[60], LYP[61] etc. were also developed. The first three functionals are without any empirical parameters and are added as a correction to the LSDA, whereas the last one is an independent functional which contains four empirical parameters that fit the He atom.

Adiabatic connection methods:[46] Using the Hellmann-Feynmann theorem, the exchange-correlation of an interacting system can be calculated from non-interacting system. The exchange-correlation energy can be computed as

$$E_{xc} = \int_0^1 \langle \Psi(\lambda) | V_{xc}(\lambda) | \Psi(\lambda) \rangle \, d\lambda \qquad 29$$

The coefficient λ varies between 0 and 1, representing the extent of inter-electronic interaction. The above equation is represented in Figure 1. When λ=0, then V =K, the exchange interaction.

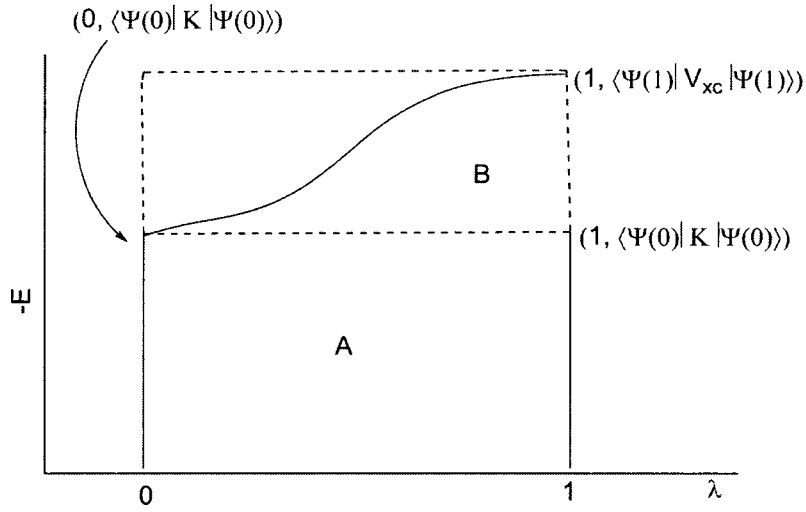

Figure 1. Energy of an interacting system represented as the sum of the energies of a non-interacting system (rectangle A) and the real exchange correlation energy (a fraction of B).[46]

When $\lambda = 0$, the expectation value is the area of the bottom rectangle, the Slater determinant for the Kohn-Sham orbitals of the non-interacting system E_X^{HF}. The area of the rectangle on the top is

$$\langle \Psi(\lambda) | V_{xc}(\lambda) | \Psi(\lambda) \rangle - E_x^{HF} \qquad 30$$

$$E_{xc} = E_x^{HF} + z(E_{xc}^{DFT} - E_x^{HF}) \qquad 31$$

where "z" is to be empirically determined, since only a fraction contributes to the E_{xc}.

The process of connecting the interacting and the non-interacting system is called the adiabatic method. Based on this Scheme, various hybrid methods such as B3PW91[62] (eq 32), B3LYP[63], mPW1PW91[64], etc. were developed.

$$E_{xc}^{B3PW91} = (1-a)E_x^{LSDA} + aE_x^{HF} + b\Delta E_x^B + E_c^{LSDA} + c\Delta E_c^{PW91} \quad 32$$

(a=0.20, b=0.72 and c=0.81)

B3PW91 uses Becke's exchange functional and the PW91 correlation functional. As an improvement over Becke's enhancement factor, Perdew[56] and co-workers developed PW exchange functional (25 % HF exchange). Even though this functional works for total atomic energies, it is not useful for long range behaviors such as hydrogen bonding, van der Waals interactions, etc. Including these non-covalent interactions, the hybrid functional mPW1PW91 was developed by Adamo and Barone[64] as a modification on PW exchange functional. In our published work on selenium compounds involving hydrogen bonding interactions, the mPW1PW91 method was used and the predicted results are consistent with expensive ab initio methods.[45] For the study (Chapters 2 and 3) using the Gaussian 03[65] software package, the mPW1PW91 method is used. In PQS[66] software, mPW1PW91 functional is not included, and hence the B97-1[67] method was used, which is a modified Becke's 1997 GGA exchange-correlation functional. In B97-1, the empirical parameters of B97 was reoptimized with an inclusion of 21% HF exchange.[67] This method was successful in predicting hydrogen bonding weak interactions,[68] and is used in Chapter 4.

Pure DFT avoids ionic interactions (underestimates barrier heights of chemical reactions), and HF, on the other hand, overestimates. In some cases, using hybrid functionals may cancel out the errors from the GGA and HF methods. For example, mPW1PW91 has a default 25 % HF exchange and the rest is from PW functional, and, to a certain extent, the errors tend to cancel out.[46]

d. Basis sets[47]

Molecular orbitals are obtained by the linear combination of atomic orbitals (LCAO) (eq 33) and basis sets are mathematical representations of atomic orbitals. In the previous sections, I have discussed the different methods that use basis sets to carry out meaningful calculations.

$$|\varphi_i\rangle = \sum c_{ip} |\varphi_{ip}\rangle \quad 33$$

Slater-type orbitals (STO) are basis functions built on an exponential mathematical form of the atomic orbitals (eq 34) similar to the solutions to hydrogenic atom, but are known to be computationally expensive. STOs can be expanded in Gaussian-type orbitals (GTO) (eq 35) which are cheap, but less accurate, representations.

$$\varphi \propto e^{-\xi r} (STO) \quad 34$$

$$\varphi' \propto e^{-\xi r^2} (GTO) \quad 35$$

In order to improve the approximation of the STO, a linear combination of several GTOs is used. For example,

$$\varphi_{STO} = \sum_i c_i \varphi_i \quad 36$$

$$\varphi_{STO-3} = c_1 \varphi_{GTF}^a + c_2 \varphi_{GTF}^b + c_3 \varphi_{GTF}^c \quad 37$$

To speed up the calculations, a fixed linear combination of GTOs (primitives), called a "contraction", is used. The representations of inner electrons are often contracted, since they do not participate in bond breaking or formation.

The representation of the molecular orbitals may also be improved by increasing the flexibility of basis set. These improvements can be done in different ways, and, in our calculations, we incorporated the following methods for this procedure.

1. Increase the basis set size for important parts of the system: As a compromise between speed and accuracy, the coefficients of the valence electrons are allowed for a free optimization, and the representation for the core electrons are kept frozen. For example, a double zeta valence basis set, in which each inner atomic orbital is assigned one basis function and each valence atomic orbital gets two basis functions, may be used for non-reacting portions of a system. For the reacting centers, triple zeta valence basis sets are assigned. The difference between double and triple zeta valence basis sets is that three basis functions are assigned per valence orbital for the latter, instead of two. Heteroatoms such as O, N, and the hydrogens attached to those atoms are assigned tzvp basis sets, whereas carbon atoms get only d95 basis set.

2. Add polarization functions: Polarization functions allow the electron density to shift toward the region of bond formation and improve the description of bonding. These functions typically have higher angular momentum quantum numbers (l+1) than the valence atomic orbitals. For example, p-type functions are used for hydrogen atoms. For the studies presented in this dissertation, all atoms, except for hydrogens bonded to carbon, are assigned polarization functions.

3. Add diffuse functions: Diffuse functions allow the charge density to expand, and are particularly important for electronegative atoms, anions, and intermolecular interactions. Diffuse functions typically have the same angular momentum as the valence

basis set, but with smaller exponents, ζ. In our calculations in the following Chapters, diffuse functions are added to Se, S, O and N atoms.

An example of how we model a reaction and designate the basis set for the present study is discussed below (Figure 2). In order to save computing time, truncated models with a small, preliminary basis sets (BSI) are used for initial mapping of the reaction coordinate to find the transition states and products. For example, in the oxidation reaction of ebselen to the corresponding oxide, we optimized the truncated reactant complex (Figure 2a) in BSI (Table 1) by retaining only the reacting skeleton of the system. Relative to ebselen, the -NHPh group is replaced by -NHMe and the phenyl ring is reduced to ethylene.

Table 1. Table of basis set I and II designation for the atoms in this study.

Atoms	BSI	BSII
Se	Ermler-Christiansen (RECP) (4s4p5d)/[3s3p3d]	BSI + s,p,d diffuse functions
S	Wadt-Hay (4s4p1d)/[3s3p1d]	BSI + s,p diffuse functions
N, O	tzvp	BSI + s,p diffuse functions
SAPE H	tzvp	BSI
CH groups	d95	BSI + d polarization functions

From the truncated versions of R, TS, and P, full models are optimized in BSI and then in BSII basis sets (Figure 2b). The activation barriers for truncated (BSI) versus full (BSII) models differ by 4 kcal/mol. More description of the DFT methods and basis sets used for modeling the reactions are given in each Chapter.

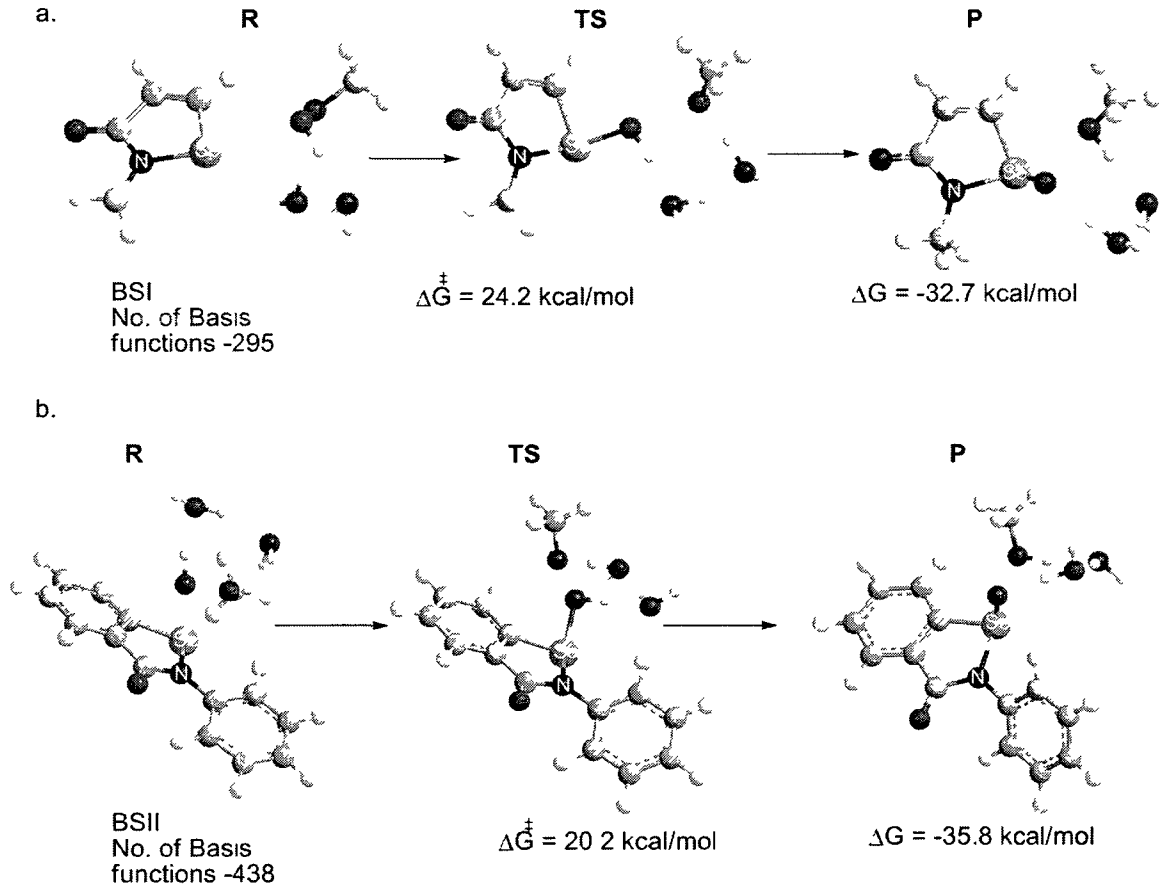

Figure 2. a. Oxidation of truncated ebselen with methyl peroxide showing the reactant, transition state and product. b. Oxidation of ebselen with methyl peroxide showing the reactant, transition state and product. [Atoms that are not labeled have the following shades/colors: carbon-gray, hydrogen-white, oxygen-black (for color copy- red). This pattern is followed throughout this dissertation.]

CHAPTER 2

MODELING THE MECHANISM OF THE GLUTATHIONE PEROXIDASE MIMIC EBSELEN USING DFT AND SOLVENT-ASSISTED PROTON EXCHANGE METHOD

Introduction

Reactive oxygen and nitrogen species (ROS/RNS) are byproducts of aerobic metabolism that cause oxidative damage of cells,[16] and are associated with aging (arthritis) and increased risk of cancer and cardiovascular disease.[14,69] ROS serve as biochemical signaling agents by activating signal transduction pathways that regulate gene expression.[70] Selenoenzymes such as glutathione peroxidase (GPx) and thioredoxin reductase (TrxR) play an important role in maintaining the optimal balance of ROS.[71] The low redox potential of Se allows it to switch readily between oxidation states.[15,72] As a result, Se is required only in trace amounts in comparison to other antioxidant molecules such as vitamin C.[73,74] Given this ability to scavenge ROS/RNS, various natural and synthetic organoselenium compounds[15,75,76] have been explored as preventatives for a number of ROS/RNS-related illnesses.[10,29,77-80]

Specifically, ebselen **1** is a non-toxic scavenger of ROS/RNS with anti-inflammatory, anti-atherosclerotic, and anti-cytotoxic properties.[17] Ebselen reacts with the peroxides in cells, membranes, lipids, and lipoproteins,[17,81] thereby inhibiting apoptosis. Studies have shown that **1** considerably reduces the oxidative damage produced by stroke.[18-21] RNS react faster than H_2O_2 with **1**, and their RNS scavenging efficiency is higher than that of other antioxidant molecules, such as ascorbate, cysteine

or methionine.[22,42,82] Ebselen also reacts with free or protein-bound nucleophilic thiols to form the corresponding selenenyl sulfide (**2**),[17] which is considered a storage form, and is also responsible for transport of the drug.[83] The reaction with thiols also includes the oxidation of cysteine ligands, which initiates the release of zinc from transcription factors.[84] Ebselen inhibits enzymes associated with inflammation (i.e., protein kinase C, NO synthase, etc.) by blocking sulfhydryl groups necessary for production of ROS/RNS.[17,82] Ebselen cannot be used as a supplement for selenium deficiency,[85] due to the bonding of Se to the aromatic ring. Ebselen is metabolized into sugar derivatives for excretion.[86]

Scheme 3. GPx catalytic cycle.

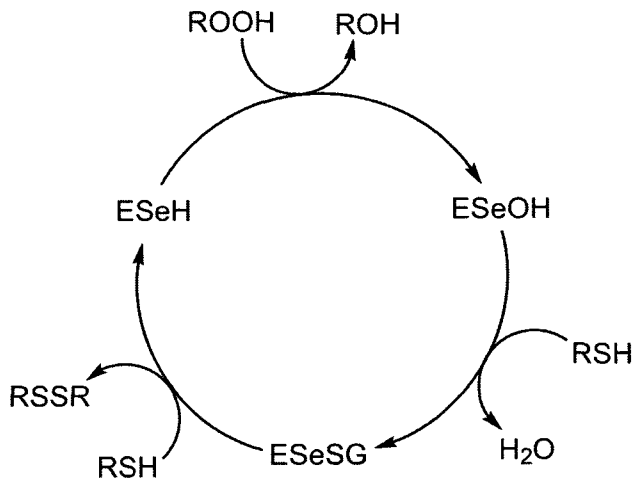

Ebselen and other organoselenium compounds catalyze the same overall reduction of ROS as the selenoprotein glutathione peroxidase (GPx).[14,87] GPx operates

by a simple, three step mechanism (Scheme 1) involving changes in oxidation state of the active-site selenocysteine (SeCys) residue. ROS oxidize the resting state selenol (GPx-SeH) to the selenenic acid (GPx-SeOH), which is reduced to the selenol by two equivalents of glutathione (GSH) through a selenenyl sulfide intermediate (GPx-SeSR). These intermediates have been characterized experimentally by ^{77}Se NMR spectroscopy except for GPx-SeOH, which air-oxidizes to the seleninic acid (GPx-SeO_2H) during crystallization.[88,89] In contrast, the covalent Se–N bond of the selenenamide functionality of **1** requires catalytic pathways more complex than the simple three-step mechanism of GPx.[39] The Se-N bond and the close proximity of highly-conserved nitrogen-containing amino acids to SeCys in GPx,[13,14,15,87] and the semisynthetic protein selenosubtilisin,[89] led to the development of a number of synthetic GPx mimics incorporating bonding and non-bonding Se···N,O interactions (e.g., cyclic selenenamides,[75] diaryl diselenides,[15] cyclic seleninates[76] and selenuranes[90,91]).

Based on experimentally observed intermediates and products, several pathways (compiled in Scheme 2) have been suggested for ROS-scavenging by **1**.[15] Daiber et al. found that the reaction of **1** with glutathione and peroxynitrite was difficult to monitor under physiological conditions because there were too many reactions and multi-equilibria systems to follow experimentally.[22] In vitro experiments by various groups have attempted to identify the pathways favored by **1**.[22,39-44] When thiols are abundant, as under normal cellular conditions, **1** is converted to **2**, but generation of selenol (**4**) for

Scheme 4. Proposed pathways for the catalytic activity of ebselen based on different experimental conditions.

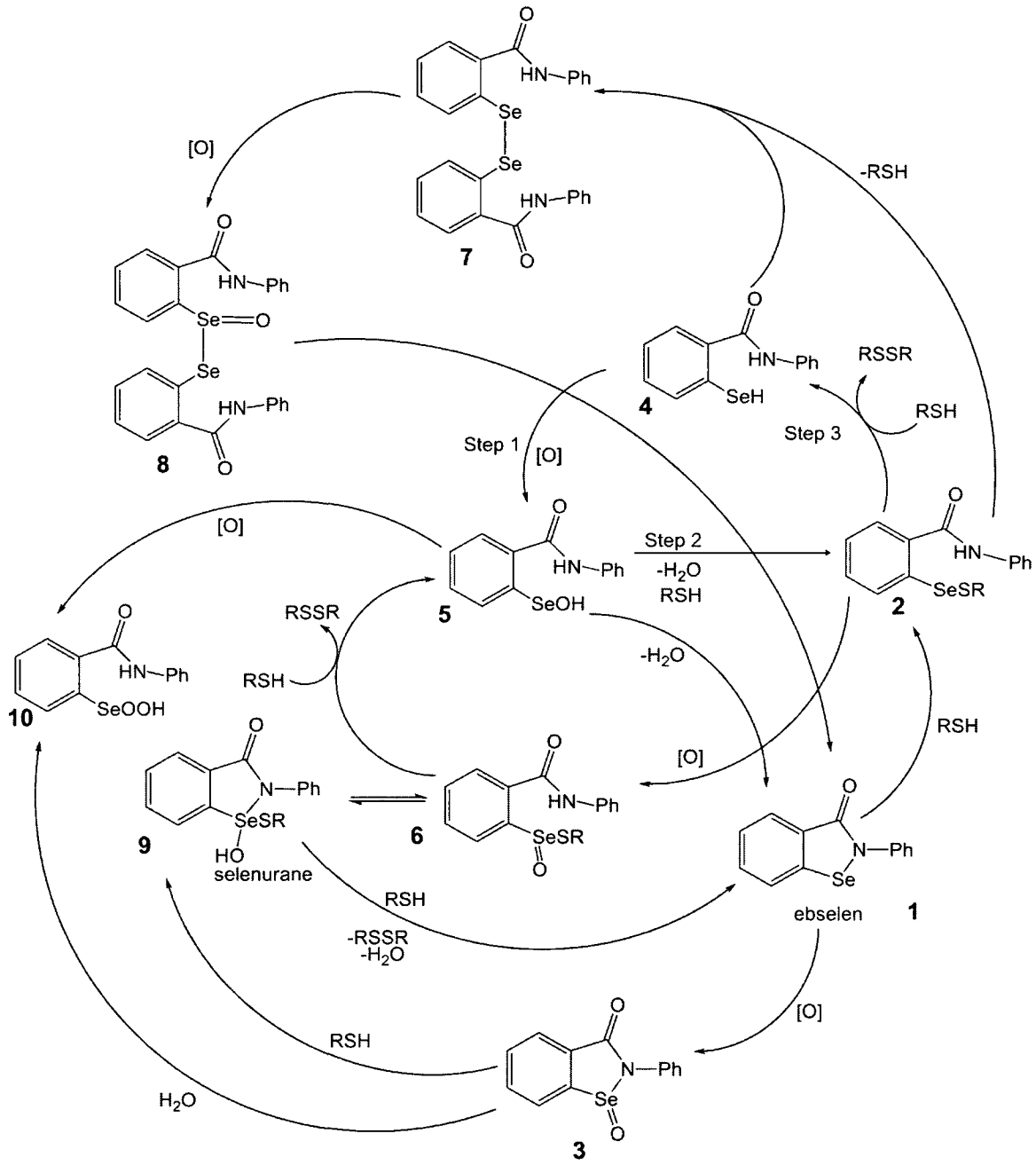

catalysis through a GPx-like cycle is hindered by the thiol-exchange reaction, limiting the capacity for ROS scavenging.[43] Intermediate **2** may slowly disproportionate to **7**, which acts as an scavenger by reacting with H_2O_2, producing the corresponding selenenamide (**1**) and seleninic acid (**10**).[87] According to Sarma and Mugesh, the reaction of **1** with H_2O_2 gives an unstable selenoxide (**3**), which then undergoes hydrolysis to seleninic acid (**10**).[44] Treatment of **10** with insufficient thiols yield ebselen, and excess thiols produce selenenyl sulfide (**2**).[92] The reaction of **3** with thiols produce ebselen and Fischer and Dereu suggested that either selenoxide selenenyl sulfide (**6**) or selenurane (**9**) is an intermediate in this step, but neither were detected by NMR spectroscopy.[39]

Although various groups have used DFT to model individual steps of the ebselen mechanism,[87,93-95] a comprehensive analysis of the full mechanism was yet to be reported. The challenge to quantum-chemical modeling of the catalytic cycle of **1** is how to represent proton transfer inherent to aqueous phase chemistry using gas-phase DFT methods. In the aqueous phase, protons are transferred with the assistance of the bulk solvent molecules, which act as mild acid/base catalysts. Gas-phase models using direct proton transfer result in strained transition states with unrealistically high activation energies. These high barriers are inherent to direct proton exchange, and cannot be remedied by solvation corrections that seek to reproduce the non-bonding effects of solvation. To approximate the role of water molecules in solution-phase proton-transfer processes, our group[45,96,97] and others[98-102] have included clusters of explicit water molecules in the gas-phase model to provide an indirect pathway for proton exchange. We have referred to this microsolvation technique as solvent assisted proton exchange (SAPE) in order to distinguish it from other methods of explicit solvation. Our group

have used SAPE to obtain realistic activation barriers for the GPx-like cycle of PhSeH,[45,94,96,97] which is comparable to the limited experimental data and DFT models of the truncated GPX active site of Morokuma et al.[103] Additionally, the barrier obtained by SAPE modeling of the ebselen oxidation, an important reaction in the scavenging of ROS/RNS, correlates to the experimental rate constant obtained for the reaction.[41]

Theoretical methods

The SAPE microsolvation models were designed based upon assumptions about how the molecular system reacts in solution. In creating a reactant complex, reacting molecules are possible relative to one another based upon the type of reaction with water molecules added to bridge the proton to the atom to which it is transferred in the product. For example, reactant complexes for S_N2-type nucleophilic attacks were obtained by orienting the nucleophile opposite the leaving group with waters added to facilitate proton transfer. SAPE models include the minimum number of solvent molecules required to connect the heavy atom proton donor and acceptor by a hydrogen-bonding network to provide a pathway for indirect proton exchange. Limiting the number of explicit solvent molecules reduces the computational effort needed to scan the reaction pathways. Although these reactions are likely to be stepwise processes in solution-phase, SAPE-derived reaction pathways are necessarily concerted as proton exchange is simultaneous with heavy atom bond breaking/forming. Also, the limited number of solvent molecules cannot adequately delocalize the proton charge to allow for a charge-separated intermediate. Additional solvent molecules are expected to similarly stabilize the charge-separated intermediate, but would require extensive conformation searches to find the global minimum within the system constraints. The smaller number of water

molecules used in our SAPE models allows for manual analysis of the conformations at the expense of a concerted pathway. However, a concerted transition state derived from SAPE modeling is expected to be an upper bound to the activation barrier of the rate-determining step of the stepwise mechanism. Few bonds are broken/formed at once in a stepwise mechanism, whereas the same bonds are broken simultaneously in a concerted mechanism.

DFT geometry optimizations and frequency calculations were performed using Gaussian 03[65] and the mPW1PW91[64] xc functional. DFT methods with 20-25% HF exchange provide activation barriers of the aqueous phase reactions of selenium compounds, similar to post-HF ab initio methods (MP2 and CCSD).[45] Pure functional tend to underestimate these activation barriers. Hybrid functionals with greater percentages of Hartree-Fock exchange overestimate the activation barriers for the reduction of methyl selenenic acid by thiols, and for the epoxidation of alkenes by H_2O_2.[102] The mPW1PW91 exchange correlation functional provided the best agreement with the post-HF methods of the tested functionals without the underestimation of the hydrogen-bonding interactions that are common for the popular B3LYP functional.[45] Models of the oxidation of MeSeH by MeOOH using a two-water SAPE network suggest that SAPE-derived activation parameters are sensitive to the admixtures of HF exchange.[45] The Ermler-Christiansen relativistic effective core potential (RECP) basis set,[104] with a set of s, p and d diffuse functions, was used for the Se atom. The Wadt-Hay RECP basis set,[105] augmented with a set of diffuse functions, was used for sulfur. Hydrogen centers involved in the SAPE network or bonded to a heteroatom were assigned Dunning's split-valence triple-ζ basis set with polarization functions (TZVP).[106]

All other hydrogens and the carbon atoms were assigned double-ζ basis set with polarization functions (i.e., d95*).[107] Transition states were confirmed as having one imaginary vibrational mode, consistent with motion along the appropriate coordinates of the atoms involved in the reaction. Solvation effects have been included using the polarizable continuum model (PCM)[108] (water ε = 78.39) for the optimized reactants, transition states, products and intermediate complexes. The ^{77}Se NMR chemical shifts were calculated using the gauge-invariant atomic orbital (GIAO) method[109] for intermediates **1** through **10**, using methods and basis sets previously described.[110,111]

Results and discussion

SAPE modeling of the catalytic reduction of ROS by ebselen using MeOOH and MeSH as the model oxidant and reductant is discussed in three sections: (a) initial oxidation and reduction of **1**, (b) the GPx-like cycle, and, (c) pathways under conditions of oxidative stress (Scheme 2). Although several groups[39,40,112] have suggested the diselenide **8** as an intermediate in the catalytic cycle, we have excluded it from our study because its formation is slow,[83] because it is second-order in selenium. Diselenides are also unlikely to occur in high concentrations in vivo due to the high concentration of nucleophiles.[113] Stationary state reactant, intermediate, transition state, and product complexes are indicated by R, RI, TS, and P respectively (Figures 1-12). For example, **1→2$_R$** represents the reactant complex in the reaction step **1→2**. GIAO-DFT ^{77}Se chemical shifts were calculated for the isolated compounds **1** through **10**, and are provided in Table 1 with available experimental values.

Ebselen oxidation versus reduction. In vivo, **1** may be reduced by thiols to selenenyl sulfide **2** or oxidized to selenoxide **3** depending upon the relative concentrations of thiol and ROS. The reaction with thiol is considered the preferred pathway under normal cellular conditions, because ebselen reacts rapidly with GSH and other thiols to form **2**,[40,114] even at -70°C.[39] When **1** is administered intravenously, more than 90% of the compound is bound to the cysteine thiols of serum albumin.[115] Under conditions of oxidative stess, **1** may be preferentially oxidized to the selenoxide **3** as observed by Fischer and Dereu[39] for the reaction of **1** with H_2O_2. However, recent studies by Mugesh suggest that the oxide is unstable and undergoes hydrolysis to selenenic acid **5**.[44] However, when **1** reacts with a 1:1 mixture of thiol and peroxynitrite, the major product is **2** with only small amount of **3** observed.[22]

The "normal" pathway **1**→**2** was modeled using a three-water SAPE network to connect the thiol proton to the selenenamide nitrogen. From this reactant complex **1**→$\mathbf{2_R}$ (Figure 3), the reaction pathway was mapped by following the S-H bond breaking coordinate. This process was continued until the thiol proton was relayed through the SAPE network to the selenenamide nitrogen resulting in the ring opening, and the formation of the product **1**→$\mathbf{2_P}$. The TS **1**→$\mathbf{2_{TS}}$ was found when the Se-S bond has decreased by 0.36 Å and Se-N distance has increased by 0.17 Å (Figure 3). The low activation barrier for **1**→**2** ($\Delta G^{\ddagger}$= 8.4 kcal/mol) relative to the reported SAPE activation barrier for step **1**→**3** (17.8 kcal/mol)[94] is consistent with the product distribution of **1** in the presence of thiols and peroxides, and the requirement of a substantial excess of oxidant for formation of **3**. Following the reaction coordinate to **1**→$\mathbf{2_P}$ produces the selenenyl sulfide **2** with a weak Se···N donor-acceptor interaction (2.93 Å) between the

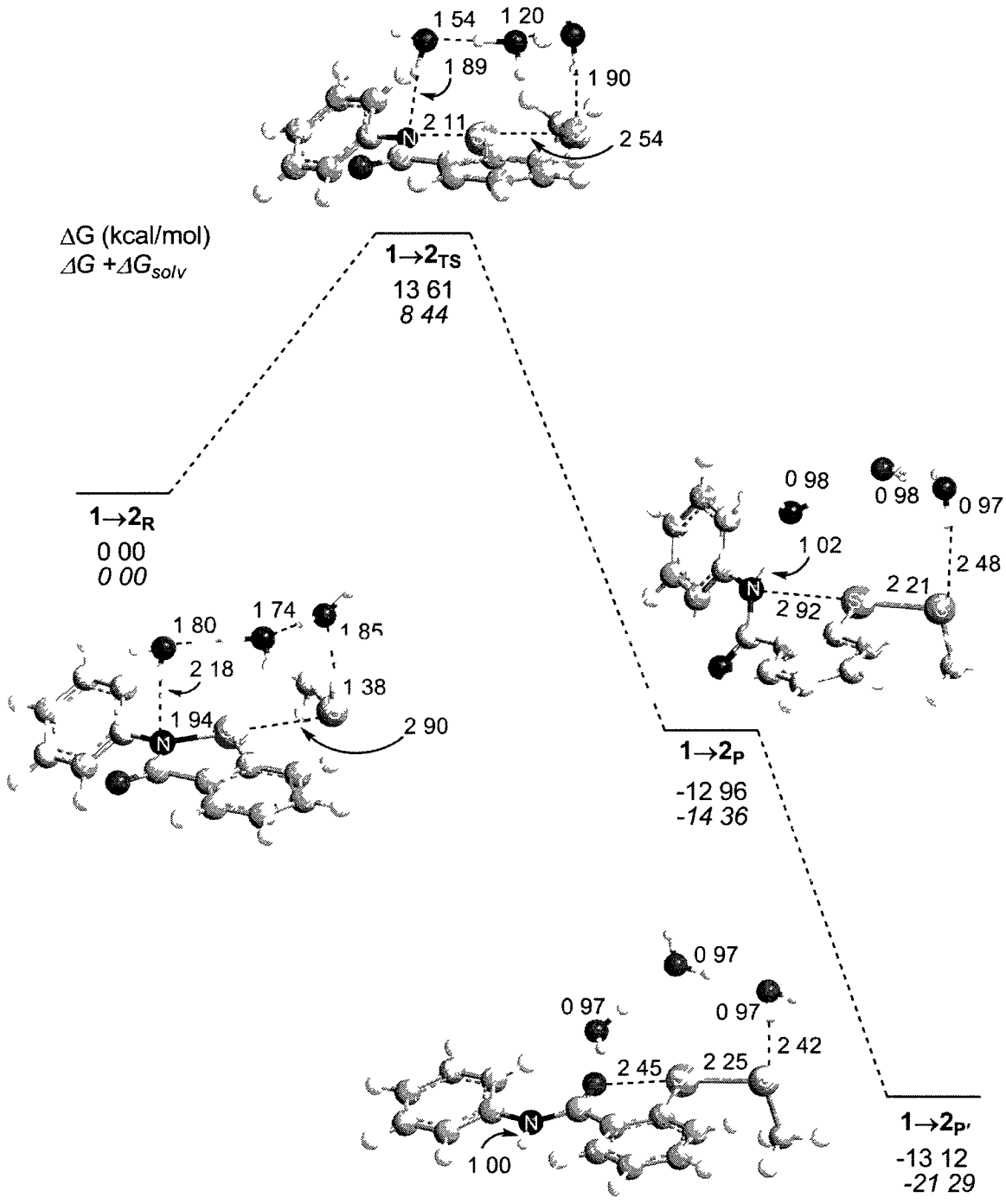

Figure 3. Reaction of **1** (ebselen) and MeSH with three water molecules in the SAPE network showing the R, TS, P and alternate product P'.

amide and the Se-S bond (Figure 3). Our previous study of the relative strengths of Se···N,O interactions with amides showed that the Se···O interaction with the carbonyl oxygen is stronger than the Se···N interaction, due to weak Lewis basicity of the amide nitrogen group.[116] Gas-phase NBO calculations on conformers of **2** show that the structure with an Se···O interaction ($\mathbf{2_O}$) is 3.6 kcal/mol lower than that with an Se···N interaction ($\mathbf{2_N}$). The Se···O distance for $\mathbf{2_O}$ is also substantially shorter than the Se···N distance for $\mathbf{2_N}$ (2.52 versus 3.01 Å), with comparable relative donor-acceptor energies $\Delta E_{d\rightarrow a}$ (14.0 versus 2.1 kcal/mol). An alternate geometry of the product complex ($\mathbf{1\rightarrow 2_{P'}}$) incorporating the stronger Se···O interaction is 6.9 kcal/mol more stable than $\mathbf{1\rightarrow 2_P}$ (ΔG=-21.3 kcal/mol).

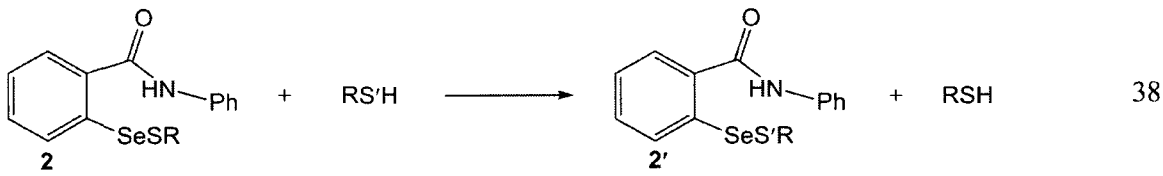

38

GPx-like cycle. If ebselen scavenges ROS through a GPx-like cycle, **1** is a procatalyst activated by reduction to **2**. In analogy to the cycle in Scheme 1, this selenenyl sulfide is reduced by thiol to **4**, which is oxidized to **5** by ROS. Reduction of this selenenic acid by a second equivalent of thiol regenerates **2**. Experimental data and theoretical calculations suggest that the reduction of the selenenyl sulfide **2**→**4** is the rate determining step.[103] Bhabak and Mugesh have proposed that thiol exchange (eq 38) competes with this step and explains the relatively low GPx-like activity of **1**.[43] The Se···O intramolecular interaction in **2** ($\Delta E_{d\rightarrow a}$ = 14.0, 19.0 (DFT(B3LYP)/6-31G*)[43] kcal/mol; d(Se-O) = 2.52, 2.47 Å[43] (DFT(B3LYP)/6-31G*)) increases the partial negative

charge at the sulfur center to favor nucleophilic attack on Se.[43] Bhabak and Mugesh have shown that tert-amide based diselenides are 10-20 times more effective than sec-amide-based diselenides (i.e., **8**), because steric interactions between the amide $-NR_2$ group and the phenyl ring prevent the strong intramolecular Se···O interactions.[92] In contrast, in our SAPE study of the GPx-like cycle of aryl selenols, we showed that weak Se···N,O interactions could be easily displaced in order for the reaction to proceed.[117] Thiol exchange is not observed for dithiols such as dihydrolipoic acid, in which the formation of **3** is not the rate-determining step because the reaction is unimolecular, and the steric factors favor attack at the sulfur.[40]

The SAPE model for reaction **2**→**4** was based upon our previous results for the selenol regeneration step in the GPx-like cycle of benzeneselenol.[97] In the reactant complex **2**→$\mathbf{4_R}$ (Figure 4), a three-water network was used to facilitate proton exchange from the thiol to the selenium center of **2**.[97] The S···S interaction (d(S-S = 3.83 Å) between MeSH and **2** in **2**→$\mathbf{4_R}$ is weak, due to the high sulfur charge induced by the strong Se···O interaction. Displacement of the amide carbonyl from the selenium in intermediate complex **2**→$\mathbf{4_{RI}}$ requires 7.7 kcal/mol, but reduces q_S for **2** by 0.30e (APT) to allow for a stronger S···S interaction (d(S-S = 3.45 Å). The structure of **2**→$\mathbf{4_{TS}}$ and its barrier calculated from **2**→$\mathbf{4_{RI}}$ (23.1 kcal/mol) is comparable to the analogous step for PhSeH (21.7 kcal/mol).[97] Calculated from **2**→$\mathbf{4_R}$, the high activation barrier (30.8 kcal/mol) is consistent with the slow rate of conversion by sec-amide GPx mimics due to competition with thiol exchange.[43,92] The product complex (**2**→$\mathbf{4_P}$) mapped from the TS has the carbonyl oxygen involved in hydrogen bonding instead of interacting with Se. Rotating about the C–Se bond axis to form an Se···O interaction with the selenol of **4**

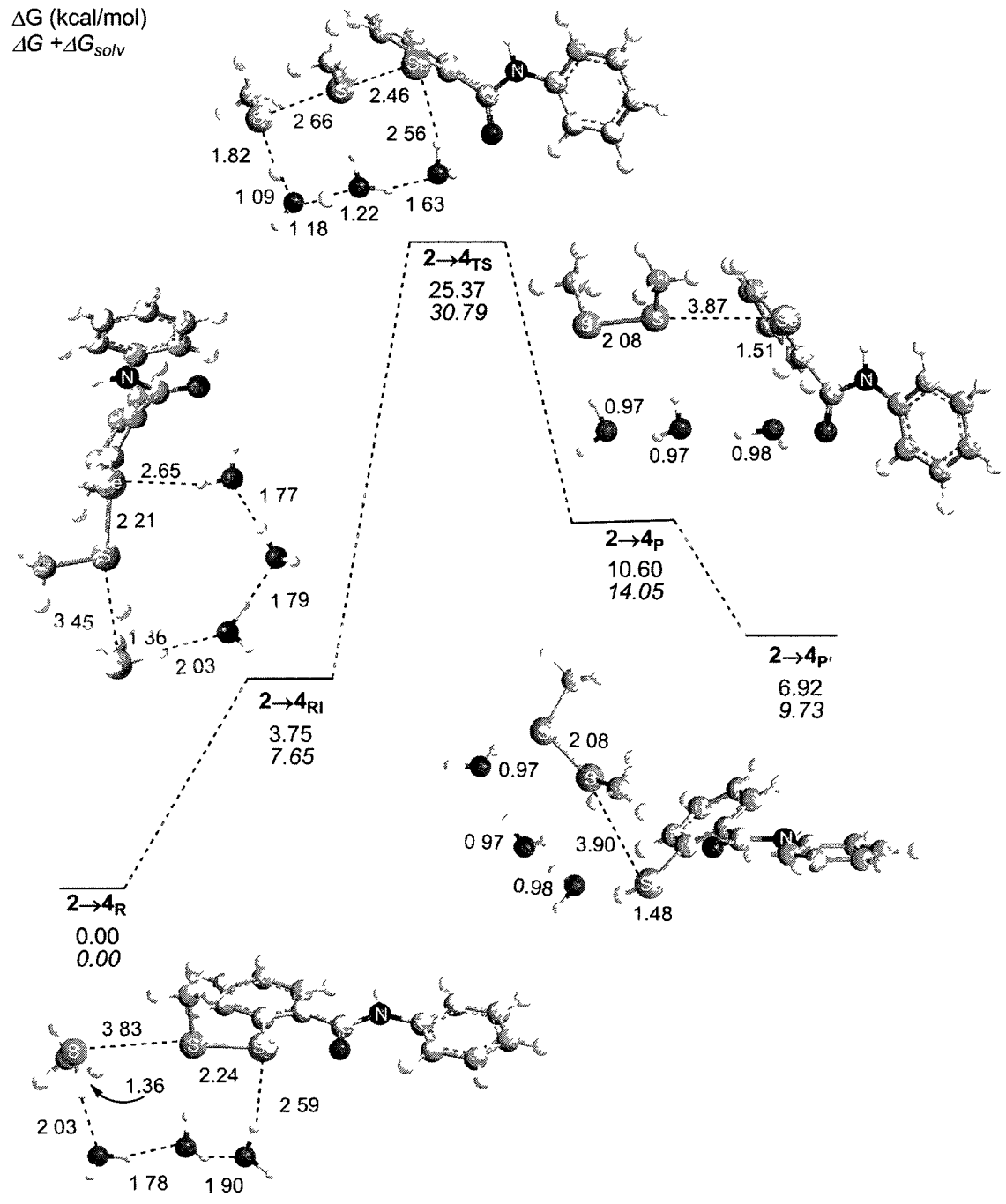

Figure 4. Reaction of **2** and MeSH with three water molecules in the SAPE network showing the R, RI, TS, P and alternate product (P').

provides a more stable geometry **2→4P'** (-4.3kcal.mol relative to **2→4P**) for an overall endergonic reaction (ΔG=9.7 kcal/mol).

Under the GPx-like mechanism, available oxidants will convert selenol **4** to the selenenic acid **5**. This reaction was modeled using a two-water SAPE network similar to the analogous step in our previous study of the PhSeH (Figure 5).[97] In the reactant complex **4→5R**, the MeOOH proton hydrogen bonds to the amide carbonyl, anchoring the oxidant close to the selenium center (dSe-O = 3.73 Å). From this complex, the transition state (**4→5TS**) is formed at the point where the Se-O distance is decreased by 1.63 Å and O-O distance increased by 0.52 Å. The imaginary frequency (260i cm^{-1}) corresponds to the appropriate bond breaking/forming coordinates, with Se-OH bond forming contributing the most character to the mode. The calculated barrier ($\Delta G^{\ddagger}+\Delta G_{sol}$ =12.8 kcal/mol) is lower than that for the PhSeOH (19.1 kcal/mol)[97] due to the increased solvation of the TS in the ebselen intermediate ($\Delta G^{\ddagger}_{sol}$ = 9.9 kcal/mol). The barrier height for this step is in agreement with the relative experimental rate constants for the oxidation of other ebselen intermediates (**1** (0.29 $mM^{-1}min^{-1}$), **2** (<0.01$mM^{-1}min^{-1}$) and **4** (2.8 $mM^{-1}min^{-1}$) with H_2O_2).[41] Our SAPE TS for the selenol would be an upper bound to the solution phase value, considering that the computational pK_a calculations by Ali et al. on the GPx protein showed that the selenolate ion, rather than the selenol form, is more reactive towards hydrogen peroxide (pK_a of SeH=4.30).[118] The overall reaction is exothermic (ΔH=-65.4 kcal/mol), forming the product complex **4→5P** with the selenenic acid stabilized by an Se···O interaction (2.35Å). Selenenic acids are generally unstable, and are rapidly reduced to selenenyl sulfides (**5→2**) or oxidized to seleninic acids (**5→10**), as shown by Goto et al. for a sterically hindered stable selenenic acid.[119] Thiol

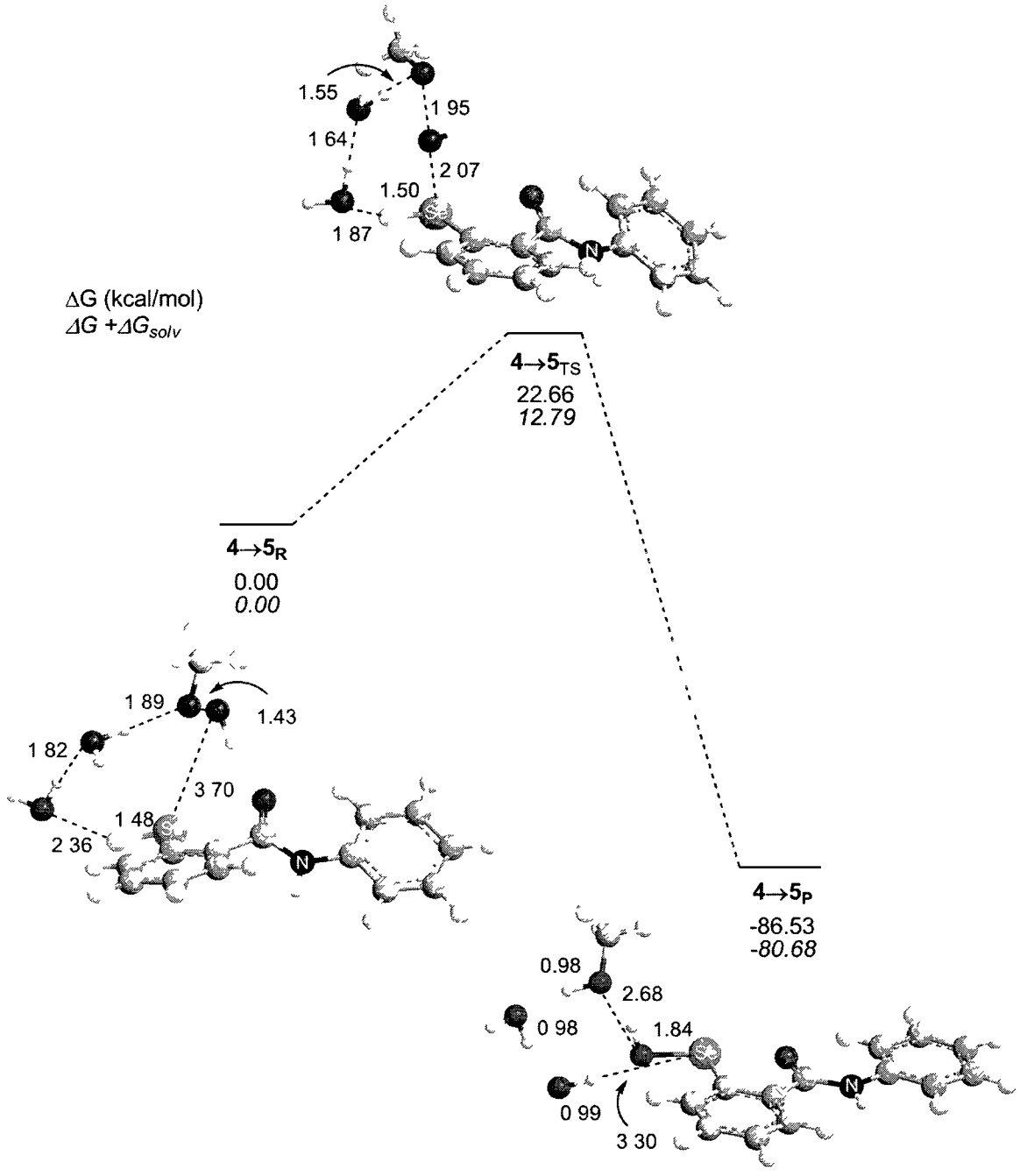

Figure 5. Reaction of **4** and MeOOH with two water molecules in the SAPE network showing the R, TS and P.

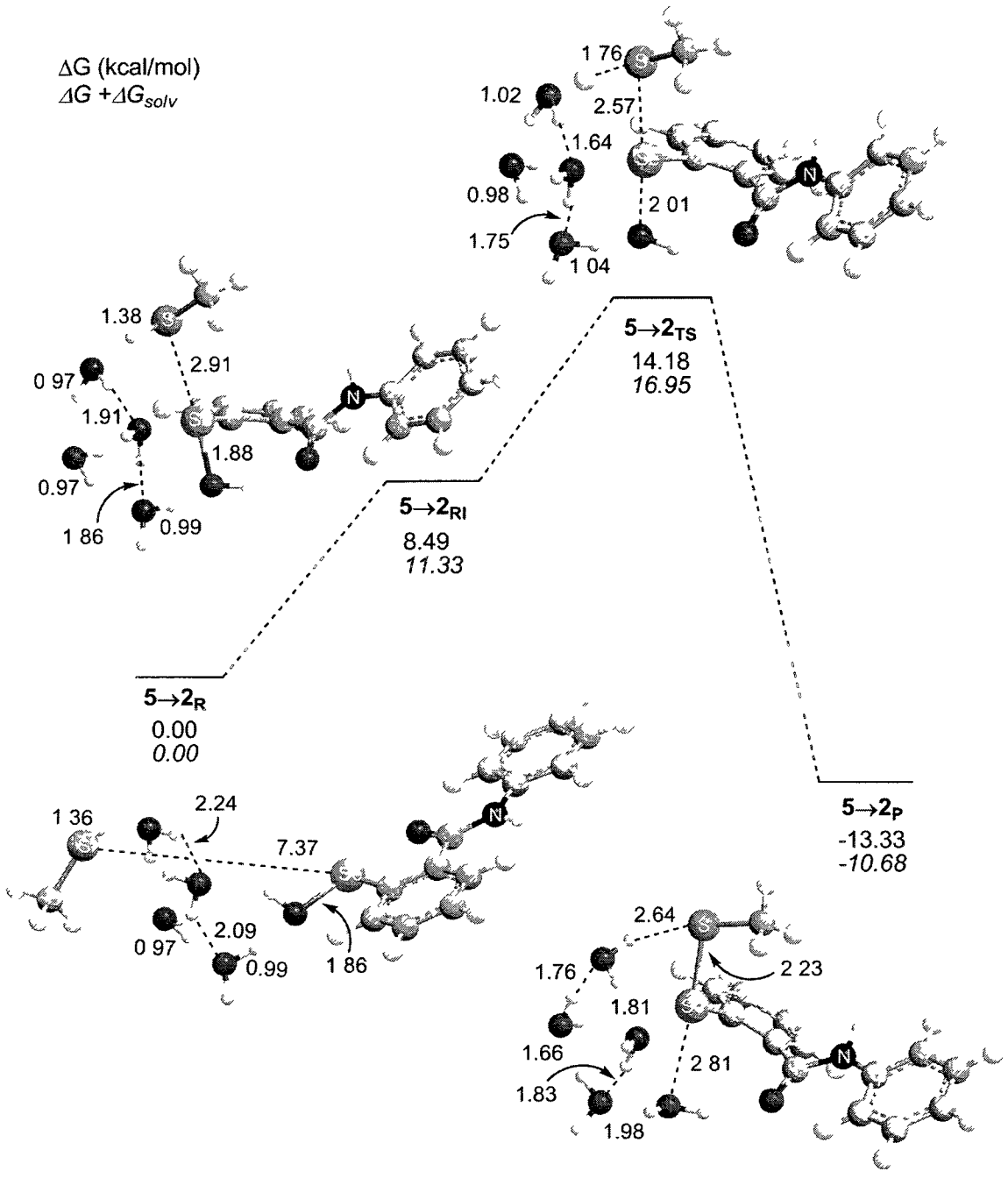

Figure 6. Reaction of **5** and MeSH with four water molecules in the SAPE network showing the R, RI, TS and P.

reduction of ebselen selenenic acid (**5**→**2**) completes the GPx-like cycle and was modeled as an S_N2-type backside attack of the thiol on Se to eliminate H_2O. Models of the analogous step in PhSeH showed that a square, four-water SAPE network gave a better approach of the nucleophile, resulting in a lower energy than a simpler two-water network.[97] The reactant complex **5**→$\mathbf{2_R}$ (Figure 6) constructed from the lowest conformation **5** has an Se···O interaction donating into the Se-OH bond, which must be replaced by the thiol in order for the reaction to proceed via a backside attack. An intermediate complex **5**→$\mathbf{2_{RI}}$ (Figure 6) with the thiol interacting with the selenium, and the amide carbonyl hydrogen-bonding to the SeOH proton is 11.3 kcal/mol higher than **5**→$\mathbf{2_R}$. From **5**→$\mathbf{2_{RI}}$, the S-H bond-breaking coordinate was followed to relay the thiol proton through the SAPE network to the leaving –OH group and form **5**→$\mathbf{2_P}$ (ΔG = -10.7 kcal/mol). The barrier calculated from **5**→$\mathbf{2_{RI}}$ ($\Delta G^{\ddagger}$=5.6 kcal/mol) is comparable to the value calculated for the conversion of PhSeOH to PhSeSMe ($\Delta G^{\ddagger}$=6.6 kcal/mol),[97] with an overall higher barrier ($\Delta G^{\ddagger}$=14.6 kcal/mol) due to stabilization of the selenenic acid by the Se···O interaction. This moderate barrier is consistent with the rapid reaction of **5** in the presence of thiols.[44]

Experimental studies by Bhabak and Mugesh have shown that cyclic selenenamides and seleninic acids are the major products of the H_2O_2–oxidation of **7** and related sec-amide-based diselenides.[87] In contrast to the tert-amide analogues, which are oxidized to selenenic acids and seleninic acids, the availability of the –NHR group allows cyclization of sec-amide-based selenenic acids. Fisher and Dereu have suggested that this pathway for selenenamide formation may be favorable for ebselen and GPx in the absence of reducing thiols.[39] Ebselen seleninic acid **10** may also be converted to **1** in the

presence of low thiol concentration through the formation of **5** as an intermediate.[44] Similarly, Mugesh et al. have shown that **1** is a product of selenoxide elimination from the *Se*-arylselenocysteine **11** (eq 39).[44]

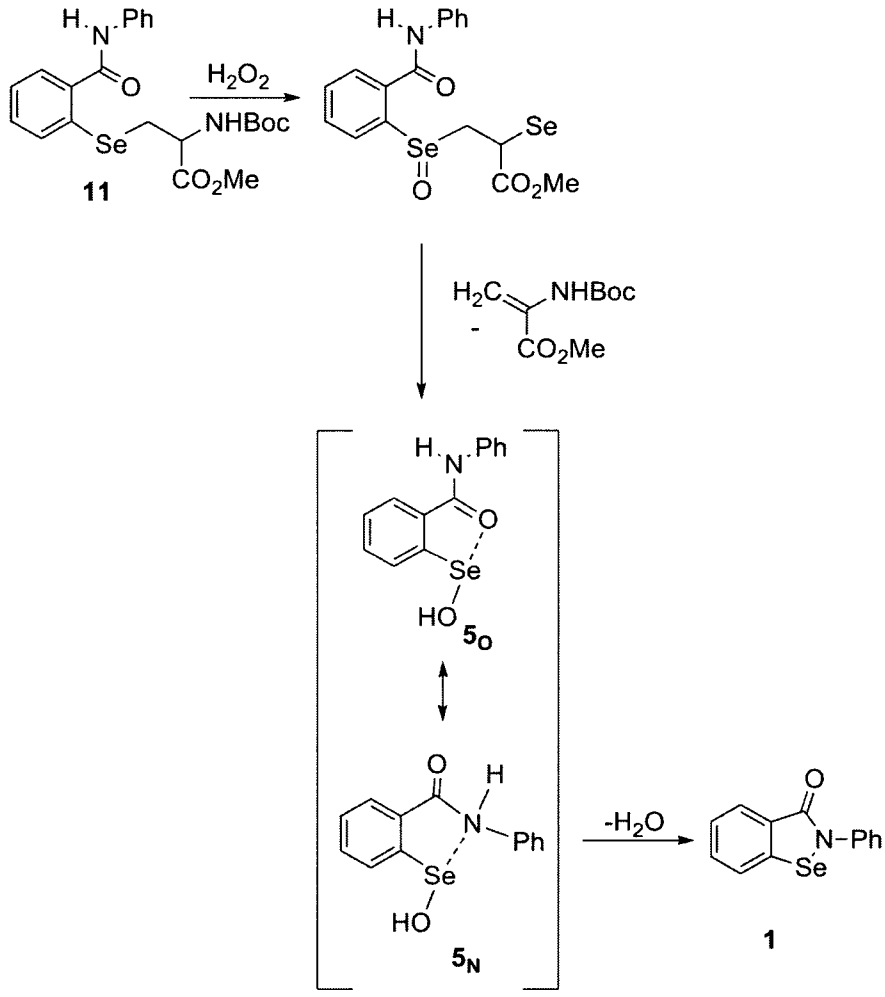

39

For step **5**→**1**, the most stable conformer of selenenic acid ($\mathbf{5_O}$) has an Se···O interaction, but the dehydration pathway likely proceeds through the Se···N conformer ($\mathbf{5_N}$). The conformer $\mathbf{5_O}$ is stabilized by 8.4 kcal/mol in comparison to $\mathbf{5_N}$ and the donor acceptor energies for $\mathbf{5_O}$ (23.2 kcal/mol) and $\mathbf{5_N}$ (3.5 kcal/mol) are higher than that for the

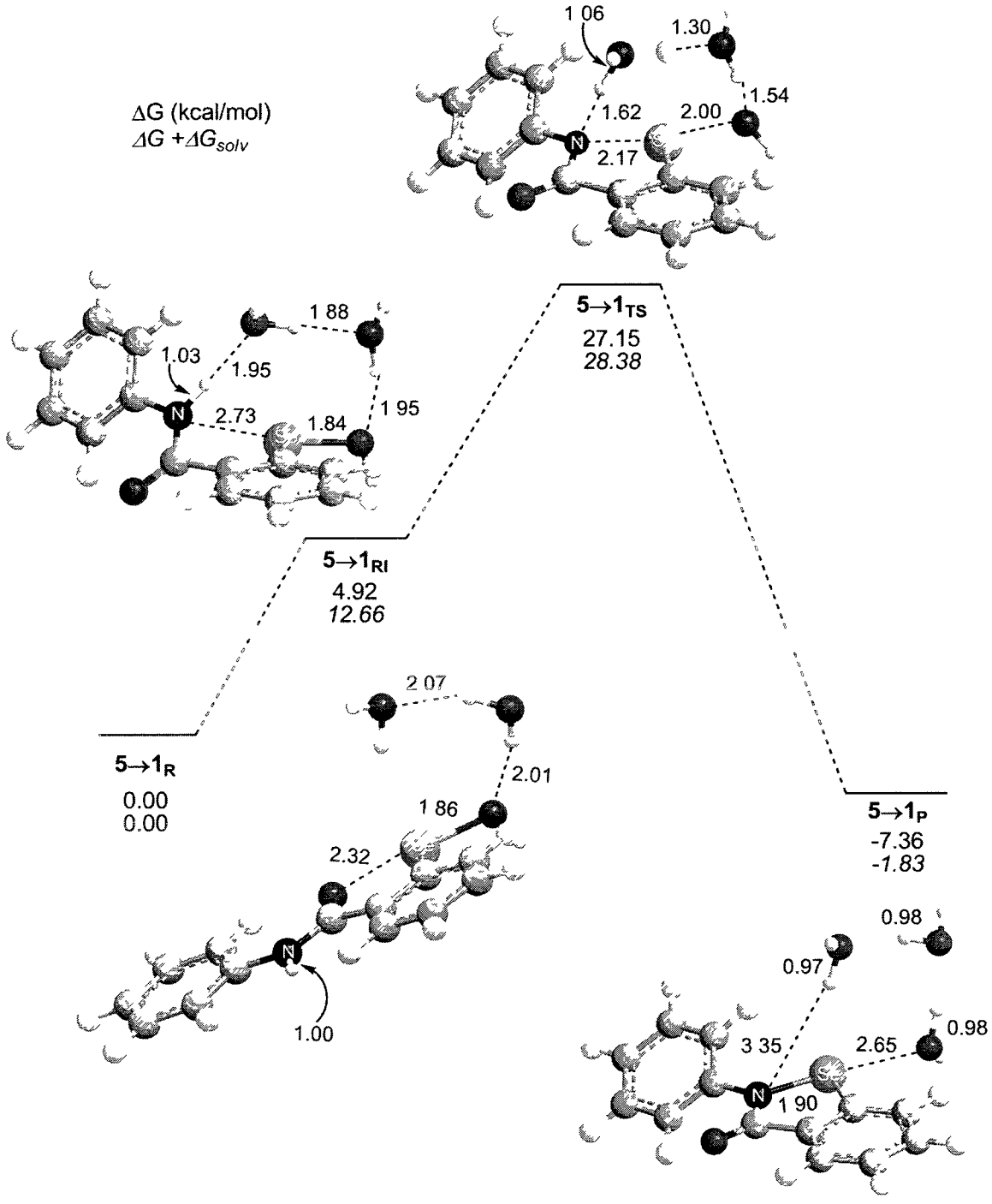

Figure 7. Dehydration reaction of **5** to **1** with two water molecules in the SAPE network showing the R, RI, TS and P.

corresponding conformers of **2** ($\Delta E_{d\rightarrow a}$=14.0 for $\mathbf{2_O}$ vs 2.1 kcal/mol for $\mathbf{2_N}$). In order to obtain the reactant complex $\mathbf{5\rightarrow 1_R}$, a two-water SAPE network is added to $\mathbf{5_O}$ that is hydrogen bonded to the selenenic acid oxygen and the carbonyl oxygen (Figure 7). The conversion energy for $\mathbf{5\rightarrow 1_R}$ to $\mathbf{5\rightarrow 1_{RI}}$ is 12.7 kcal/mol is higher than that for $\mathbf{2\rightarrow 4_R}$ to $\mathbf{2\rightarrow 4_{RI}}$ (7.7 kcal/mol), which is in accordance to the donor-acceptor energies. At the TS ($\Delta G^{\ddagger}$=28.4 kcal/mol), the imaginary frequency corresponds to the formation of the Se-N bond and the breaking of the Se-OH bond. Schewe suggested that **1** is thermodynamically stable relative to its derivatives, due to the energetically-favored five-membered ring.[17] The step **5→2** discussed earlier is a low barrier reaction ($\Delta G^{\ddagger}$=16.9 kcal/mol) in comparison to the ebselen formation (**5→1,** ΔG=-1.8 kcal/mol), suggesting that the ring formation may occur only in the absence of sufficient thiols.

To compare the overoxidation of **5** to other possible reactions of the selenenic acid (**5→1** and **5→2**), the reaction **5→10** was modeled as an oxygen-atom transfer from MeOOH facilitated by a two-water network (Figure 8). From $\mathbf{5\rightarrow 10_R}$, the attacking oxygen approaches selenium perpendicularly to the Se-OH plane in the TS, and the activation barrier ($\Delta G^{\ddagger}$=18.5 kcal/mol) is comparable to that of the oxidation of **1**.[45] Step **5→10** is exergonic (ΔG=-44.2 kcal/mol), and the product complex $\mathbf{5\rightarrow 10_p}$ has an Se···O distance of 2.68 Å (2.46 Å for **10**)[44], this deviation is due to the hydrogen bonding interactions of the seleninic acid functional group with the SAPE network. Comparing the energetics of the competitive reactions that selenenic acid may undergo, the oxidation of **5** happens only in excess of peroxides and in the absence of sufficient thiols, otherwise **5→2** ($\Delta G^{\ddagger}$=16.9 kcal/mol) is highly favorable.

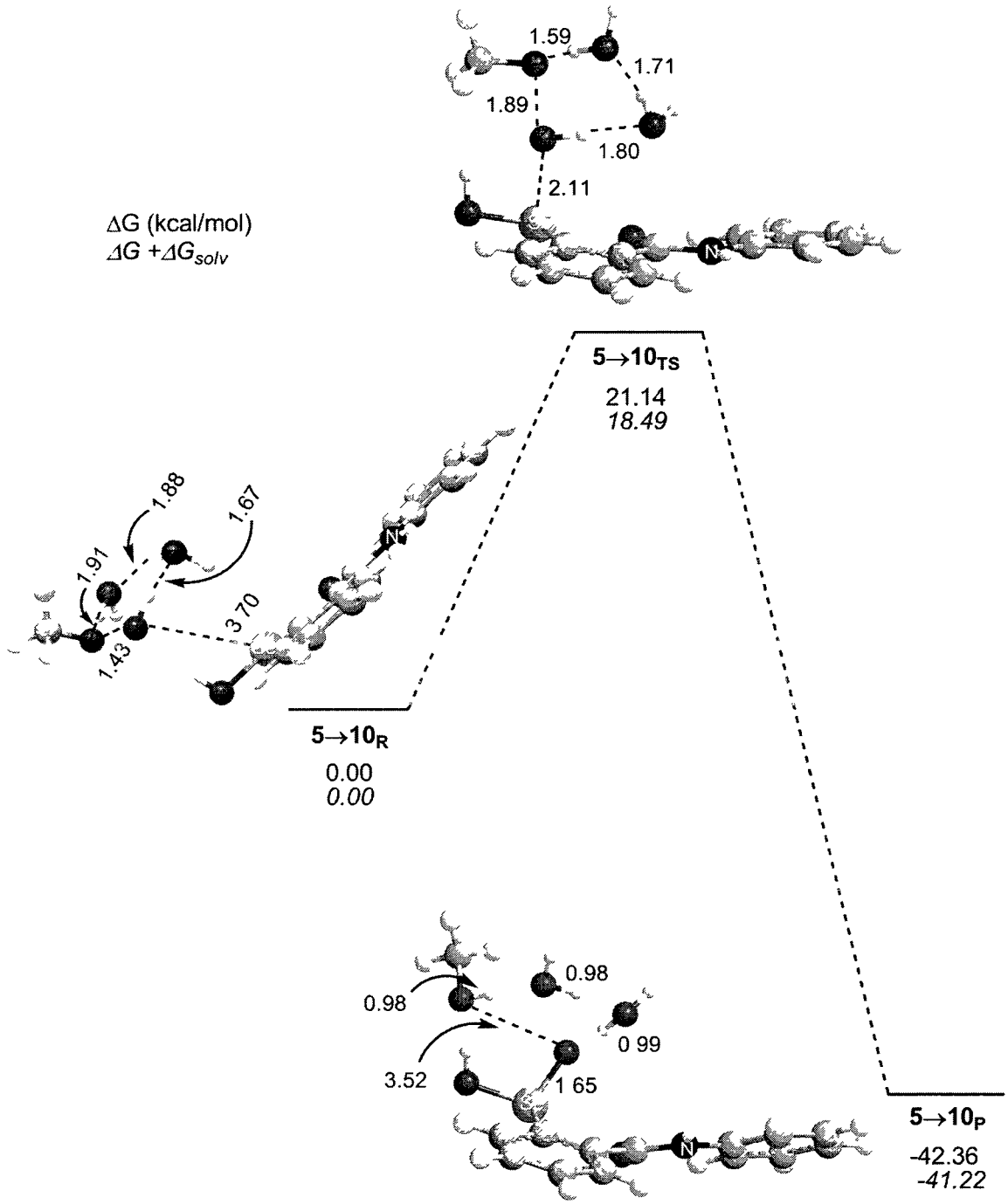

Figure 8. Oxidation of **5** to **10** with MeOOH and two water molecules in the SAPE network showing the R, TS, and P.

Pathways under conditions of oxidative stress. The activity of ebselen as an ROS scavenger in spite of the high barrier obtained for step **2**→**4** of the GPx-like cycle suggests that the molecule's antioxidant properties will be most effective under conditions of oxidative stress (e.g., $rate_{1\rightarrow3} > rate_{1\rightarrow2}$). Fischer et al. showed that **1** is regenerated from **3** by two equivalents of thiol.[39] Mechanistic pathways were proposed through either seleninyl sulfide **6** or the hypervalent selenurane **9**, but neither of these intermediates could be detected experimentally.[39] Thiol can easily attack the Se (IV) center of **3** to either reduce the selenoxide to **6** or form **9** without ring opening. The intermediates react with a second equivalent of thiol to form the selenenic acid **5** or regenerate **1** directly. Models of these pathways are based on our previous SAPE study of the reduction of methyl- and benzeneseleninic acid[96] to the selenenic acid **15** by two possible pathways: through seleninyl sulfide intermediate **13**, or by thiol addition to

Scheme 5. Mechanism used for DFT-SAPE modeling of the thiol reduction of a seleninic acid.

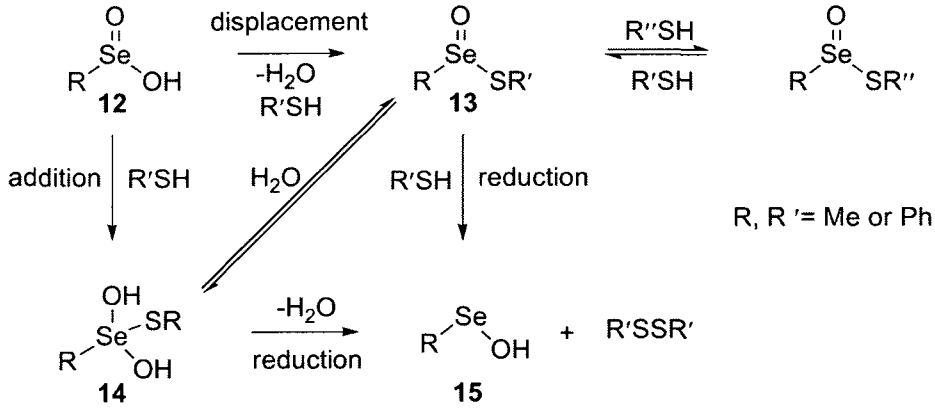

selenurane intermediate **14** (Scheme 5). The results from this study suggest that the first step of the reduction produces **14**, which interconverts to **13** prior to subsequent reduction with thiol, which generates **15**. The models for these steps have been adapted for the thiol-reduction of ebselen selenoxide **3** forming **6** (analogous to **13**) or **9** (analogous to **14**).

Thioselenurane formation from the selenoxide **3→9** was modeled as a thiol addition using a two-water SAPE network to direct the proton to the cis oxo group (Figure 9). At the TS **3→9$_{TS}$** ($\Delta G^{\ddagger}$ = 7.3 kcal/mol), the attacking thiol approached the central selenium with a simultaneous protonation of the oxide, leading to expansion of the selenium coordination sphere through Se-S bond formation ($\Delta d_{Se\text{-}S}$ = -0.52 Å relative to the reactant complex). In the related reaction of the seleninic acid (**12→14**),[96] the solvation-corrected Gibbs free energy of activation is similar to that of step **3→9,** despite a lower decrease in the Se-S distance (0.39 Å) progressing from R to TS. The above mentioned discrepancy in the bond distance in **12→14** and **3→9** are due to the difference in the basicity of the group attached to Se, trans to the attacking thiol. The selenurane in product complex **3→9$_P$** (ΔG=0.6 kcal/mol) formed by following the reaction coordinate from the TS is an unstable conformation with the -SMe group trans to the amide. However, the most electronegative groups of the three-center-four-electron bond of a hypervalent species like **9** should be trans (i.e., the amide and the hydroxyl).[120] Pseudorotation of the unstable **9'** conformation in **3→9$_P$** to **9** should be rapid.[121] The rearranged product complex **3→9$_{P'}$** was 3.6 kcal/mol more stable than **3→9$_P$**. The energy of the reaction (-3.0 kcal/mol) and the low activation barrier suggest that the presence of sufficient thiols keeps the reaction going forward instead of decomposing **9** back to **3**.

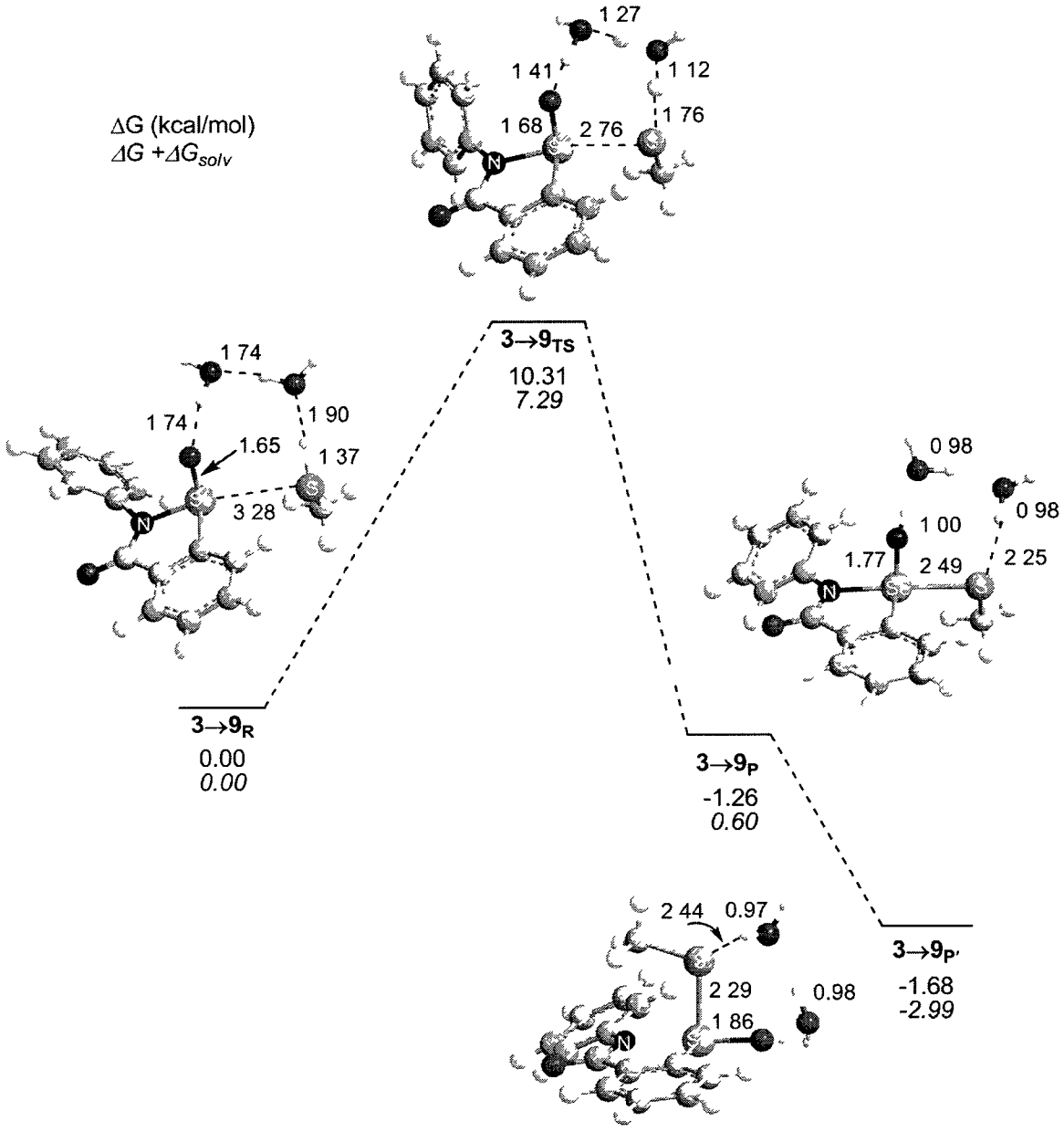

Figure 9. Reaction of **3** to **9** with two water molecules in the SAPE network showing the R, TS, P and alternate product P'.

The selenurane may be isomerized to seleninyl sulfide ($\Delta E_{6\rightarrow 9}$=-2.5 kcal/mol) by a ring opening process, resulting in a proton transfer from the –OH to the nitrogen of **9**. As our previous study showed that the interconversion energy between selenurane and seleninyl sulfide is very low,[96] we did not model this reaction.

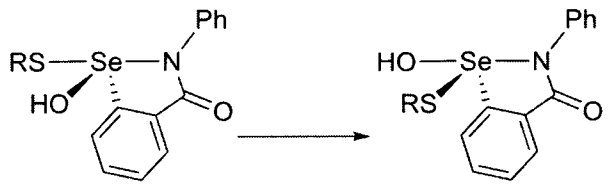

9′ **9**

Further reaction of **9** with thiol regenerates **1** through the elimination of disulfide and water. The SAPE model of **9**→**1** used a three-water network to bridge the thiol proton to the leaving –OH group. In the reactant complex **9**→$\mathbf{1_R}$, the sulfur of the attacking thiol is at a distance of 2.93 Å from the S attached to the selenium center and collinear to the Se-S bond (Figure 10). Although the Se (IV) center of **9** is positive (APT charge = 1.523 e), steric hindrance around this center and the more positive charge on S of **9** (APT charge = -0.169e vs -0.243e for **2**) allows for a nucleophilic attack at the sulfur. Comparing to reactant complex **2**→$\mathbf{4_R}$, the S-S distance is longer (3.83 Å) and the Se-S bond length is shorter (2.24 Å vs 2.34 Å in **9**→$\mathbf{1_R}$) than the corresponding distances in **9**→$\mathbf{1_R}$. At **9**→$\mathbf{1_{TS}}$ ($\Delta G^{\ddagger}$=6.5 kcal/mol), the Se-S bond length increased to 2.71 Å and the S-S distance decreased to 2.32 Å, whereas in **2**→$\mathbf{4_{TS}}$ these distances are 2.46 Å and 2.66 Å, respectively.

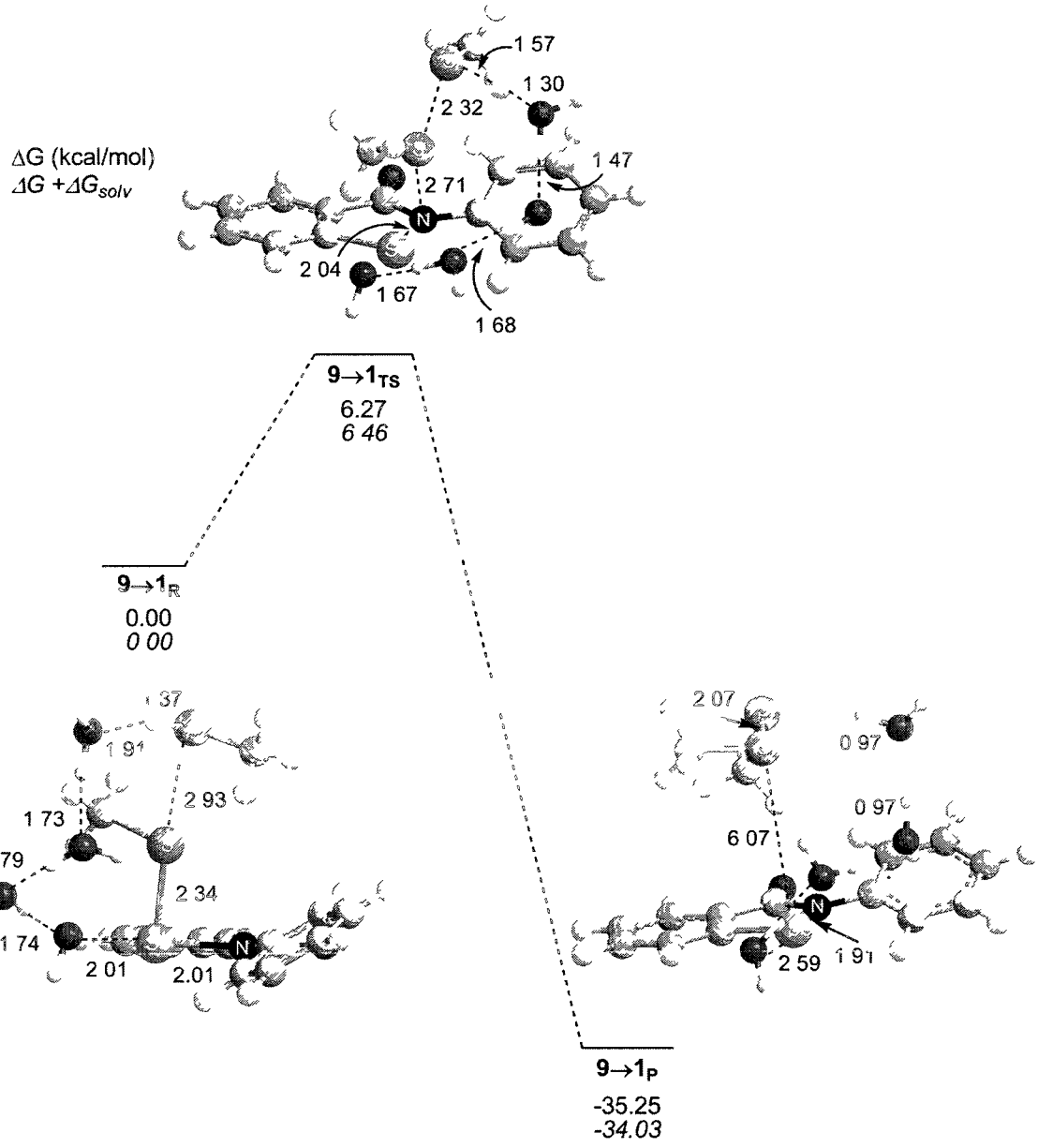

Figure 10. Reaction of **9** to **1** with three water molecules in the SAPE network showing the R, TS and P.

These differences in structural parameters in the reactant and TS complexes and the activation barriers are indicative of an early transition state in the case of **9**→**1** relative to **2**→**4**. The early transition state is also consistent with the exothermicity of **9**→**1**$_P$ (ΔG=-34.0 kcal/mol).

Thiol reduction of **3** was modeled as an S_N2-type attack, resulting in the breaking of Se-N bond, thereby forming **6**. The nucleophilic thiol approaches the selenium through the backside of –OH, the leaving group, with three water molecules in the SAPE network, similar to the conversion of methyl seleninic acid to **12**. In the case of **3**, the amide nitrogen is accessible for protonation through the plane perpendicular to that of the heterocyclic ring, where the =O group is absent (Figure 11). The activation barrier for **3**→**6**$_{TS}$ ($\Delta G^{\ddagger}$=9.2 kcal/mol) is comparable to that for selenurane formation, but it is lower than that for the methyl selenenyl sulfide (**11**) formation ($\Delta G^{\ddagger}$=20.5 kcal/mol).[96] The drastic reduction in the barrier for step **3**→**6** is gained through the solvation correction due to the positioning of the oxo group away from the water cluster. The subsequent step **6**→**5** (Figure 12) is based on the model **13**→**15**, and the barrier obtained is ($\Delta G^{\ddagger}$=18.4 kcal/mol) almost three times higher than that for **9**→**1**. In **6**→**5**, the presence of the Se···O interaction and the aromatic substituent on Se, instead of the methyl group in **13**, account for the higher activation barrier in comparison to **13**→**15** ($\Delta G^{\ddagger}$=15.8 kcal/mol). Since **6** is in equilibrium with **9**, and the conversion of **6**→**5** is a high-barrier reaction, the formation of **1** from **9** is more likely to happen.

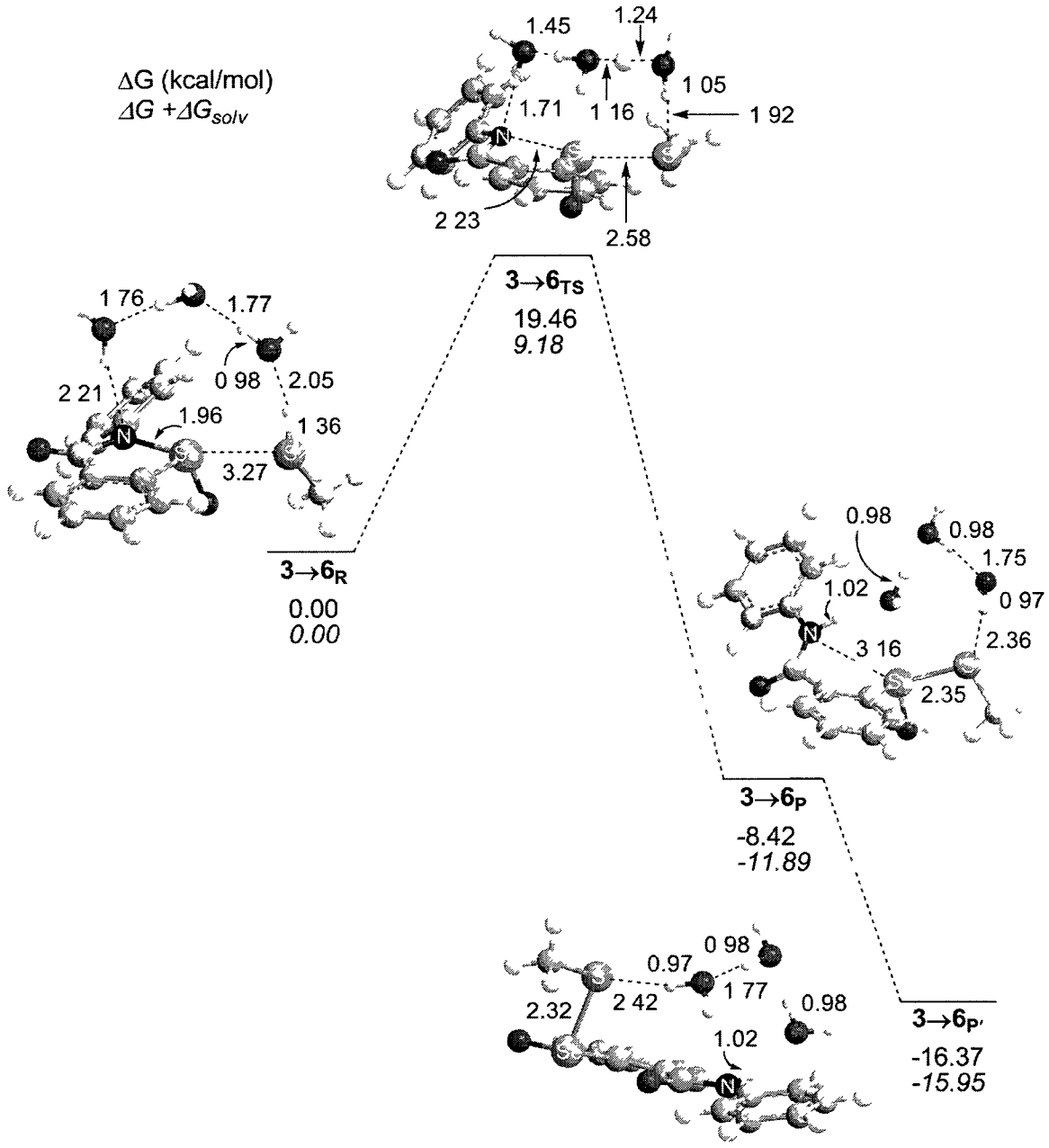

Figure 11. Reaction of **3** to **6** with three water molecules in the SAPE network showing the R, TS, P and alternate product P'.

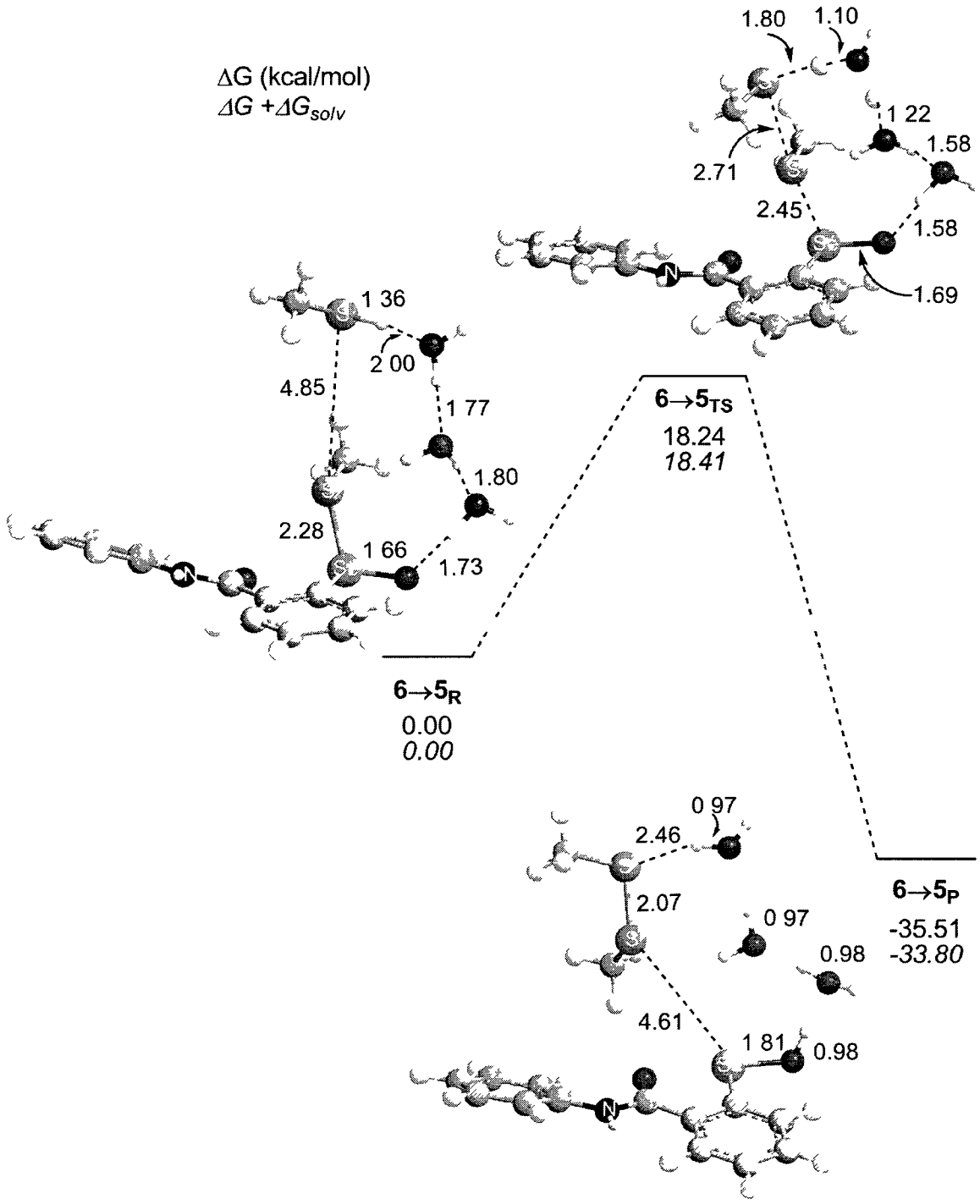

Figure 12. Reaction of **6** to **5** with three water molecules in the SAPE network showing the R, TS and P.

Although **6** and **9** appear to be important intermediates, Fischer and Dereu may not have been able to detect these species in their ^{77}Se NMR study of the thiol reduction of **3** to **1**, due to the short half-lives expected from the DFT-SAPE activation barriers. GIAO-DFT(mPW1PW91) calculations on some selenium compounds were shown to predict the ^{77}Se chemical shifts (δ) with an average absolute error of 9% for well-behaved systems, and 13% for hypervalent compounds.[111] The chemical shifts of **1** through **10** were calculated using the DFT (mPW1PW91)/BSII-optimized geometries with the Se RECP basis set replaced by TZVP. Calculated chemical shift values (Table 2) are in good agreement with available experimental chemical shifts with errors ranging from 0% to 14 %. The DFT predicted chemical shifts of intermediates **6** (1123ppm) and **9** (839ppm) are separated well for identification. In a previous NMR study on the selenomethione oxidation, the signals at 703 and 716 ppm are assigned to the diastereoisomeric hypervalent compounds (error of 1-2% for theoretical prediction) similar to **9**.[122] For the ebselen analogue **9**, the downfield shift indicates a different chemical environment and less positive charge around selenium in comparison to the selenomethionine derivatives. A related thioselenurane intermediate **16** (eq 40) for a reaction similar to **3**→**1** was confirmed by Cowan et al. by mass spectrometry, but not by NMR.[123] If the lifetimes of **6** and **9** were within the NMR scale, then a definitive pathway would have been ascribed for the catalytic pathway of ebselen.

Ebselen selenoxide, **3** may undergo an alternate pathway, hydrolysis, to form **10**, and Mugesh et al. suggests that the instability of the oxide leads to the formation of seleninic acid.[44] Comparing the experimental and theoretical ^{77}Se NMR chemical shifts

Table 2. Theoretical and experimental ^{77}Se chemical shifts (ppm) of ebselen and its intermediates.

Compounds	GIAO-DFT $\delta_{Se}{}^{g, a}$	GIAO-DFT $\delta_{Se}{}^{c, b}$	Exp. δ_{Se}
1	915	960	959[39]
2	632	633	588[124]
3	1060	1099	1190[39]
4	218	205	232[43]
5	1003	996	1143[43]
6	1091	1123	
7	501	504	440[43]
8	1067, 700	1088, 744	
9	839	880	
10	1113	1143	1130[44]

a. $\delta_{Se}{}^{g}$ chemical shift calculated in gas phase.

b. $\delta_{Se}{}^{c}$ chemical shift calculated in chloroform solvent.

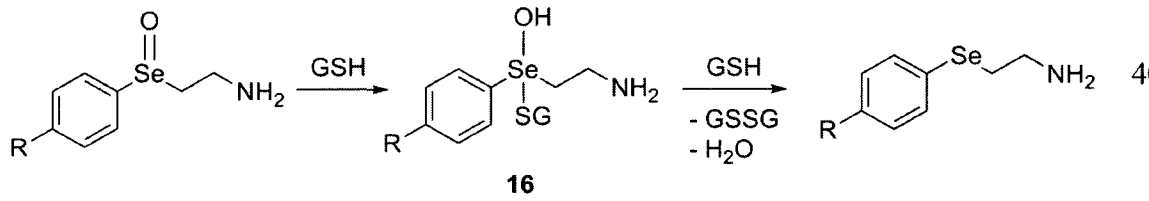

40

of **3** and **10** suggests that the values (Table 2) may be too close to distinguish between the two compounds.[44] The reactant complex **3**→**10**$_R$ is similar to **3**→**6**$_R$, except that the thiol is replaced by water as the nucleophile. For the reaction **3**→**10**, the Se-OH distance decreased by 0.67 Å, and the Se-N bond distance increased by 0.30 Å, when TS complex ($\Delta G^{\ddagger}$=20.1 kcal/mol) is formed, and the product complex has a Se-OH bond distance of 1.85 Å (Figure 13). The barrier for this reaction from our calculations is higher than that for the reactions **3**→**6** and **3**→**9**, and the value suggests step **3**→**10** (ΔG = 2.5 kcal/mol), occurs in the absence of sufficient thiols, and **10** is not an important intermediate in the antioxidant catalytic cycle of ebselen.

As an alternative to the selenoxide cycle, the ROS scavenging ability of **2** was examined through the formation seleninyl sulfide **6**. In the reactant complex **2**→**6**$_R$, the oxidant MeOOH is connected to two solvent molecules, forming a closed loop with the attacking oxygen anchored at a distance of 4.86 Å. This arrangement facilitates the protonation of the methoxy group from the nearest water molecule in the SAPE network as soon as the oxygen from MeOOH is transferred to the selenium (Figure 14). At TS, the Se-O distance is reduced to 2.00 Å and the activation barrier (21.3 kcal/mol) obtained is comparable to that of **2**→**4**, but the latter one is endergonic (11.8 kcal/mol vs -24.5

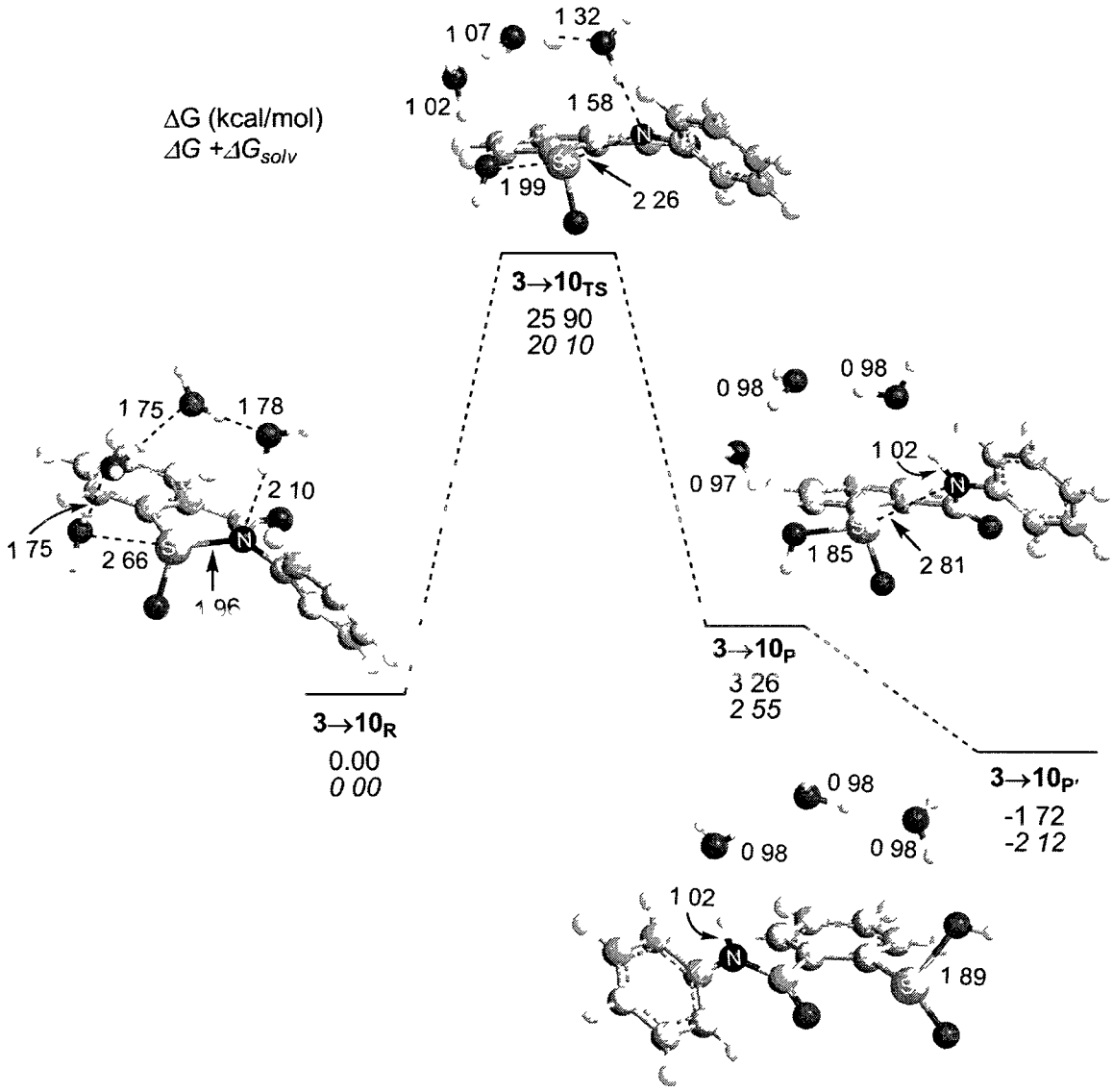

Figure 13. Hydrolysis of **3** to **10** with four water molecules in the SAPE network showing the R, TS, P and alternate product P'

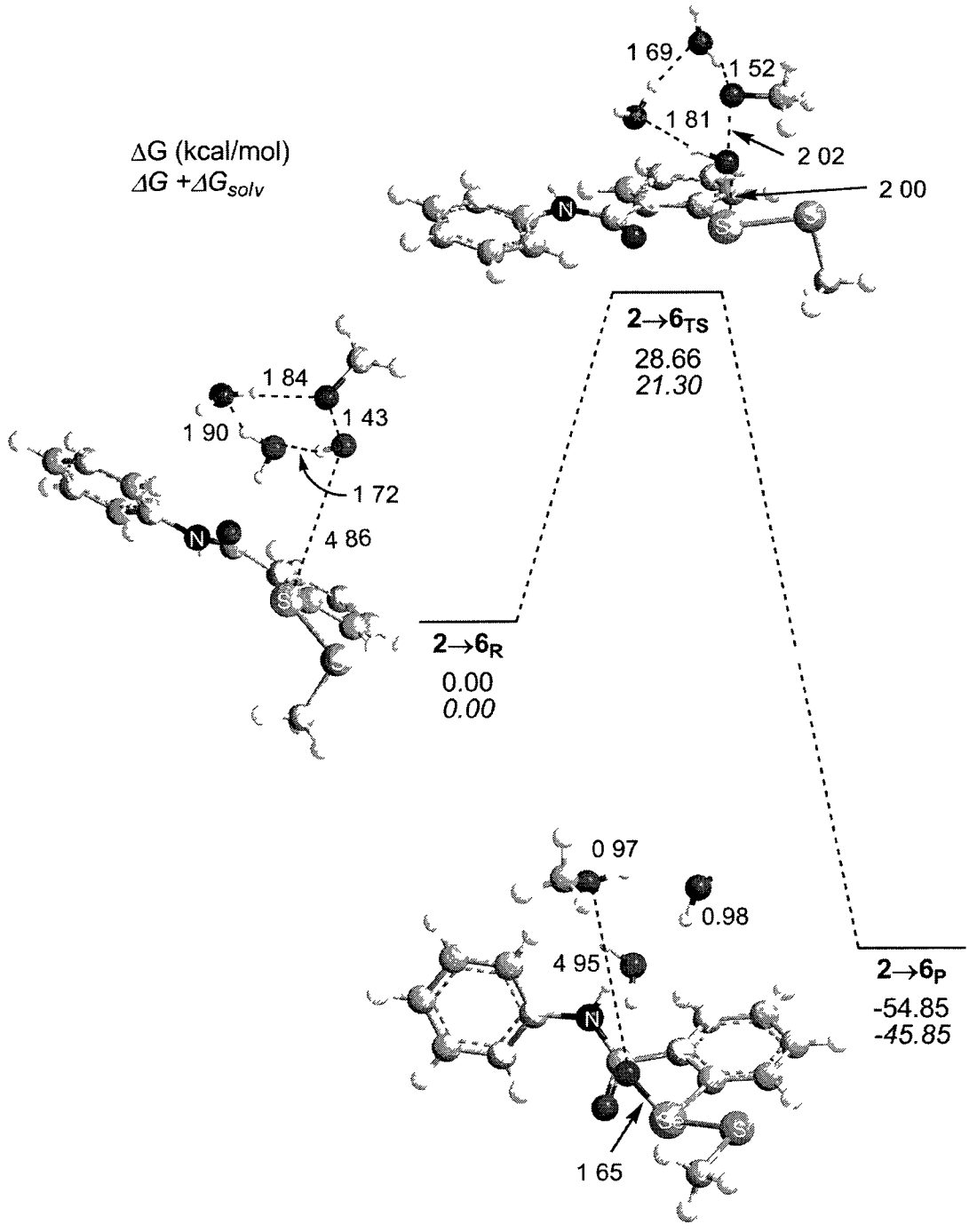

Figure 14. Reaction of **2** to **6** with three water molecules in the SAPE network showing the R, TS and P.

kcal/mol). The $\Delta G^{\ddagger}$ values for the reactions **1**→**3** (0.29 $mM^{-1}min^{-1}$), **4**→**5** (2.8 $mM^{-1}min^{-1}$), and **2**→**6** (<0.01$mM^{-1}min^{-1}$) correlates with the experimental second order rate constants for the reaction with hydrogen peroxide.[41] These results further suggest that the initial reduction of ebselen, yielding **2,** is a terminal pathway for any ROS scavenging reactions of **1**. Since the formation of **4**, the previously-thought active form of **1**, is a slow step, the ROS scavenging by ebselen to form the selenoxide is an essential reaction for the antioxidant catalytic activity of ebselen.

Conclusions

The SAPE reported values for the reaction of ebselen under oxidative stress and normal cellular condition correlate to the experimental observation. Two major mechanistic pathways have been proposed for the initial reaction of ebselen:

a. Under normal cellular conditions (high concentration of thiols and low amount of oxidants), ebselen preferentially undergoes reduction by thiols to form selenenyl sulfides. If the reacting thiols are simple ones, then the formation of **2** is a terminal pathway for the ROS scavenging mechanism. The initial reduction reaction of ebselen has other implications as well, since it reacts with free thiols such as glutathione, cysteine, and protein-bound thiols, including zinc finger, to form the corresponding selenenyl sulfide. This reaction can occur with other reducible ebselen intermediates, such as selenenic acid, seleninic acid, selenurane etc. The oxidation of zinc finger cysteines ejects zinc from its coordination site, leading to an unfolded, non-functional protein. Excess selenium oxidants may be beneficial in inhibiting many inflammatory enzymes. The reaction of ebselen with zinc finger models is to be dealt in Chapter 4.

b. Under oxidative stress, ebselen reacts with peroxides to form ebselen oxide, which in turn reacts with thiol to form a short lived thioselenurane intermediate **9**. The latter reaction occurs without ring opening, and it expands the selenium coordination sphere. Intermediate **9** has a very short half-life, since Fischer and Dereu were unable to detect it using ^{77}Se NMR. The chemical shift calculation using the GIAO method suggests that δ values of **3** and **9** are separated well for detection. A second equivalent of thiol reacts with **9** to regenerate ebselen, and this pathway may continue for a while until no more of **3** is formed, and the intermediates of **1** are in selenenyl sulfide form. Instead, a dithiol could undergo a GPx-like cycle and the catalaytic efficiency of **1** is increased, because both the initial reduction and oxidation regenerates ebselen.

CHAPTER 3

A DFT STUDY ON THE THIOL REDUCTION OF SELENIOUS ACID

Introduction

Selenite is a potential selenium supplement, as studies have shown that it is a Se source for selenoenzymes. However, selenite is very toxic at low concentrations (LD_{50} of Na_2SeO_3 - 5mg/kg), due, in part, to depletion of the cellular thiol pool.[26,125] Selenium is typically obtained from food sources in the form of selenomethionine, selenocysteine, Se-methylselenocysteine, selenate, and selenite.[126] Selenium content in food can be increased by enriching soil with inorganic forms, such as SeO_4^{2-} and SeO_3^{2-}. Plants take up these forms of selenium and convert them into selenoamino acids.[126] Additionally, selenium enriched yeast, a nutritional supplement for humans, is grown in a selenite-rich medium to produce selenomethionine.[126]

The conversion of selenite into other forms of selenium is dependent upon the availability of thiols. Non-enzymatic reductive reactions of selenite with sulfhydryls form selenotrisulfides (RS-Se-SR) and disulfide, as established by Painter[127] (eq 41).

$$H_2SeO_3 + 4RSH \rightarrow RSSeSR + RSSR + 3H_2O \qquad 41$$

An equivalent reaction was observed with proteins such as human serum albumin.[128] The reaction of selenite with cellular thiols also yields the selenotrisulfide (e.g., the glutathione derviative GS-Se-SG, identified in yeast extract by mass spectrometry). Selenotrisulfide derivatives are either taken up by enzymes (GPx[129]) as substrate, or react

further with two equivalents of thiol to produce H_2Se. Selenotrisulfides are unstable at higher pH,[28] depending on the type of thiols used. For example, the selenotrisulfide of penicillin was found to be chemically stable even at physiological pH.[130] Selenite is used as an antidote for heavy metal poisoning, where the selenotrisulfide forms an adduct with the metal such as Hg or As.[131,132] Selenite inhibits the activity of the zinc finger transcription factors, such as TFIIIA, Sp1, and AP1, by oxidizing the thiolate ligands to eject the zinc ion from the coordinating site, which disrupts the 3D structure of the protein. Labaree et al. also observed that a selenotrisulfide derivative was obtained from reaction of sodium selenite with a zinc finger model compound.[38]

Modeling the reactions of selenite with thiols can be considered as a preliminary investigation into its reactivity with zinc finger and other thiol-rich proteins. The reactions of selenite with thiols have been experimentally monitored, and two different pathways were suggested at acidic and alkaline conditions, but a conclusive mechanism at biological pH has not yet been determined. In the proposed mechanism (Scheme 6), selenious acid (**1**) first reacts with one mole of thiol producing the intermediate RSSe(=O)OH (**2**). Subsequent reaction with thiol forms dimethylthiolate selenoxide (**3**), followed by the thioselenurane (**4**). In the final step, selenotrisulfide and disulfide are produced from the reaction of the fourth equivalent of thiol with the thioselenurane. Since all these intermediates react with thiols, they may also interact with the thiolate of the zinc finger proteins as well. Like the reactions of ebselen in Chapter 2, the participation of the water solvent in these reactions cannot be neglected, therefore SAPE networks were included in the modeling of the mechanism of thiol reduction of selenite.

Scheme 6. Steps involved in the reaction of selenious acid to selenotrisulfide.

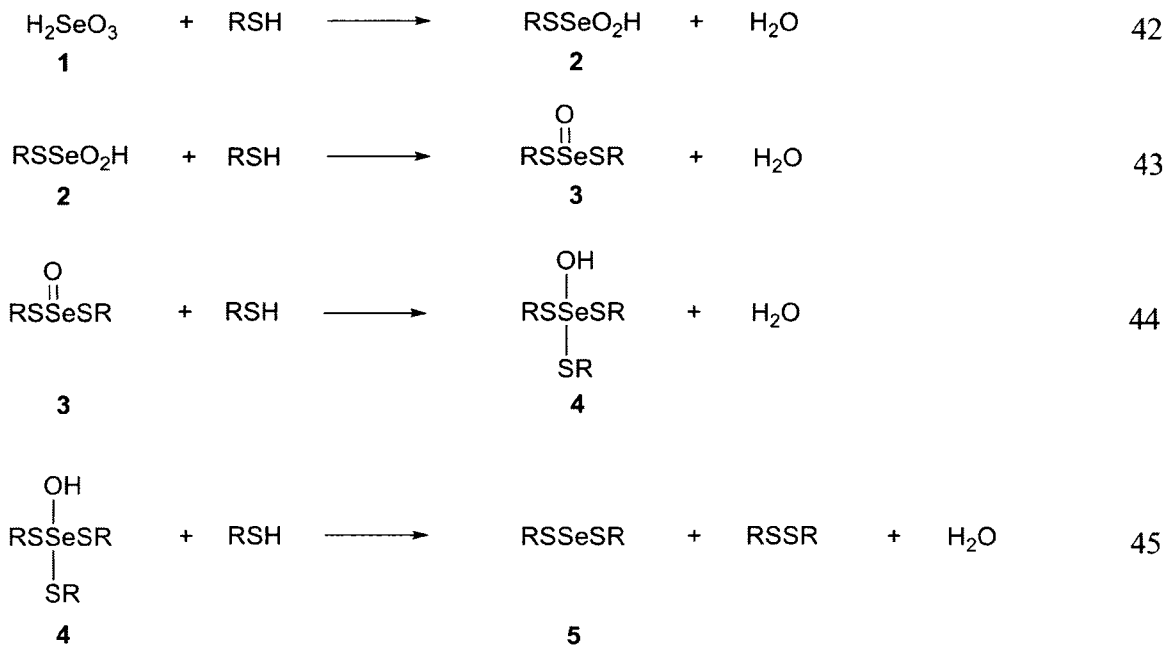

Theoretical methods

Geometry optimizations and frequency calculations were performed using Gaussian 03 at the DFT (mPW1PW91[64]) level of theory. The Ermler-Christiansen relativistic effective core potential (RECP) basis set with a set of s, p and d functions was used for the Se atom.[104] The Wadt-Hay RECP basis set augmented with a set of diffuse functions was used for sulfur.[105] All the protons involved in the SAPE network, and the ones attached to the heteroatoms, were assigned split valence triple-ζ basis set with polarization functions (TZVP).[106] All other hydrogens and the carbon atoms were assigned double-ζ basis set with polarization functions (d95*).[107] Solvation effects have been included using the polarizable continuum model (PCM) [108] (water ε = 78.39) for the optimized reactants, transition states, products and intermediate complexes. The ^{77}Se

NMR chemical shift was calculated using the gauge-invariant atomic orbital (GIAO) method[109] for intermediates **1** through **5,** using methods and basis sets previously described.[110,111]

Results and Discussion

^{77}Se NMR calculations of the optimized structures of compounds **1** through **5** were predicted as a means of identifying experimentally observed intermediates. The chemical shift of compounds **1**, **2** and **3** are indicative of a more positive selenium center than **4** and **5** (Table 3). The APT charges correlate with the calculated shifts of compounds **1**, **2**, **3** and **5**. For the thioselenuane intermediate **4**, the up-field shift and more positive Se charge are a result of the three-centered-four-electron bonding of the hypervalent selenium center. The calculated chemical shift of **5** is consistent with the experimental value. An experimental investigation on the selenotrisulfides of different thiols showed that the chemical shift is very sensitive to the environment around selenium.[133] Depending upon the type of selenotrisulfide, the chemical shift usually ranges from 500-700 ppm relative to the resonance of dimethyl selenide.[133] For mixed selenotrisulfides, the chemical shift is midway between that of the corresponding pure bis(alkylthio) selenides.[133] The pH is inversely correlated to the chemical shift value.[133]

The model reaction for each step was examined separately (Scheme 7). The first two steps are S_N2 type reactions, in which the thiol attacks from the backside of the leaving group. A square SAPE network was used for the proton transfer, where three water molecules actively participate in the reaction, and the fourth stabilizes the solvent network through hydrogen bonding. The third step is an addition reaction with no

leaving group, and is modeled similarly to the first two steps, with proton transfer to the oxo group. The final step is a reductive elimination mechanism with the formation of the selenotrisulfide. This step was modeled as a nucleophilic thiol attack at the sulfur of the selenurane with the simultaneous protonation of the hydroxyl ligand through a three-water SAPE network.

Table 3. Theoretical (solvent corrected) and experimental ^{77}Se chemical shifts (ppm) of selenious acid and its intermediates with calculated APT charges.

Compounds	APT charges	GIAO-DFT δ_{Se}	Exp. δ_{Se}
1 H_2SeO_3	1.709	1232	1282[133]
2 $CH_3SSe(=O)OH$	1.401	1338	
3$(CH_3S)_2Se=O$	1.072	1257	
4$(CH_3S)_3SeOH$	1.414	882	
5$(CH_3S)_2Se$	0.261	822	785[134]

Scheme 7. Mechanistic pathways involved in the reaction of selenite with thiols.

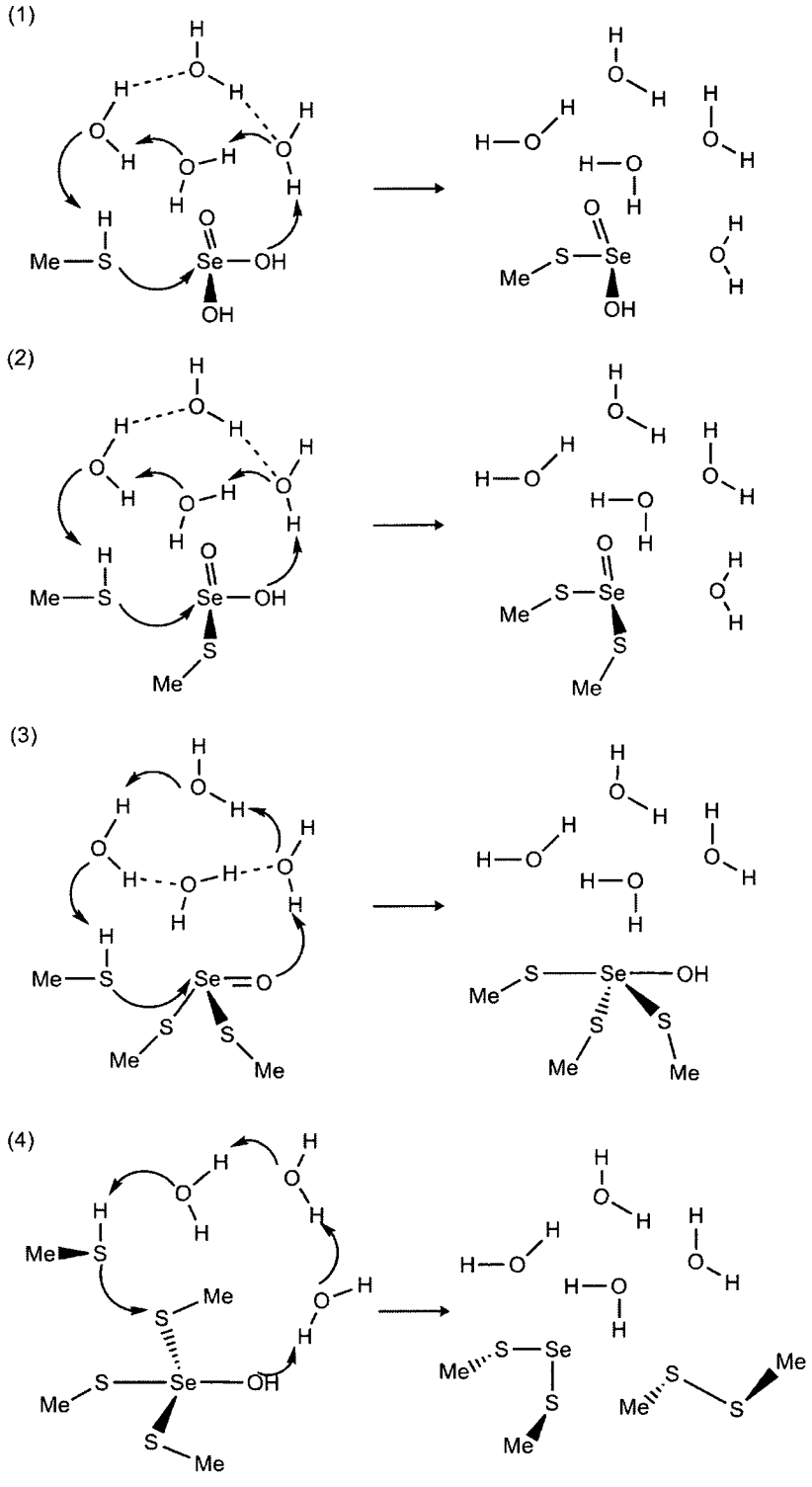

Table 4. Activation energy and energy of the reaction of the mechanistic steps involved in the reaction of selenious acid with thiols.

Reactions	Energy	R→TS (kcal/mol)	R→P (kcal/mol)
Step 1	ΔE+ZPE	4.0	-22.0
	ΔH	2.8	-22.2
	ΔG	5.8	-23.9
	$\Delta G+ \Delta G_{sol}$	6.2	-24.7
Step 2	ΔE+ZPE	2.5	-15.4
	ΔH	1.1	-15.4
	ΔG	5.3	-15.7
	$\Delta G+ \Delta G_{sol}$	6.6	-16.0
Step 3	ΔE+ZPE	13.8	1.0
	ΔH	11.4	0.0
	ΔG	19.4	4.7
	$\Delta G +\Delta G_{sol}$	19.2	3.8
Step 4	ΔE+ZPE	6.1	-40.6
	ΔH	4.7	-39.8
	ΔG	8.6	-44.1
	$\Delta G+ \Delta G_{sol}$	7.8	-43.9

Step 1 (Reaction of selenious acid with thiol yielding the first intermediate): The first step is the reaction of methyl thiol with selenious acid, yielding RSSe(=O)OH. Optimization of H_2SeO_3 led to a trigonal pyramidal geometry with an APT charge of 1.71e on selenium, the site of nucleophilic attack. Step 1 is modeled as a S_N2-type mechanism, where the nucleophilic thiol attacks Se from the back side of the leaving group, –OH (Figure 15). The reactant complex was constructed with a square SAPE network of four water molecules, which connects the thiol proton and the leaving group. The optimized reactant complex had a short Se-S distance (2.80 Å), due to a high positive charge (Table 3). The TS ($\Delta G^{\ddagger}$=6.3 kcal/mol) structure obtained by following the S-H coordinate is see-saw shaped, with the nucleophile and leaving group almost linear (169.4°). The low barrier (Table 4) may be attributed to the positively-charged Se center, and the predicted value is comparable to the reaction of PhSeOH→PhSeSMe ($\Delta G^{\ddagger}$=6.6 kcal/mol), previously modeled with a four-water network.[97] After the product (ΔG=-24.7 kcal/mol) formation, the SAPE network shifted towards the leaving group, due to preferences in hydrogen bonding.

Step 2 (Reaction of $CH_3SSe(=O)OH$ with thiol giving the second intermediate): In Step 2, the product from the first reaction reacts with a second molecule of thiol to form RSSeOSR (Figure 16). The reactant complex was constructed similar to the first step, with the nucleophilic thiol approaching the Se from the backside of the leaving group (OH). The lower positive charge on the selenium of **3** is evident from the weaker Se…S interaction (2.91 Å) relative to the first step. By following the S-H distance, the TS was found at 1.67 Å (ΔG=6.6 kcal/mol), the Se-S and S-H bond distances increased by 0.25 Å and 0.28 Å, respectively. The TS was confirmed by one imaginary frequency

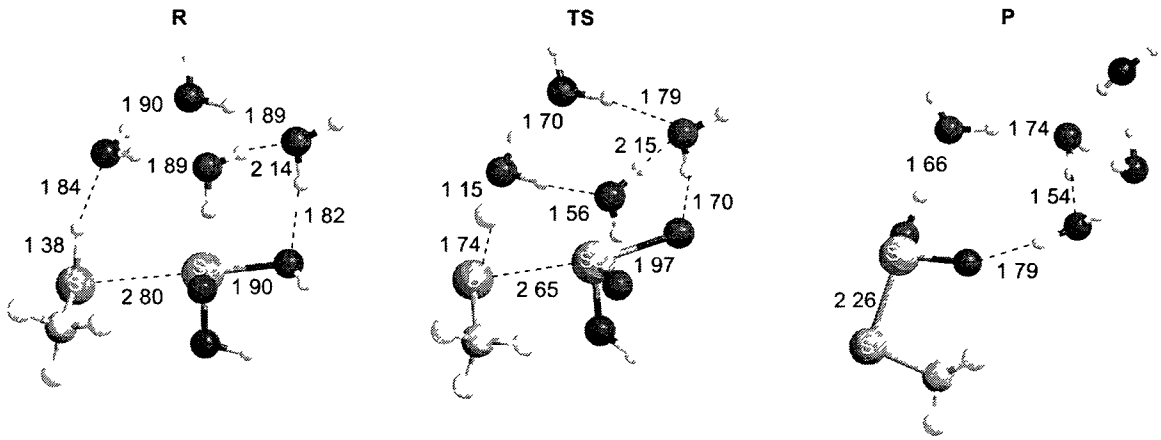

Figure 15. Optimized structures of the stationary states in step 1 with selected bond distances.

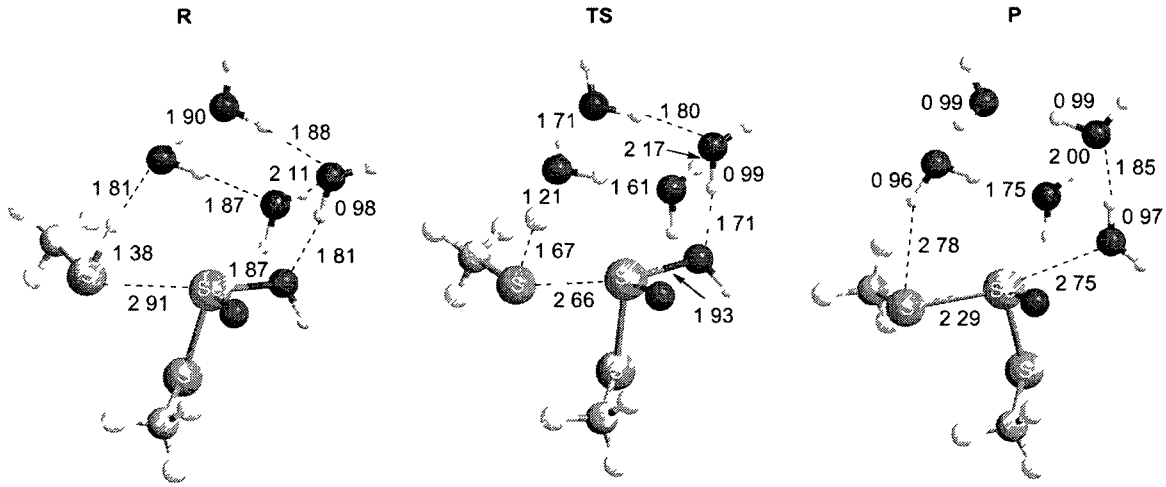

Figure 16. Optimized structures of the stationary states in step 2 with selected bond distances.

with major motion along the S-H coordinate. The barrier is comparable to the previous step, but the reaction is less exothermic (-16.8 kcal/mol).

Step 3 (Reaction of $(CH_3S)_2Se(=O)$ with thiol giving selenurane): Step 3 involves the formation of the hypervalent compound $(RS)_3SeOH$ from $(RS)_2Se=O$ by the addition of a –SR group and a proton to the Se=O bond. The reactant complex was constructed with a four-water molecule SAPE network, and the nucleophilic thiol approaching the Se center (d_{Se-S} = 3.37 Å) trans to the Se=O bond (Figure 17). The Se-S interaction is longer than the corresponding distance for the reactant complexes in step 1 and step 2. In addition, the decreased positive charge on Se, in comparison to the reactants in previous steps, contributes to the high activation barrier ($\Delta G^{\ddagger}$=19.2 kcal/mol). The water molecule providing the proton for the oxo group (O=Se-) is stabilized through hydrogen bonding on either side by the SAPE network. For a similar reaction between ebselen oxide and thiol in Chapter 2, a lower barrier ($\Delta G^{\ddagger}$=7.3 kcal/mol) was predicted for the formation of the corresponding thioselenurane. In step 3, the approach of the nucleophile must be trans to the Se=O group, whereas for ebselen, the nucleophile is cis to the Se=O group. In the latter case, fewer O-H bonds must be broken in the SAPE network for the proton transfer to form products, resulting in a lower activation barrier. The product complex $(RS)_3SeOH$ is a hypervalent selenium compound with a see-saw structure, with Se-S and S-OH bonds in the trans positions. Consistent with other selenuranes, the axial bonds are elongated, with the most electronegative groups trans to each other. The energy of the reaction (ΔG=3.8 kcal/mol) is comparable to that of the selenurane formation in Chapter 2.

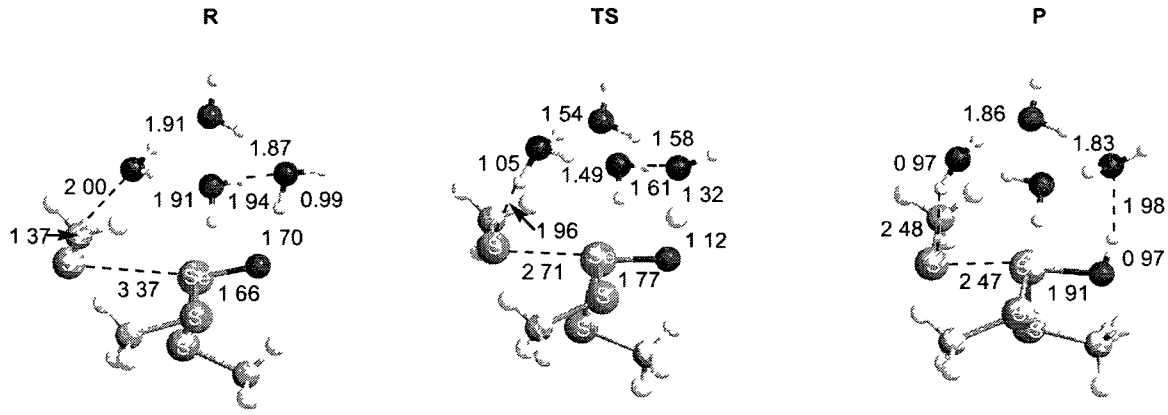

Figure 17. Optimized structures of the stationary states in step 3 with selected bond distances.

Step 4 (Decomposition of selenurane to selenotrisulfide): The final step in the formation of selenotrisulfide is the attack of a nucleophilic thiol on the selenurane. In this selenurane, the axial S_a, Se, and O atoms are involved in a linear three-center-four-electron (3c4e) bond. Resonance structures (Scheme 8) show that the axial thiol is more negatively charged (-0.552e) than the other sulfurs (-0.222e). This increased negative charge on the axial thiol, along with the steric hindrance around the selenium center, drives the attack of the incoming nucleophile on one of the non-axial –SR ligands. In the reactant complex, the Se-S_a bond (2.36 Å) cis to –OH is longer than the other Se-S_b bonds (2.28 Å), due to its involvement in the delocalized 3c4e bond (Figure 18). The nucleophilic thiol attacks one of the non-axial sulfurs (S-S_b 3.13Å), and the reactant complex optimized with three water molecules in the SAPE network connecting the leaving groups. The transition state ($\Delta G^{\ddagger}$=7.8 kcal/mol) for this step is found when the S_b-S distance has decreased to 1.61 Å and Se-S_b has increased to 2.59 Å. The activation

barrier and the energy of the reaction suggest that this step is rapid with a stable product (ΔG=-43.9 kcal/mol). The energetics of this reaction suggest that as soon as the product from step 3 is formed, it is converted into selenotrisulfide.

Scheme 8. Resonance structures of hypervalent selenurane.

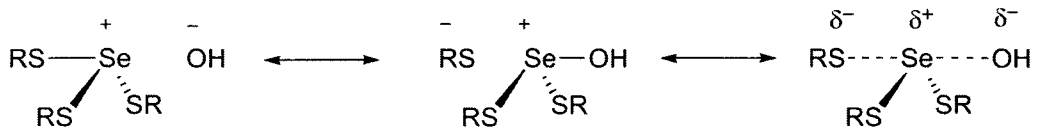

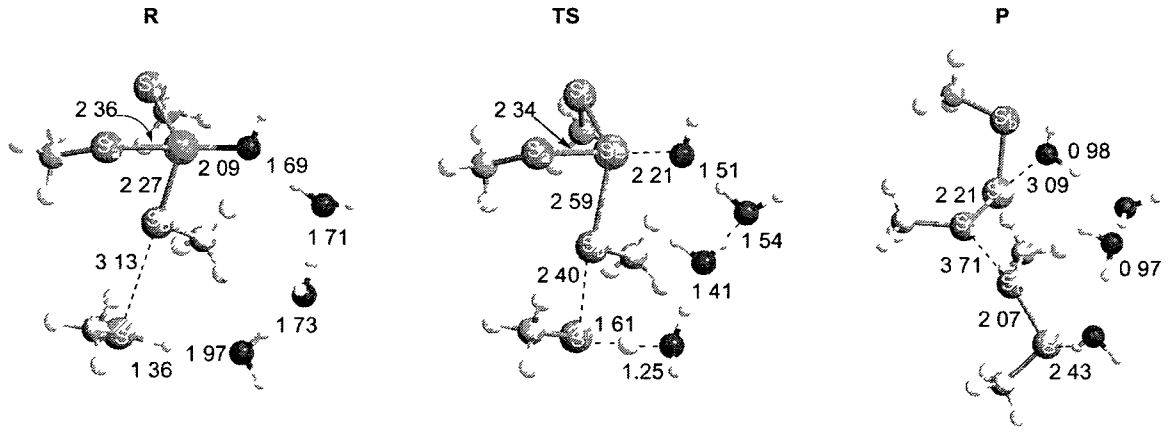

Figure 18. Optimized structures of the stationary states in step 4 with selected bond distances.

Kice et al.[135] studied the reaction of selenious acid with thiols in 60% dioxane solution under acidic conditions. Compound **2** was detected as the first stable intermediate, and the identity of the second intermediate was not established, because of the short half life. Kice et al.[135] suggested that **1** is in equilibrium with SeO_2, and that the dehydrated form reacts faster than the acid to form the first intermediate (**2**), also the rate is higher for the first step in comparison to the subsequent steps. Forastiere et al.[136] studied the same reaction under alkaline condition and excess of selenite, and assigned **2** as the first intermediate and selenotrisulfide **5** as the product. Our calculations suggest that the first two steps have low activation barriers, such that **2** is unlikely to be an observable intermediate. The barrier for the third step is relatively high, suggesting that the selenotrisulfide oxide **3** must be the stable intermediate at pH 7.

Conclusions

A SAPE DFT study of the four steps involved in the reaction of selenious acid with thiols suggests that the protonation of the oxygen in $(RS)_2Se{=}O$ to a selenurane is the rate-determining step. However, alternate pathways may be involved under acidic or basic conditions, and should be examined in the future study. The product compound of the slow step is a selenurane, and the energy of the reaction shows that it is unstable and it decomposes into selenotrisulfide. This selenotrisulfide is a stable product, which has been observed experimentally by various groups. RS-Se-SR may further react with thiols, or can be a substrate for certain enzymes and get incorporated into proteins. The models of this study may be used as a basis for examining the reactions of selenite and its derivatives with zinc finger proteins.

CHAPTER 4

A DFT STUDY ON THE INITIAL MECHANISTIC STEP INVOLVED IN THE REACTION OF ZINC FINGER WITH EBSELEN

Introduction

Zinc is an essential element and the second most abundant transition metal in the human body (2.3g/70kg) after iron.[137] In eukaryotes, zinc is predominately bound to proteins, in which the metal plays a structural or catalytic role.[138] Free Zn^{2+} ions are present in nanomolar to picomolar concentrations.[139,140] Zinc acts as a signaling agent, as the dynamics of extracellular and extracellular Zn pools are related to cell growth and apoptosis.[141] Zinc finger (ZF) transcription factors (TF) are a class of Zn^{2+} binding proteins that interact with DNA, RNA, and proteins,[142] and are associated with gene expression and growth.[143] In transcription factors, zinc is tetrahedrally-coordinated to cysteine (C) and/or histidine (H) ligands.[144] Based on the number of ligands in the coordination sphere, zinc fingers can be classified as C2H2, C3H, or C4.[145] The C2H2-type zinc finger is one of the largest gene families in the human genome.[146] Zn must be coordinated to the C and the H ligands for the proper folding to the tertiary structure of the zinc finger proteins for protein-nucleic acid binding.[147] In functional zinc fingers, the cysteine residues coordinated to the Zn^{2+} are in the reduced, thiolate form.[148] Biological oxidants/reductants in our system regulate gene expression by altering the oxidation state of these cysteines to allow for folding/unfolding of the zinc finger proteins (eq 46).[140,149] Xenobiotic oxidants can also oxidize these cysteines to release zinc and disrupt the 3D structure of the protein.[149]

$$-S\text{-}Zn^{2+}\text{-}S- + \text{oxidant} \rightarrow Zn^{2+} + -S\text{-}S- \quad (46)$$

Reducible selenium compounds such as phenylselenenic acid, phenyl selenenyl chloride, ebselen, and 2-nitrophenyl selenocyanate are found to release Zn from the transcription factor XPAzf (C4 type), while methylselenocysteine or selenomethionine did not have any effect.[150] Ebselen also oxidizes the thiolate of the zinc finger, resulting in the release of Zn^{2+} and unfolding of the protein.[150] Another study observed that ebselen and selenite displaced zinc from TFIII and sp1 TFs (C2H2 type).[38] Selenium compounds also release Zn^{2+} from metallothionein (MT), a zinc-binding protein involved in regulating the uptake, storage, and distribution of Zn^{2+} ions.[151] These selenium compounds are either supplements or have therapeutic effects, which may also affect the intracellular and extracellular Zn^{2+} concentration.[141] Since the pool of zinc is a signaling system associated with gene expression, apoptosis, and cell growth,[141] it is important to understand the redox chemistry of zinc fingers with selenium compounds.

The proposed mechanism for the release of Zn^{2+} from a zinc finger model compound by ebselen is shown in Scheme 9. First, the zinc-bound thiol attacks the Se of ebselen, followed by the protonation of amide nitrogen and hydroxylation of zinc. In the second step, the nucleophilic sulfur attached to the zinc attacks the S in the Se-S bond, forming a disulfide, a selenol, and a (dihydroxo, diimidazole)- zinc complex. In the protein, this zinc complex would be an intermediate in the complete release of Zn^{2+} from the protein. In this Chapter, we model the first step of the mechanism of the reaction of ebselen with C2H2-type zinc fingers. The thiolate in the zinc finger is attached to the metal ion, making this reaction different from reaction of ebselen with simple thiols which was discussed in Chapter 2.

To reduce the system size for DFT calculations, the C2H2 zinc finger model complex **A** was truncated by removing the majority of the protein, replacing the histidines with imidazoles, and replacing the cysteines with a propylene-based dithiolate. In the ZF protein, the two cysteine ligands are connected through 2-5 hydrophobic amino acids, which provide additional structural stability.[152,153] The second cysteine is connected to histidine through many amino acid residues, and the fourth and third ligands are linked in the same fashion.[152] In our study, the thiol groups are tethered, so that the system mimics the protein by retaining the thiolate groups in the vicinity of the zinc, and the selenenyl sulfide formed in the first step will not drift away from the zinc coordination site. In the discussion below, we first discuss the energetics (ΔE) of the reaction, specifically, the strength of the interaction of the Se···S interaction in the initial ebselen-zinc finger complex (**C**) and the Se···O interaction in the immediate product complex (**D**), followed by the SAPE modeling of the expected rate-determining step **C→D**.

Theoretical Methods

Geometry optimizations and frequency calculations were performed using parallel quantum solution (PQS)[66] software at the DFT/(B97-1)[67] level of theory. The Ermler-Christiansen relativistic effective core potential (RECP) basis set with a set of s, p and d functions was used for the Se atom.[104] The Wadt-Hay RECP basis set augmented with a set of diffuse functions was used for sulfur.[105] Protons involved in the SAPE network or bonded to heteroatoms were represented by the Dunning triple-ζ basis set with polarization functions (TZP), and an additional diffuse function (TZP+) defined the O and N atoms.[106] The rest of the protons were assigned double-ζ basis set (DZ), and the

Scheme 9. Mechanistic steps involved in the reaction of zinc finger model with ebselen.

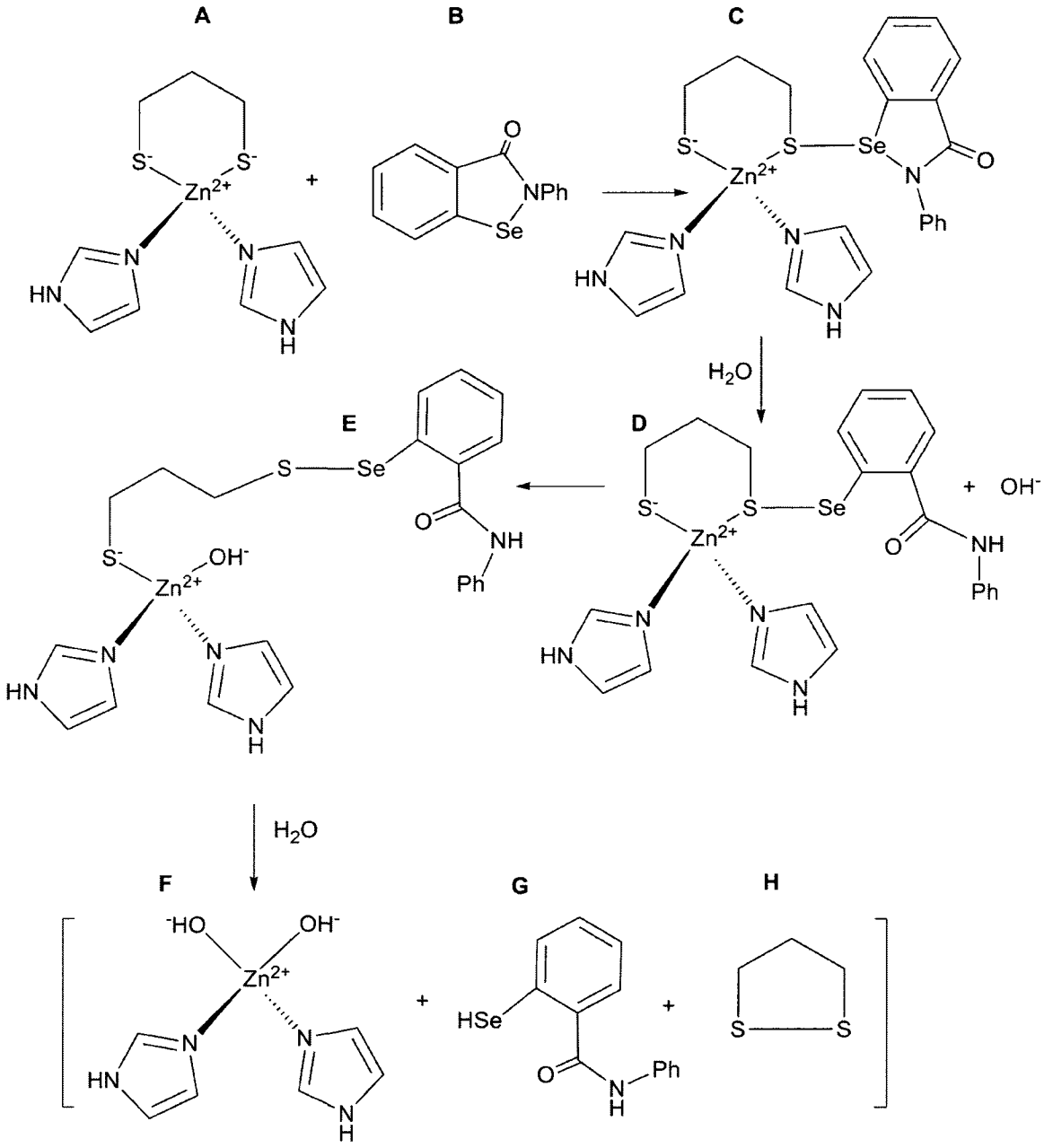

carbon atoms with polarization functions on DZ basis set (DZP).[107] All the remaining hydrogens and carbons were assigned double-ζ basis set (DZ) with polarization functions (DZP) added to carbon.[107] The LANL2DZ[154], CRENBL[104], and B2[155] basis sets were used for the Zn atom. The B2 basis set for zinc was developed to validate exchange-correlation functionals against benchmark values obtained by expensive ab initio methods for different types of complexes. The B2 basis set takes into account the fact that zinc is a borderline transition metal (filled 3d orbitals), and has a small, but not negligible, relativistic effect.[155]

Results and Discussion

The energy of the reactions in Scheme 9 was obtained from the optimized structures of the intermediates in Figure 19 (Table 5). The tetrahedral zinc finger model compound (**A**) resulted in a tetrahedral geometry with Zn-N (2.14 Å) and Zn-S (2.28 Å) distances comparable to the 1SP2 protein[156] (2.07 Å and 2.25 Å). The association of zinc finger model (**A**) and ebselen (**B**) to form a complex **C** is energetically favorable by -18.0 kcal/mol. The intermediate complex **E** may be obtained from the complex **C** (ΔE=-2.2 kcal/mol), or from the reaction of **A** and **B** with water (ΔE=-20.1 kcal/mol), where the latter reaction is energetically favorable. The energy of formation of disulfide, ebselen selenol, and dihydro,diimidazole zinc complex (**F**) is endothermic (26-28 kcal/mol) from **C** or **D**, whereas from **A**, **B** and 2 water molecules, ΔE is 8.1 kcal/mol. The endothermicity may be due to the lack of solvent participation in the mechanistic step and/or the ejection of zinc is not taken into account. In the actual protein, **F** is not the final product, but an intermediate in the full release of Zn^{2+} from the binding site followed by unfolding of the functional TF.

Table 5. Energy of the reaction with ZPE correction, enthalpy and Gibb's free energy of the intermediates and products of the reaction in Scheme 7.

Reaction	E+ZPE	H	G
A+B →C	-17.99	-17.1	-1.29
A+B +H_2O→E	-20.14	-18.58	9.88
A+B +2H_2O→F+G+H	8.12	8.02	16.05
C + H_2O →E	-2.15	-1.49	11.17
C +2H_2O→F+G+H	26.12	25.11	17.34
E+ H_2O→F+G+H	28.27	26.60	6.17

The model ZF-ebselen complex **C** is a donor-acceptor pair with the S donating to the antibonding orbital of Se-N bond, and has an elongated Zn-S bond (2.36 Å) with a Se···S interaction (2.76 Å). The NBO calculation on the optimized geometry of this complex predicted a donor-acceptor energy of 36.2 kcal/mol; suggesting a strong interaction between the zinc finger model compound and ebselen. The abstraction of a proton by the amide nitrogen in complex **C** resulted in the product formation (**D**) with the Se-S bond (2.32 Å), and a further increase in the Zn-S (2.43 Å) bond. The NBO calculation of complex **D** showed that it is stabilized by an Se···O interaction ($\Delta E_{d\rightarrow a}$= 30.91 kcal/mol). The strength of these interactions suggests that the selenium of the ebselen can bind to thiolate while maintaining the tetrahedral geometry. These analyses

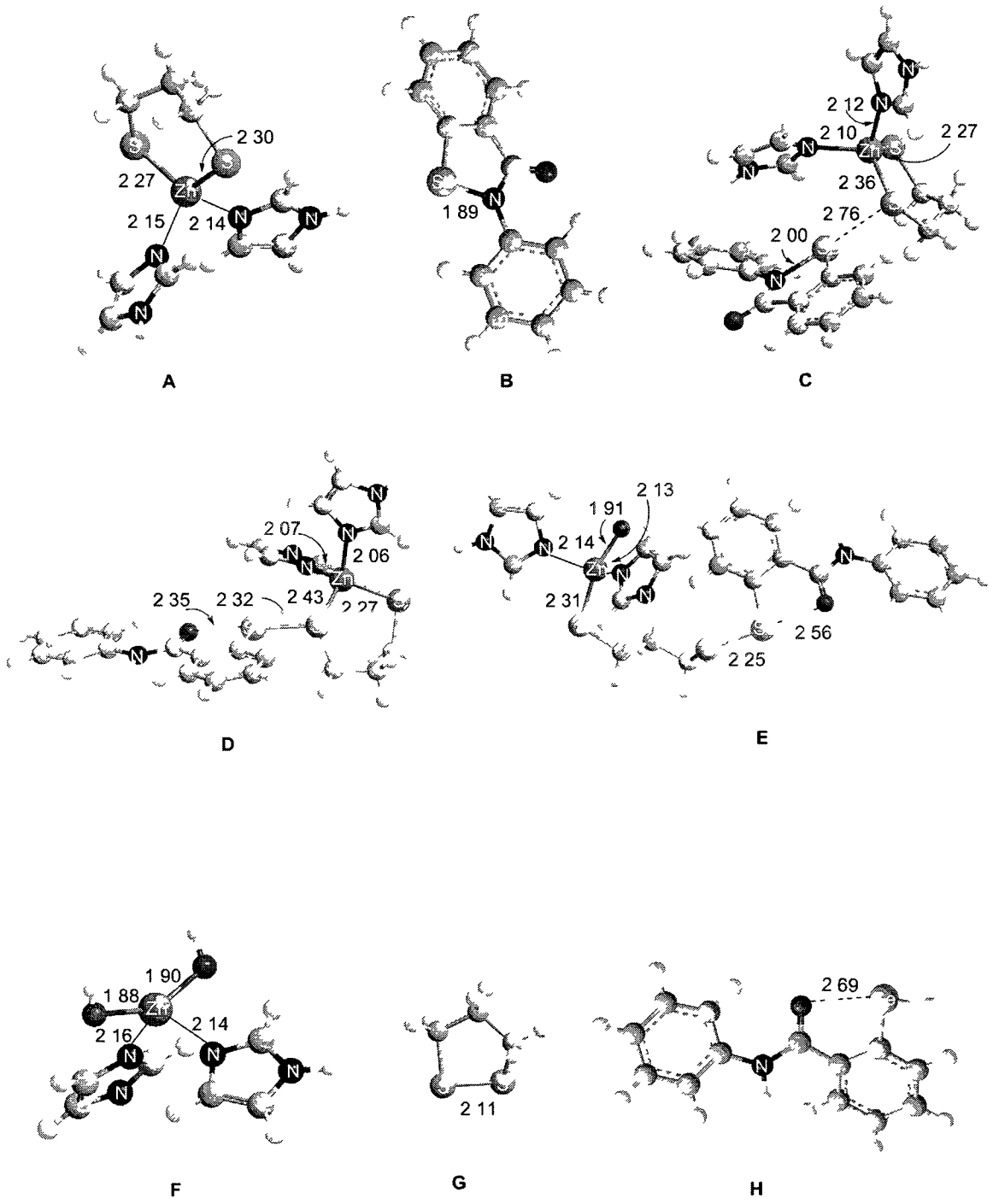

Figure 19. Optimized structures of reactants, possible intermediates and products of the reaction of zinc finger model complex and ebselen.

suggest that the approach of water for the formation of Zn-OH bond is very important for the release of zinc.

Scheme 10. SAPE model for the initial reaction of ebselen with zinc finger model compound.

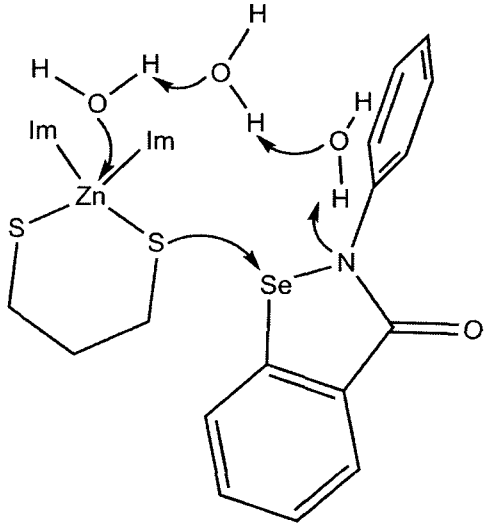

SAPE modeling of the transition state for the initial reaction of ebselen with the zinc finger model was done using the LANL2DZ basis set for zinc at the DFT/(B3PW91)[62] level of theory. The starting geometry of the reactant complex had three water molecules connecting the amide nitrogen of ebselen-Zn finger model complex **C** and the zinc center, so as to form complex **E**, the intermediate product in Scheme 9. The SAPE network in the reactant complex is arranged in such a way that the

nitrogen of the amide group abstracts a proton from the nearby water molecule, and the network of the solvent assists in the replacement of the thiolate attached to the zinc by a hydroxyl group (Scheme 10). The reactant complex optimized to a five-coordinate, trigonal-bipyramidal geometry around Zn with an H_2O from the SAPE network as the fifth ligand (Figure 20). The pentavalent zinc complex was based on the enzyme carbonic anhydrase (CA), where zinc is coordinated to 3 histidines and 2 oxygens of HCO_3^-, and on some zinc finger model compounds that were synthesized by Almaraz et al. to study DNA binding interactions.[157] The x-ray diffraction studies of the Zn(N,N'-bis(2-mercaptoethyl)-1,4-diazacylcoheptane) dimer showed a trigonal bipyramidal or a square pyramidal geometry with the fifth coordination site occupied by the bridging sulfur ligands. The average Zn-S and Zn-N distances were 2.41 Å and 2.22 Å, respectively,[157] comparable to bond distances in the LANL2DZ-optimized reactant complex (Figure 20), suggesting that five-coordinate zinc may be an important intermediate in its release from transcription factors by ebselen.

However, the LANL2DZ designation for a zinc basis set is misleading in the Gaussian software, instead it is LANL1DZ (3s2p5d)/[2s2p2d], a large core ECP-small basis set, which has a core representation for the 18 inner electrons without any relativistic effects.[158] Calculations using this basis set have been shown not to be reliable[159] because the valence s and p orbitals do not have radial nodes.[158] This problem can be solved using a basis set that includes the (n-1) s and p electrons in the basis set, rather than the ECP. CRENBL (7s6p6d)/[7s6p6d] is one of those basis sets that results in a node, and is fully uncontracted if used as obtained from the EMSL basis set exchange.[160,161] B2 (15s11p6d2f)/[10s7p4d2f], an all-electron basis set which includes

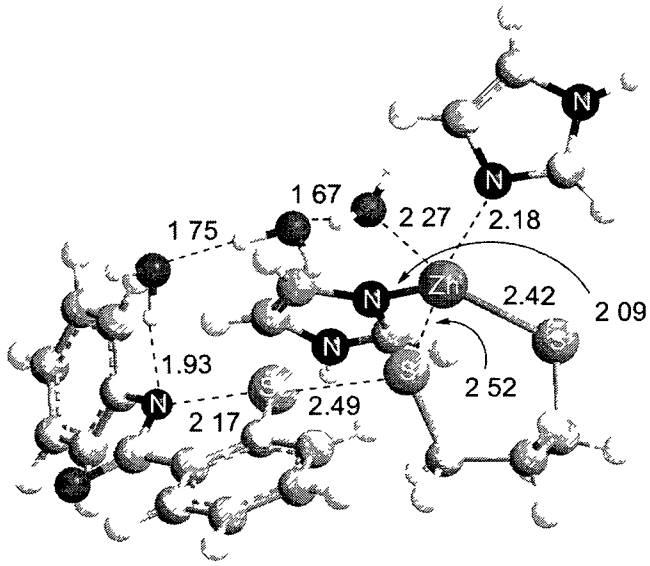

Figure 20. LANL2DZ optimized reactant complex of zinc finger model and ebselen with three water molecules in the SAPE network.

the relativistic effect, is used in this study for the reasons mentioned in the method section. After the complete optimizations in CRENBL and B2 basis sets with the inclusion of polarization and diffuse functions on the ligands, the zinc complex optimized to a four-coordinate, tetrahedral geometry, instead of the pentavalent structure observed with LANL1DZ. For this reactant complex, the geometry was similar for both the basis sets, with the water molecule having drifted away from the Zn center ($d_{Zn\text{-}O}$=4.74 Å), and the amide nitrogen still maintaining the hydrogen bonding interaction with the SAPE network ($d_{N\text{-}H}$ =2.09 Å). The Se-S (2.64 Å) and Se-N (2.08 Å) bond lengths are

comparable to the corresponding distances (2.76 Å and 2.00 Å) in complex C. The discussion of geometry and energetics is based on B2 basis set unless specified otherwise.

Using the reactant complex geometry in BSI, the transition state was found by following the N-H bond formation. The optimized structure of the TS was associated with an imaginary frequency (843i cm^{-1}) along the expected modes of bond breaking/forming. In the TS, the thiolate attached to the zinc (d_{Zn-S}=3.03 Å) was displaced, allowing the Zn-O (2.06 Å) bond formation (Figure 22). The breaking of Se-N (2.82 Å) bond resulted in the abstraction of the proton by the amide nitrogen (d_{N-H} =1.24 Å), suggestive of a progression towards the product complex. The activation barrier without solvation correction is 11.03 kcal/mol, which is indicative of a rapid reaction, as observed with MT and ebselen ($t_{1/2}$ < 1m).[84] The barrier calculated using CRENBL basis set is 3 kcal/mol lower than that for B2, but the stabilization energy of the product with respect to the TS has similar values. If the activation barrier were to be calculated from the ebselen-zinc finger model compound (**C**) and an independent three water cluster, then $\Delta G^{\ddagger}$ is 16.9 kcal/mol. This suggests that, even with the truncated model, the approach of the water molecule to form the Zn-O bond is important for the release of zinc. The energy of the reaction forming an immediate product complex is endothermic (0.78 kcal/mol). Experimental studies of the reaction of ebselen with simple thiols and MT show that the former ($t_{1/2}$<1s) is much faster than the latter ($t_{1/2}$<1m).[84] This difference in rate may be due to steric hindrance on the thiolate of zinc fingers. In order to study the complete reaction, the reactant complex for the mechanistic step for the formation of disulfide should be either from the immediate product complex or from an alternate one with an Se···O interaction.

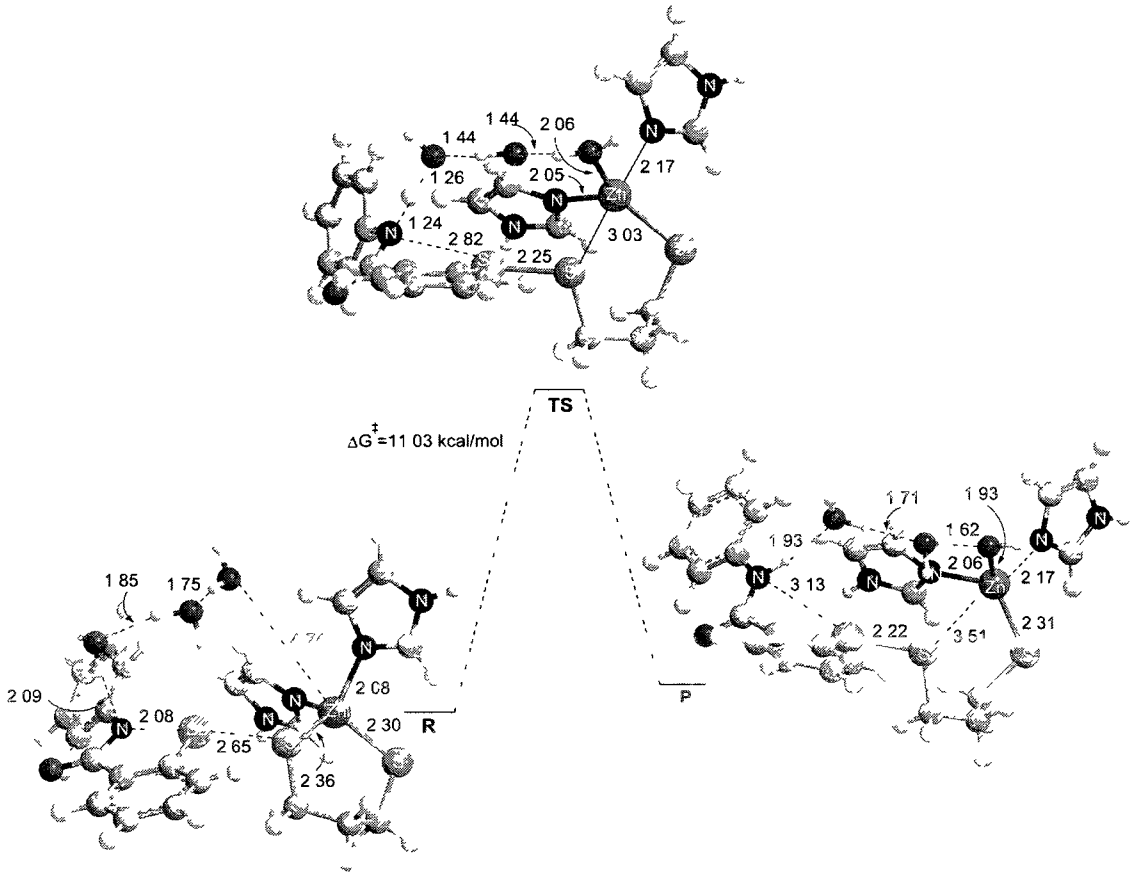

Figure 21. Reaction of zinc finger model compound and ebselen with three water molecules in the SAPE network showing R, TS and P complexes.

Conclusions

DFT modeling of the oxidation of the first thiolate in the C2H2-type zinc finger model is a low barrier reaction and comparable to the reaction of ebselen with simple thiols (Chapter 2). With the truncated coordination site of the zinc finger, the ligands have more flexibility, and the core hydrophobic residues were not included in the model. As a result, the imidazole rings are closer to the phenyl ring of ebselen with some interaction. The barrier obtained may be lower than the actual value. The CRENBL basis set from the PQS library and the B2 representation for zinc are computationally expensive, as was observed during the optimization procedures. In order to run these calculations in a reasonable time, an ECP basis set of B2 or CRENBL quality should be used.

The model from this study may be extended to full models of the reaction of ebselen with the C2H2, C3H and C4 type zinc fingers using a QM/MM study, which can be used to examine the energetics and structural change of the protein due to cysteine oxidation. This study may also be extended to other reducible selenium compounds (phenylselenenic acid, ebselen selenenic acid, selenite, selenate, etc.) that have been shown to release zinc from transcription factors as well as other zinc proteins known to reaction with selenium compounds such as MT.[84] These results will enhance our understanding of the beneficial and detrimental effects different selenium compounds.

CONCLUSIONS

Selenium is an important trace element required for maintaining the redox balance in biological systems. The mechanisms of the organoselenium compound ebselen, a mimic of the antioxidant selenoenzyme GPx, are not well understood. DFT calculations incorporating SAPE suggest that under normal cellular conditions, ebselen reacts with the thiols forming the selenenyl sulfide. An intra-molecular Se···O interaction prevents the conversion of selenenyl sulfide to the ROS-scavenging selenol, making the initial reduction of ebselen a terminal pathway in the peroxide removing cycle. Conditions of oxidative stress lead to the initial oxidation of ebselen yielding the corresponding oxide. Our calculations suggest that subsequent reaction with two equivalents of thiols completes the catalytic cycle, through a hypervalent selenurane intermediate with low barrier consistent with the experimental observation.

SAPE modeling the mechanistic pathways for the thiol reduction of selenious acid to selenotrisulfide predict the formation of thioselenurane to be the rate-determining step. The selenotrisulfide, an important derivative which can react with thiols to form selenide, is a substrate for the selenium incorporation into proteins. Since selenite is found to inhibit certain transcription factors, the models from this Chapter could be used as a starting point for models of the reaction of selenious acid and its derivatives with zinc finger proteins.

Zinc finger transcription factors have oxidizable thiols that control the quaternary structure of the protein. Studies have shown that ebselen inhibit some zinc finger proteins by blocking the sulfhydryl group necessary for the activity. The initial reaction

of a zinc finger model with ebselen by DFT-SAPE methods is predicted to be a low-barrier reaction in agreement with experimental data. The work should be expanded through QM/MM type calculations to include the hydrophobic core of the zinc finger protein which has a role in protein stability. Even though this process adds significant computational cost, this study would give a better representation of how the protein reacts to the reduction of the cysteinates over the course of the reaction. Understanding these mechanisms can lead to the design of new selenium compounds that target specific zinc fingers involved in the cancer growth.

SAPE modeling is an important technique for determining activation barriers for aqueous phase reactions, and the predicted results are consistent with available experimental observations. The microsolvation is applied only to the necessary bond formation/breaking sites. The rest of the system does not experience the effect of the solvent, and to evaluate the contribution of explicit solvation, a QM/MM approach should be used for future studies of aqueous-phase reactivity. An appropriate water box with 7-10 hydration shells should be employed for solvation. QM (DFT) should be applied for the stationary states with the SAPE network as well as for the first shell of solvation, and the rest of the water molecules in the box should be treated by MM. Activation barriers evaluated from the optimized geometries using QM/MM approach may give an improved picture on the influence of solvent for the whole system.

LITERATURE CITED

(1) Reilly, C. In *Selenium in Food and Health*; Springer US: 2006, p 1.

(2) Moxon, A. L.; Rhian, M. *Physiol. Rev.* **1943**, *23*, 305.

(3) Schwarz, K.; Foltz, C. M. *J. Am. Chem. Soc.* **1957**, *79*, 3292.

(4) Rederstorff, M.; Krol, A.; Lescure, A. *Cell. Mol. Life Sci.* **2006**, *63*, 52.

(5) Beck, M. A.; Levander, O. A.; Handy, J. *J. Nutr.* **2003**, *133*, 1463S.

(6) Tan, J. a.; Zhu, W.; Wang, W.; Li, R.; Hou, S.; Wang, D.; Yang, L. *Sci. Total Environ.* **2002**, *284*, 227.

(7) Papp, L. V.; Lu, J.; Holmgren, A.; Khanna, K. K. *Antioxid. Redox Signaling* **2007**, *9*, 775.

(8) Arthur, J.; Nicol, F.; Beckett, G. *Biol. Trace Elem. Res.* **1992**, *34*, 321.

(9) Zimmermann, M. B.; Köhrle, J. *Thyroid* **2002**, *12*, 867.

(10) Rayman, M. P. *Lancet* **2000**, *356*, 233.

(11) Rotruck, J. T.; Pope, A. L.; Ganther, H. E.; Swanson, A. B.; Hafeman, D. G.; Hoekstra, W. G. *Science* **1973**, *179*, 588.

(12) Flohe, L.; Günzler, W. A.; Schock, H. H. *FEBS Lett.* **1973**, *32*, 132.

(13) Epp, O.; Ladenstein, R.; Wendel, A. *Eur. J. Biochem.* **1983**, *133*, 51.

(14) Mugesh, G.; du Mont, W.-W.; Sies, H. *Chem. Rev.* **2001**, *101*, 2125.

(15) Mugesh, G.; Singh, H. B. *Chem. Soc. Rev.* **2000**, *29*, 347.

(16) Mugesh, G.; du Mont, W.-W. *Chem. –Eur. J.* **2001**, *7*, 1365.

(17) Schewe, T. *Gen. Pharmacol.* **1995**, *26*, 1153.

(18) Ramakrishnan, N.; Kalinich, J. F.; McClain, D. E. *Biochem. Pharmacol.* **1996**, *51*, 1443.

(19) Namura, S.; Nagata, I.; Takami, S.; Masayasu, H.; Kikuchi, H. *Stroke* **2001**, *32*, 1906.

(20) Piantadosi, C. A.; Zhang, J. *Stroke* **1996**, *27*, 327.

(21) Lapchak, P. A.; Zivin, J. A. *Stroke* **2003**, *34*, 2013.

(22) Daiber, A.; Zou, M.-H.; Bachschmid, M.; Ullrich, V. *Biochem. Pharmacol.* **2000**, *59*, 153.

(23) Suzuki, K. T. *J. Health Sci.* **2005**, *51*, 107.

(24) Wendel, A.; Fausel, M.; Safayhi, H.; Tiegs, G.; Otter, R. *Biochem. Pharmacol.* **1984**, *33*, 3241.

(25) Zeng, H.; Uthus, E. O.; Combs Jr, G. F. *J. Inorg. Biochem.* **2005**, *99*, 1269.

(26) Dumont, E.; Vanhaecke, F.; Cornelis, R. *Anal. Bioanal. Chem.* **2006**, *385*, 1304.

(27) Kim, I. Y.; Stadtman, T. C. *Proc. Natl. Acad. Sci. U. S. A.* **1997**, *94*, 12904.

(28) Ganther, H. E. *Biochemistry* **1968**, *7*, 2898.

(29) Ganther, H. E. *Carcinogenesis* **1999**, *20*, 1657.

(30) Ren, X.; Bjoernstedt, M.; Shen, B.; Ericson, M. L.; Holmgren, A. *Biochemistry* **1993**, *32*, 9701.

(31) Ogasawara, Y.; Lacourciere, G. M.; Ishii, K.; Stadtman, T. C. *Proc. Natl. Acad. Sci. U. S. A.* **2005**, *102*, 1012.

(32) Veres, Z.; Tsai, L.; Scholz, T. D.; Politino, M.; Balaban, R. S.; Stadtman, T. C. *Proc. Natl. Acad. Sci. U. S. A.* **1992**, *89*, 2975.

(33) Veres, Z.; Kim, I. Y.; Scholz, T. D.; Stadtman, T. C. *J. Biol. Chem.* **1994**, *269*, 10597.

(34) Handel, M. L.; Watts, C. K.; deFazio, A.; Day, R. O.; Sutherland, R. L. *Proc. Natl. Acad. Sci. U. S. A.* **1995**, *92*, 4497.

(35) Larabee, J. L.; Hocker, J. R.; Hanas, R. J.; Kahn, F. M.; Hanas, J. S. *Biochem. Pharmacol.* **2002**, *64*, 1757.

(36) Spyrou, G.; Björnstedt, M.; Kumar, S.; Holmgren, A. *FEBS Lett.* **1995**, *368*, 59.

(37) József, L.; Filep, J. G. *Free Rad. Biol. Med.* **2003**, *35*, 1018.

(38) Larabee, J. L.; Hocker, J. R.; Hanas, J. S. *J. Inorg. Biochem.* **2009**, *103*, 419.

(39) Fischer, H.; Dereu, N. *Bull. Soc. Chim. Belg.* **1987**, *96*, 757.

(40) Haenen, G. R.; De Rooij, B. M.; Vermeulen, N. P.; Bast, A. *Mol. Pharmacol.* **1990**, *37*, 412.

(41) Morgenstern, R.; Cotgreave, I. A.; Engman, L. *Chem.-Biol. Interact.* **1992**, *84*, 77.

(42) Masumoto, H.; Sies, H. *Chem. Res. Toxicol.* **1996**, *9*, 262.

(43) Sarma, B. K.; Mugesh, G. *J. Am. Chem. Soc.* **2005**, *127*, 11477.

(44) Sarma, Bani K.; Mugesh, G. *Chem. Eur. J.* **2008**, *14*, 10603.

(45) Bayse, C.; Antony, S. *Main Group Chem.* **2007**, *6*, 185.

(46) Cramer, C. J. *Essentials of computational chemistry: theories and models*; John Wiley & Sons, Ltd.: Chichester, England., 2004.

(47) Szabo, A.; Ostlund, N. S. *Modern quantum chemistry: introduction to advanced electronic structure theory*; Dover Publications, Inc.: Mineola, N.Y., 1996.

(48) Levine, I. N. *Quantum Chemistry*; 6th ed.; Pearson Prentice Hall: Upper Saddle River, N.J., 2009.

(49) Hohenberg, P.; Kohn, W. *Phys. Rev.* **1964**, *136*, B864.

(50) Kohn, W.; Sham, L. J. *Phys. Rev.* **1965**, *140*, A1133.

(51) Koch, W.; Holthausen, M. C. *A chemist's guide to density functional theory*; 2nd ed.; Wiley -VCH: Weinheim, Germany, 2001.

(52) Ceperley, D. M.; Alder, B. J. *Phys. Rev. Lett.* **1980**, *45*, 566.

(53) Vosko, S. H.; Wilk, L.; Nusair, M. *Can. J. Phys.* **1980**, *58*, 1200.

(54) Becke, A. D. *J. Chem. Phys.* **1988**, *88*, 1053.

(55) Becke, A. D. *Phys. Rev. A* **1988**, *38*, 3098.

(56) Perdew, J. P. *Phys. Rev. B* **1986**, *33*, 8822.

(57) Perdew, J. P.; Burke, K.; Ernzerhof, M. *Phys. Rev. Lett.* **1996**, *77*, 3865.

(58) Perdew, J. P.; Burke, K.; Ernzerhof, M. *Phys. Rev. Lett.* **1997**, *78*, 1396.

(59) Becke, A. D. *J. Chem. Phys.* **1986**, *84*, 4524.

(60) Perdew, J. P.; Chevary, J. A.; Vosko, S. H.; Jackson, K. A.; Pederson, M. R.; Singh, D. J.; Fiolhais, C. *Phys. Rev. B* **1992**, *46*, 6671.

(61) Lee, C.; Yang, W.; Parr, R. G. *Phys. Rev. B.* **1988**, *37*, 785.

(62) Becke, A. D. *J. Chem. Phys.* **1993**, *98*, 5648.

(63) Stephens, P. J.; Devlin, F. J.; Chabalowski, C. F.; Frisch, M. J. *J. Phys. Chem.* **1994**, *98*, 11623.

(64) Adamo, C.; Barone, V. *J. Chem. Phys.* **1998**, *108*, 664.

(65) Gaussian 03, R. C.; Gaussian, Inc., Wallingford CT: 2004.

(66) PQS version 4.0, P. Q. S., 2013 Green Acres Road, Suite A, Fayetteville, AR 72703.

(67) Hamprecht, F. A.; Cohen, A. J.; Tozer, D. J.; Handy, N. C. *J. Chem. Phys.* **1998**, *109*, 6264.

(68) Zhao, Y.; Truhlar, D. G. *J. Chem. Theory Comput.* **2005**, *1*, 415.

(69) de Magalhães, J. P.; Church, G. M. *Experimental Gerontol.* **2006**, *41*, 1.

(70) Palmer, H. J.; Paulson, K. E. *Nutr. Rev.* **1997**, *55*, 353.

(71) Nordberg, J.; Arnér, E. S. J. *Free Rad. Biol. Med.* **2001**, *31*, 1287.

(72) Jacob, C.; Giles, G. I.; Giles, N. M.; Sies, H. *Angew. Chem., Int. Ed.* **2003**, *42*, 4742.

(73) Thomson, C. D. *Eur. J. Clin. Nutr.* **2004**, *58*, 391.

(74) Carr, A. C.; Frei, B. *Am. J. Clin. Nutr.* **1999**, *69*, 1086.

(75) Back, T. G.; Dyck, B. P. *J. Am. Chem. Soc.* **1997**, *119*, 2079.

(76) Back, T. G.; Moussa, Z. *J. Am. Chem. Soc.* **2003**, *125*, 13455.

(77) Heliövaara, M.; Knekt, P.; Aho, K.; Aaran, R. K.; Alfthan, G.; Aromaa, A. *Ann. Rheum. Dis.* **1994**, *53*, 51.

(78) Kardinaal, A. F. M.; Kok, F. J.; Kohlmeier, L.; Martin-Moreno, J. M.; Ringstad, J.; Gomez-Aracena, J.; Mazaev, V. P.; Thamm, M.; Martin, B. C.; Aro, A.; Kark, J. D.; Delgado-Rodriguez, M.; Riemersma, R. A.; van Veer, P. t.; Huttunen, J. K. *Am. J. Epidemiol.* **1997**, *145*, 373.

(79) Hatfield, D. L.; Berry, M. J.; Gladyshev, V. N. *Selenium: its molecular biology and role in human health*; Springer: New York, 2006.

(80) Allan, C. B.; Lacourciere, G. M.; Stadtman, T. C. *Annu. Rev. Nutr.* **1999**, *19*, 1.

(81) Lass, A.; Witting, P.; Stocker, R.; Esterbauer, H. *Biochim. Biophys. Acta - Lipids Lipid. Metabol.* **1996**, *1303*, 111.

(82) Sies, H.; Masumoto, H. *Adv. Pharmacol.* **1996**, *38*, 229.

(83) Sies, H. *Free Rad. Biol. Med.* **1993**, *14*, 313.

(84) Jacob, C.; Maret, W.; Vallee, B. L. *Biochem. Biophys. Res. Commun.* **1998**, *248*, 569.

(85) Müller, A.; Cadenas, E.; Graf, P.; Sies, H. *Biochem. Pharmacol.* **1984**, *33*, 3235.

(86) Müller, A.; Gabriel, H.; Sies, H.; Terlinden, R.; Fischer, H.; Römer, A. *Biochem. Pharmacol.* **1988**, *37*, 1103.

(87) Bhabak, K. P.; Mugesh, G. *Acc. Chem. Res.* **2010**, *43*, 1408.

(88) Ren, B.; Huang, W.; Åkesson, B.; Ladenstein, R. *J. Mol. Biol.* **1997**, *268*, 869.

(89) Syed, R.; Wu, Z.; Hogle, J.; Hilvert, D. *Biochemistry* **1993**, *32*, 6157.

(90) Back, T. G.; Kuzma, D.; Parvez, M. *J. Org. Chem.* **2005**, *70*, 9230.

(91) Press, D. J.; Mercier, E. A.; Kuzma, D. a.; Back, T. G. *J. Org. Chem.* **2008**, *73*, 4252.

(92) Bhabak, K.; Mugesh, G. *Chem.--Asian J.* **2009**, *4*, 974.

(93) Pearson, J. K.; Boyd, R. J. *J. Phys. Chem. A* **2007**, *111*, 3152.

(94) Bayse, C. A.; Antony, S. *J. Phys. Chem. A* **2009**, *113*, 5780.

(95) Musaev, D. G.; Hirao, K. *J. Phys. Chem. A* **2003**, *107*, 1563.

(96) Bayse, C. A. *J. Inorg. Biochem.* **2010**, *104*, 1.

(97) Bayse, C. A. *J. Phys. Chem. A* **2007**, *111*, 9070.

(98) Zakharov, M.; Masunov, A. E.; Dreuw, A. *J. Phys. Chem. A* **2008**, *112*, 10405.

(99) Efremenko, I.; Poverenov, E.; Martin, J. M. L.; Milstein, D. *J. Am. Chem. Soc.* **2010**, *132*, 14886.

(100) Chen, P.-T.; Wang, C.-C.; Jiang, J.-C.; Wang, H.-K.; Hayashi, M. *J. Phys. Chem. B* **2011**, *115*, 1485.

(101) Silverman, D. N.; McKenna, R. *Acc. Chem. Res.* **2007**, *40*, 669.

(102) Lundin, A.; Panas, I.; Ahlberg, E. *J. Phys. Chem. A* **2007**, *111*, 9080.

(103) Prabhakar, R.; Vreven, T.; Morokuma, K.; Musaev, D. G. *Biochemistry* **2005**, *44*, 11864.

(104) Hurley, M.; Pacios, L. F.; Christiansen, P.; Ross, R.; Ermler, W. *J. Chem. Phys.* **1986**, *84*, 6840.

(105) Wadt, W. R.; Hay, P. J. *J. Chem. Phys.* **1985**, *82*, 284.

(106) Dunning, Jr. T. H. *J. Chem. Phys.* **1971**, *55*, 716.

(107) Dunning Jr, T. H. *J. Chem. Phys.* **1970**, *53*, 2823.

(108) Tomasi, J.; Mennucci, B.; Cammi, R. *Chem. Rev.* **2005**, *105*, 2999.

(109) Wolinski, K.; Hinton, J. F.; Pulay, P. *J. Am. Chem. Soc.* **1990**, *112*, 8251.

(110) Bayse, C. A. *Inorg. Chem.* **2004**, *43*, 1208.

(111) Bayse, C. A. *J. Chem. Theory Comput.* **2005**, *1*, 1119.

(112) Maiorino, M.; Roveri, A.; Coassin, M.; Ursini, F. *Biochem. Pharmacol.* **1988**, *37*, 2267.

(113) Rooseboom, M.; Commandeur, J. N. M.; Floor, G. C.; Rettie, A. E.; Vermeulen, N. P. E. *Chem. Res. Toxicol.* **2000**, *14*, 127.

(114) Glass, R. S.; Farooqui, F.; Sabahi, M.; Ehler, K. W. *J. Org. Chem.* **1989**, *54*, 1092.

(115) Wagner, G.; Schuch, G.; Akerboom, T. P. M.; Sies, H. *Biochem. Pharmacol.* **1994**, *48*, 1137.

(116) Bayse, C. A.; Baker, R. A.; Ortwine, K. N. *Inorg. Chim. Acta* **2005**, *358*, 3849.

(117) Bayse, C. A.; Pavlou, A. *submitted.*

(118) Ali, S. T.; Jahangir, S.; Karamat, S.; Fabian, W. M. F.; Nawara, K.; Kóňa, J. *J. Chem. Theory Comput.* **2010**, *6*, 1670.

(119) Goto, K.; Nagahama, M.; Mizushima, T.; Shimada, K.; Kawashima, T.; Okazaki, R. *Org. Lett.* **2001**, *3*, 3569.

(120) Allenmark, S. *Chirality* **2008**, *20*, 544.

(121) Sato, S.; Matsuo, M.; Nakahodo, T.; Furukawa, N.; Nabeshima, T. *Tetrahedron Lett.* **2005**, *46*, 8091.

(122) Ritchey, J. A.; Davis, B. M.; Pleban, P. A.; Bayse, C. A. *Org. Biomol. Chem.* **2005**, *3*, 4337.

(123) Cowan, E. A.; Oldham, C. D.; May, S. W. *Arch. Biochem. Biophys.*, *506*.

(124) Bhabak, K. P.; Mugesh, G. *Chem. Eur. J.* **2008**, *14*, 8640.

(125) Tarze, A.; Dauplais, M.; Grigoras, I.; Lazard, M.; Ha-Duong, N. T.; Barbier, F.; Blanquet, S.; Plateau, P. *J. Biol. Chem.* **2007**, *282*, 8759.

(126) Whanger, P. D. *J Am Coll Nutr* **2002**, *21*, 223.

(127) Painter, E. P. *Chem. Rev.* **1941**, *28*, 179.

(128) Haratake, M.; Hongoh, M.; Miyauchi, M.; Hirakawa, R.; Ono, M.; Nakayama, M. *Inorg. Chem.* **2008**, *47*, 6273.

(129) Sunde, R. A.; Hoekstra, W. G. *Biochem. Biophys. Res. Commun.* **1980**, *93*, 1181.

(130) Nakagawa, T.; Hasegawa, Y.; Yamaguchi, Y.; Tanaka, H.; Chikuma, M.; Sakurai, H.; Nakayama, M. *Biochem. Biophys. Res. Commun.* **1986**, *135*, 183.

(131) Gailer, J.; George, G. N.; Pickering, I. J.; Madden, S.; Prince, R. C.; Yu, E. Y.; Denton, M. B.; Younis, H. S.; Aposhian, H. V. *Chem. Res. Toxicol.* **2000**, *13*, 1135.

(132) Gailer, J. *Biochimie* **2009**, *91*, 1268.

(133) Rabenstein, D. L.; Tan, K.-S. *Magn. Reson. Chem.* **1988**, *26*, 1079.

(134) Fleischer, H.; Glang, S.; Schollmeyer, D.; Mitzel, N. W.; Buhl, M. *Dalton Trans.* **2004**, 3765.

(135) Kice, J. L.; Lee, T. W. S.; Pan, S.-T. *J. Am. Chem. Soc.* **1980**, *102*, 4448.

(136) Forastiere, D. O.; Borghi, E. B.; Morando, P. J. *Helv. Chim. Acta* **2007**, *90*, 1152.

(137) Junker, M.; Rodgers, K. K.; Coleman, J. E. *Inorg. Chim. Acta* **1998**, *275-276*, 481.

(138) Vallee, B. L.; Auld, D. S. *Biochemistry* **1990**, *29*, 5647.

(139) Krężel, A.; Maret, W. *J. Biol. Inorg. Chem.* **2006**, *11*, 1049.

(140) Maret, W. *BioMetals* **2009**, *22*, 149.

(141) Hershfinkel, M. In *Molecular Biology of Metal Homeostasis and Detoxification*; Tamas, M., Martinoia, E., Eds.; Springer Berlin / Heidelberg: 2006; Vol. 14, p 131.

(142) Laity, J. H.; Lee, B. M.; Wright, P. E. *Curr. Opin. Struct. Biol.* **2001**, *11*, 39.

(143) Dreosti, I. E. *Mutat. Res., Fundam. Mol. Mech. Mutagen.* **2001**, *475*, 161.

(144) Witkiewicz-Kucharczyk, A.; Bal, W. *Toxicol. Lett.* **2006**, *162*, 29.

(145) Maret, W. *J. Anal. At. Spectrom.* **2004**, *19*, 15.

(146) Becker, K. G.; Nagle, J. W.; Canning, R. D.; Biddison, W. E.; Ozato, K.; Drew, P. D. *Hum. Mol. Genet.* **1995**, *4*, 685.

(147) Miura, T.; Satoh, T.; Takeuchi, H. *Biochim. Biophys. Acta, Protein Struct. Mol. Enzymol.* **1998**, *1384*, 171.

(148) Maret, W. *Biochemistry* **2004**, *43*, 3301.

(149) Hanas, J. S.; Larabee, J. L.; Hocker, J. R. In *Zinc Finger Proteins*; Iuchi, S., Kuldell, N., Eds.; Springer US: 2005, p 39.

(150) Blessing, H.; Kraus, S.; Heindl, P.; Bal, W.; Hartwig, A. *Eur. J. Biochem.* **2004**, *271*, 3190.

(151) Rana, U.; Kothinti, R.; Meeusen, J.; Tabatabai, N. M.; Krezoski, S.; Petering, D. H. *J. Inorg. Biochem.* **2008**, *102*, 489.

(152) Wolfe, S. A.; Nekludova, L.; Pabo, C. O. *Annu. Rev. Biophys. Biomol. Struct.* **1999**, *3*, 183.

(153) Sénèque, O.; Latour, J.-M. *J. Am. Chem. Soc.* **2010**, *132*, 17760.

(154) Hay, P. J.; Wadt, W. R. *J. Chem. Phys.* **1985**, *82*, 270.

(155) Amin, E. A.; Truhlar, D. G. *J. Chem. Theory Comput.* **2008**, *4*, 75.

(156) Narayan, V. A.; Kriwacki, R. W.; Caradonna, J. P. *J. Biol. Chem.* **1997**, *272*, 7801.

(157) Almaraz, E.; de Paula, Q. A.; Liu, Q.; Reibenspies, J. H.; Darensbourg, M. Y.; Farrell, N. P. *J. Am. Chem. Soc.* **2008**, *130*, 6272.

(158) Couty, M.; Hall, M. B. *J. Comp. Chem.* **1996**, *17*, 1359.

(159) Gourlaouen, C.; Piquemal, J.-P.; Saue, T.; Parisel, O. *J. Comp. Chem.* **2006**, *27*, 142.

(160) Feller, D. *J. Comp. Chem.* **1996**, *17*, 1571.

(161) Schuchardt, K. L.; Didier, B. T.; Elsethagen, T.; Sun, L.; Gurumoorthi, V.; Chase, J.; Li, J.; Windus, T. L. *J. Chem. Inf. Model.* **2007**, *47*, 1045.

VITA

SONIA ANTONY

EDUCATION

Ph.D., Chemistry, Old Dominion University, Virginia, U.S.A., May 2011
Dissertation: "Theoretical studies on the reactions of selenium compounds" Advisor: Dr. Craig A. Bayse.

M.S., Chemistry, Old Dominion University, Virginia, U.S.A., 2006.

M.Sc., Chemistry, University of Kerala, India, 2001.

B.Sc., Chemistry, University of Kerala, India, 1999.

PROFESSIONAL EXPERIENCE

Computational chemistry research using quantum mechanical software- Gaussian 03 and PQS.

Teaching Assistant for Laboratory courses: General Chemistry, Organic Chemistry.

Familiar with IR, NMR, GC and HPLC instruments.

HONORS

Old Dominion University Office of Academic Affairs Enhancement Award, 2002-2003.

PROFESSIONAL AFFILIATION

American Chemical Society, 2009-present.

PUBLICATIONS

Antony, Sonia; Bayse, Craig A. "Theoretical studies of models of the active site of the tungstoenzyme acetylene hydratase" *Organometallics,* 2009, 28, 4938-4944.

Bayse, Craig A.; Antony, Sonia. "Theoretical studies of [2,3]-sigmatropic Rearrangements of allylic selenoxides and selenimides" *Molecules*, 2009, 14, 3229-3236.

Bayse, Craig A.; Antony, Sonia. "Modeling the oxidation of ebselen and other organoselenium compounds using explicit solvent network" *J. Phys. Chem. A*, 2009, 113, 5780-5785.

Bayse, Craig A.; Antony, Sonia. "Molecular modeling of bioactive selenium compounds" *Main Group Chem.*, 2007, 6, 185-200.

Albin, Sacharia; Zheng, Jianli; Xiao, Bing; Cooper, John. B.; Jeffers, Robert B.; Antony, Sonia. "Chemical vapor deposited diamond films for self-referencing fiber optic Raman probes" *New Diam. Front. Carbon Technol.*, 2003, 13, 341-351.

ORAL PRESENTATIONS

Antony, Sonia and Bayse, Craig A, "Computational investigation of the reactions of ebselen." Graduate Research Symposium, College of William and Mary, Virginia, United States, March 2011.

Antony, Sonia and Bayse, Craig A, "Molecular modeling of intermediates in the mechanism of the tungsten enzyme acetylene hydratase." 238th ACS National Meeting, Washington, DC, United States, August 16-20, 2009.

Antony, Sonia and Bayse, Craig A, "Understanding the reactivity of ebselen using SAPE and DFT methods." Virginia Academy of Science meeting, Hampton University, Virginia, United States, May 2008.

POSTERS

Antony, Sonia and Bayse, Craig A, "Modeling the mechanism of the glutathione peroxidase mimic ebselen." 238th ACS National Meeting, Washington, DC, United States, August 16-20, 2009.

Antony, Sonia and Bayse, Craig A, "DFT analysis of the role of ebselen in delaying undesired apoptosis due to removal of reactive oxygen species." Chemical Biology Symposium, Virginia Commonwealth University, Virginia, United States, April 2009.

Bayse, Craig A.; Antony, Sonia. "Molecular modeling of the tungstoenzyme acetylene hydratase." 236th ACS National Meeting, Philadelphia, PA, United States, August 17-21, 2008.

Bayse, Craig A.; Antony, Sonia. "Molecular Modeling of Ebselen and Other Mimics of the Selenoprotein Glutathione Peroxidase." 35th Northeast Regional Meeting of the American Chemical Society, Burlington, VT, United States, June 29-July 2, 2008

Dobrydneva, Yuliya; Weatherman, Ross; Trebley, Joseph; Fitzgerald, Megan; Antony, Sonia; Chatterjie, Nithiananda; Blackmore, Peter. "Tamoxifen, diethylstilbestrol and other non-steroidal estrogens, a novel class of store operated calcium channel modulators that affect platelet activation and thrombosis: Two faces of one pharmacophore." 232nd ACS National Meeting, San Francisco, CA, United States, Sept. 10-14, 2006.